1-1-1996

Star formation in Lynds 1641.

Lori E. Allen
University of Massachusetts Amherst

Star Formation in Lynds 1641

A Dissertation Presented

by

Lori E. Allen

Submitted to the Graduate School of the
University of Massachusetts Amherst in partial fulfillment
of the requirements for the degree of

Doctor of Philosophy

February 1996

Department of Physics and Astronomy

Star Formation in Lynds 1641

A Dissertation Presented

by

Lori E. Allen

Approved as to style and content by:

Karen M. Strom, Chair

Stephen E. Strom, Member

Ronald L. Snell, Member

John Kwan, Member

Monroe Rabin, Outside Member

John F. Dubach, Department Head
Department of Physics and Astronomy

Acknowledgments

Many people have had a hand in the work that is presented here. First among them is Karen Strom, who has devoted a significant fraction of her professional life to the study of Lynds 1641, and who turned over to me a terrific project that came with much of the data already acquired! Fortunately, we did have to spend some time in the Southwest getting more, which led to a several day drive through Arizona and New Mexico and a lasting friendship. Karen's ability to remember the details of any randomly chosen star field in L1641 is matched only by her instinctive navigation among unmarked dirt roads in Navajo country. I hope we will have the chance to explore other deserts together. Steve Strom has been a great co-advisor, and a good friend. I'll always be grateful to Steve for the support and encouragement he gave me at a crucial time, as well as all the scientific guidance he has provided. I look forward to many years of both work and play with Karen and Steve.

Mike Meyer, as friend, colleague, and officemate, has been a prominent person in my life the last few years, much to my good fortune. I have learned more from Mike than I can record here, not least of which is the value of colored pencils. Lynne Hillenbrand broke a lot of ground before me, making my work easier. Her energetic presence has been missed here in Amherst since she moved West. Chigurupati Murali, in addition to talking over some of this work with me, has been a good friend, a co-conspirator, and a great guy to hear jazz with. I'm so glad my time here overlapped with Nuria Calvet, a good friend who is always willing to talk over a scientific problem, and who I just enjoy talking with, about anything. Suzan Edwards provided an always insightful and clear perspective on my work, which I should have taken advantage of more often.

So many of my fellow grad students have made life in the GRC tolerable. Special thanks go to Doug McGonagle, for being one of my very best friends in the world, in addition to providing some eleventh hour typesetting help that made all the difference. Beth Berry (honorary Astronomer), has been very supportive over the years, but I thank her most for introducing me to UMass hoops back in the days of Will (the thrill) and company. Thanks to the residents of Happy House (Meg, Mrinal, and Jess), I haven't had to sleep in my car the last two months.

Finally, I acknowledge the limitless support of my family, my parents Royal and Helen, my sisters Mary Ann and Royallynn.

Abstract

Star Formation in Lynds 1641

February 1996

Lori E. Allen, B.A., University of California Santa Cruz

Ph.D., University of Massachusetts Amherst

Directed by: Professor Karen M. Strom

We conducted an extensive multi-wavelength study of the nearest giant molecular cloud, L1641, with the goal of characterizing its stellar populations. At a distance of approximately 500 pc, L1641 provides an excellent opportunity for studying star formation over the entire range of stellar masses, and the star formation history in a region thought representative of those dominating stellar production in the Milky Way.

Our approach combines imaging surveys at optical and infrared wavelengths with spectroscopic surveys at $\lambda\lambda 6000 - 9000 \AA$ to measure stellar luminosities and effective temperatures. Stellar ages and masses are then estimated from comparison of L_*, T_{eff} with pre-main sequence evolutionary tracks. The stars for which we have obtained classifiable spectra as well as optical (R, I) and near-infrared (J, H, K) photometry number $\sim$300, and are contained within four regions, each approximately $20'$ square (2.5×2.5 pc).

Our 2.2μm images reveal both modest aggregates of several tens of stars and stars distributed at random across the face of the cloud; we find no evidence of rich (N >> 100 stars) clusters. The aggregate members appear to have formed within the past 1 Myr, while the distributed population contains both young stars (t<1 Myr) and stars ranging in age up to 30 Myr. From comparison of the fraction of the youngest stars forming in aggregates and in isolation, we conclude that stars born initially in aggregates comprise 25–50% of the total stars formed in L1641.

The observed frequency distribution of stellar ages enables a discussion of the star-forming history of the cloud. The L1641 cloud has been producing stars for nearly 30 Myr and over the last 10 Myr, the SFR has been roughly constant. We explore the implications of this result for the "off-cloud" spatial distribution of young stars.

Finally, we examine the circumstellar disk properties of stars in our spectroscopic sample. The frequency of disks, as inferrred from infrared excess emission, is found to be higher for stars less massive than 1 $M_{\odot}$ than for more massive stars. We also find that at least six stars in L1641 have apparently retained their accretion disks beyond an age of 3 Myr.

Table of Contents

List of Tables

List of Figures

Chapter 1

Introduction

It is believed that most of the stars in the solar neighborhood originated in giant molecular clouds. Orion is the nearest GMC complex, at a distance of ~500 parsecs. We know that star formation in Orion occurred as long ago as 10^7 yr, based on the ages derived for the oldest subgroup of the Ori OB association (Blaauw 1991; Warren & Hesser 1978; Brown *et al.* 1994). Stars have formed there very recently, as well; the famous Orion nebula cluster, with its luminous young Trapezium stars, is the archetypal stellar nursery. Elsewhere throughout the cloud complex, deeply embedded luminous sources, detectable only at infrared wavelengths and frequently associated with molecular outflows and optical jets, serve as signposts of current star formation. Thus, Orion offers a unique opportunity: to study a nearby GMC in depth, to observe star formation over the full range of masses, from O stars (40 $M_\odot$) to late M stars at the hydrogen-burning mass limit (0.08 $M_\odot$), and to determine the star formation history of a GMC over the past 10 million years.

Until recently, our understanding of star formation in Orion was based primarily on large-scale surveys at optical wavelengths. From these studies we learned much about the luminous O and B stars in the complex, but little about fainter low-mass stars, especially those which are still partially embedded in the molecular cloud and therefore invisible at optical wavelengths. Early infrared detectors made possible the detection of embedded sources, but they were limited in both size and sensitivity, leading to studies of small regions only a few arcminutes across. Only recently have infrared arrays become large and sensitive

enough that *unbiased* imaging surveys of nearby molecular clouds can be conducted. Thus, for the first time we are able to investigate significant portions of giant molecular clouds, with the goal of understanding the relation between the initial conditions in clouds and the stars that form.

This thesis summarizes my contribution to that effort. It is largely motivated by recent IR imaging studies, which have identified three possibly distinct modes of star formation in Orion: clusters (N> 100; not necessarily bound), aggregates (N=10-50; most likely unbound), and isolated (individual stars). I have focussed on the Lynds 1641 molecular cloud, in which the aggregate and isolated modes of star formation dominate. My goal is to characterize these populations, as part of a larger effort aimed at understanding how molecular cloud properties relate to the observed modes of star formation. The questions addressed in this work include:

- What fraction of stars in L1641 form in aggregates, and what fraction in isolated, individual events?
- What is the star formation history (N[t]) of the cloud?
- What is the initial mass function (N[m]) for the cloud? Does it vary with location in the cloud?
- What fraction of young stars in L1641 are surrounded by circumstellar disks? How does this fraction depend on stellar age? On stellar mass?

To answer these questions we must estimate stellar masses and ages. Our approach will be to combine spectroscopic and photometric data to calculate L_* and T_{eff}, in order to place stars on the H-R diagram. Stellar ages and masses are derived from comparison with evolutionary models for pre-main sequence stars.

The key observational aspect of this work, which distinguishes it from previous studies of L1641, is the spectral classification of over 300 young stars in the cloud. With spectral type comes effective temperature as well as intrinsic color, which

combined with photometric observations provides a measure of interstellar extinction, and enables us to accurately estimate stellar luminosity. Most of the young stars in this study are too red for spectroscopic observations in the B and V bands, where most stellar classification work has been done. For example, a typical R magnitude for late-type M star in our study is 17, which translates to 19 mag at V. Add to that 5 A_v of extinction, and the star becomes spectroscopically unobservable at V =24 mag. Thus it was necessary to obtain classification spectra at a longer wavelength. However, in order to obtain spectra of a sufficiently large sample of stars, it was important to take advantage of capabilities available only at $\lambda < 1\mu$m, where large-format CCDs and multi-object spectrometers enable spectroscopy of $\sim$100 sources simultaneously; hence our choice of the $\lambda\lambda 6000 - 9000$Å region.

Additional observational data include imaging surveys at both optical and infrared wavelengths, which are used in combination with intrinsic color (based on spectral type) to measure extinction and calculate source luminosity. Millimeter-wave spectral line observations are used to determine column densities across the surveyed regions, both to examine the molecular environments of the young stars, and as an aid in estimating the contamination of the cloud population by background stars.

Analysis of the data has led to several results. We find that low-mass stars form individually in L1641, as well as in small groups of 10-50. These "modes" of star formation may be equally responsible for the existing stellar population in the cloud. The distributions of stellar ages in the cloud are *not* consistent with a scenario in which star formation throughout the cloud was "triggered" by the nearby OB association. Instead, it appears that stars have been forming in the cloud for the past 10 million years, with occasional localized bursts in which a relatively rich (N$\sim$100) group is formed.

The work toward these conclusions is described in the following chapters of this thesis. Details of the observations are provided in Chapter 2. In Chapter 3 we examine our sample to identify and quantify the extent of stellar aggregates. The procedure developed to place stars in H-R diagrams is described in Chapter 4, and this is followed in Chapter 5 by an anlysis of the temporal and spatial distributions of stars placed in the H-R diagrams. In Chapter 6 we determine the circumstellar disk frequency as a function of age and mass. A brief discussion of our results and how they fit into the broader picture of star formation throughout the Orion GMC complex occurs in Chapter 7, where we also compare star formation in L1641 with star formation in the Taurus-Auriga molecular cloud. Our main conclusions are listed in Chapter 8.

Chapter 2

Observations

2.1 The Sample

Optical and infrared images were obtained in 1990 and 1992 for a large, representative sample of the cloud (0.77 square degrees; SSM). These surveys provided photometric measurements and astrometric positions which guided our selection of a spectroscopic sample suitable to our program. In particular, we selected regions located at the the northen and southern ends of the cloud. The areas included in both the imaging and spectroscopic surveys are marked in Figure 2.1, and include the following:

1. L1641N: A 26.4′ x 22′ region (centered at $\alpha = 5^h33^m35^s$, $\delta = -6°\ 24'$ (1950)) which includes *IRAS* PSC 05336−0632, the driving source for the energetic L1641N molecular outflow (Fukui *et al.* 1988). Five other *IRAS* PSC sources are included in this region as well.

2. V380: A 26.4′ x 21′ region (centered at $\alpha = 5^h33^m35^s$, $\delta = -6°\ 44'$ (1950)) which includes the driving source for the HH 1, 2 outflow (Pravdo *et al.* 1985; Herbig and Jones 1981). Also contains the Ae/Be star V380 and 10 *IRAS* sources.

3.&4. L1641 South/Cohen-Kuhi Group: Combined, a 43.7′ x 17.5′ region (centered at $\alpha = 5^h39^m15^s$, $\delta = -8°\ 09'$ (1950)) which includes a cluster (N∼150 stars), the continuum+emission classical T Tauri star DL Ori, and the "Cohen-Kuhi" group (Cohen & Kuhi 1979), an aggregate of partially embedded young stars. A total of 12 *IRAS* sources are found within this region.

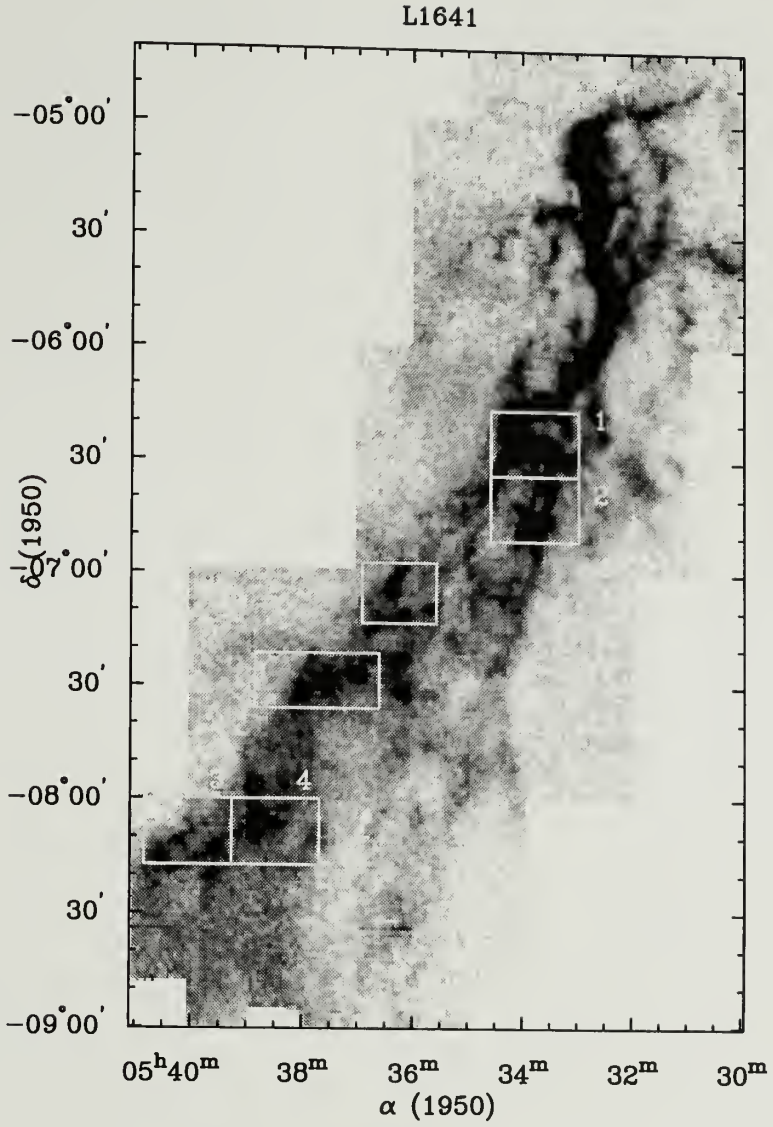

Figure 2.1. Map of the integrated intensity at ^{13}CO of L1641. Regions covered by the imaging survey of SSM are outlined, and those included in the spectroscopic survey are numbered. CO map from Bally *et al.* 1987.

2.2 Infrared and Optical Imaging

Infrared mapping of selected regions in L1641 was carried out during 1992 January using the SQIID infrared camera at the 1.3-m telescope at KPNO. Simultaneous images in the J (1.25μm), H (1.65μm), and K (2.2μm) bands were made at a spatial resolution of 1.36″ per pixel. Individual fields of size 5.4′ x 5.4′ were used to construct larger maps of the regions. Total integration time was 6 minutes in each band. Details of the mosaicking and reduction procedures are given in SSM.

Sources were identified using DAOFIND in IRAF, and stellar photometry was obtained using the APPHOT routine. JHK measurements were placed on a standard magnitude system using observations of stars from the list of Elias *et al.* (1982). Extinction corrections were derived using observations of Elias standards and a "local standard" field within L1641 at a variety of air masses. Completeness limits are estimated to be 16.8, 15.8, and 14.75 mag, at J, H, and K, respectively.

R (7000Å) and I (9000Å) band images were obtained in 1990 November, 1992 January, and 1994 March with a Tektronix 2048 x 2048 CCD on the KPNO 0.9-m telescope. The plate scale for the camera/telescope combunation is 0.77″ per pixel. Integration times were 5 and 3 minutes in R and I, respectively. Details regarding the data reduction are provided in SSM. The measurements were placed on the Cousins photometric system by observing stars from Landolt's (1983) catalog. Air-mass corrections were derived from the observations of Landolt standards at several different elevations. Estimated completeness limits are 20.2 mag at R and 19.3 mag at I.

Both the optical and infrared images were placed on an astrometric coordinate system defined by stars contained within the SAO Catalog (1966) and the Guide Star Catalog (1992), using the ASTROMETRY package in IRAF. The 1σ

uncertainties in derived positions were typically $\pm 1.1''$ and $\pm 0.8''$ for the SQIID mosaics and CCD images respectively.

2.3 *R*-band Spectroscopy

Spectra were obtained using Hydra, a multiple-fiber optic fed spectrograph used in conjunction with the 4-m telescope at Kitt Peak National Observatory, on the nights 1-4 January 1993 and 21-24 December 1993. We used the red fiber cable in conjunction with the BL181 grating (316 l/mm) set at a central wavelength of 7600Å, and a Tektronix 2048x2048 CCD to obtain spectra in the range $\lambda\lambda 5500 - 9500$Å. The spectral dispersion was ~ 1.9Å per pixel; the effective resolution was $\sim$3 pixels or 6Å. Typical integration times were 1.5 hr, consisting of three 0.5 hr integrations co-added. The signal-to-noise of the spectra is high; ~ 50 for a star with I=18 mag.

The spectra were reduced using the DOHYDRA package within IRAF[2], and further analysed using the HYDRA and ONEDSPEC packages. The reduction included flat-fielding and wavelength calibration, but no attempt was made to flux calibrate the spectra. Spectra were normalized by fitting a third order spline function to continuum points at 6530, 7040, 7560, 8130, 8840, and 9040Å.

The luminosity coverage of the spectral survey is shown in Figure 2.2 , where the number distributions of observed I magnitudes in the photometry and spectroscopy samples are plotted.

On the same nights that spectra were obtained for stars in L1641, spectra were also obtained for some 275 stars in the open clusters Praesepe and M67 (plus some field giants), in order to construct a standard grid. Details regarding our classification system and our grid of spectral standards are provided in Appendix A.

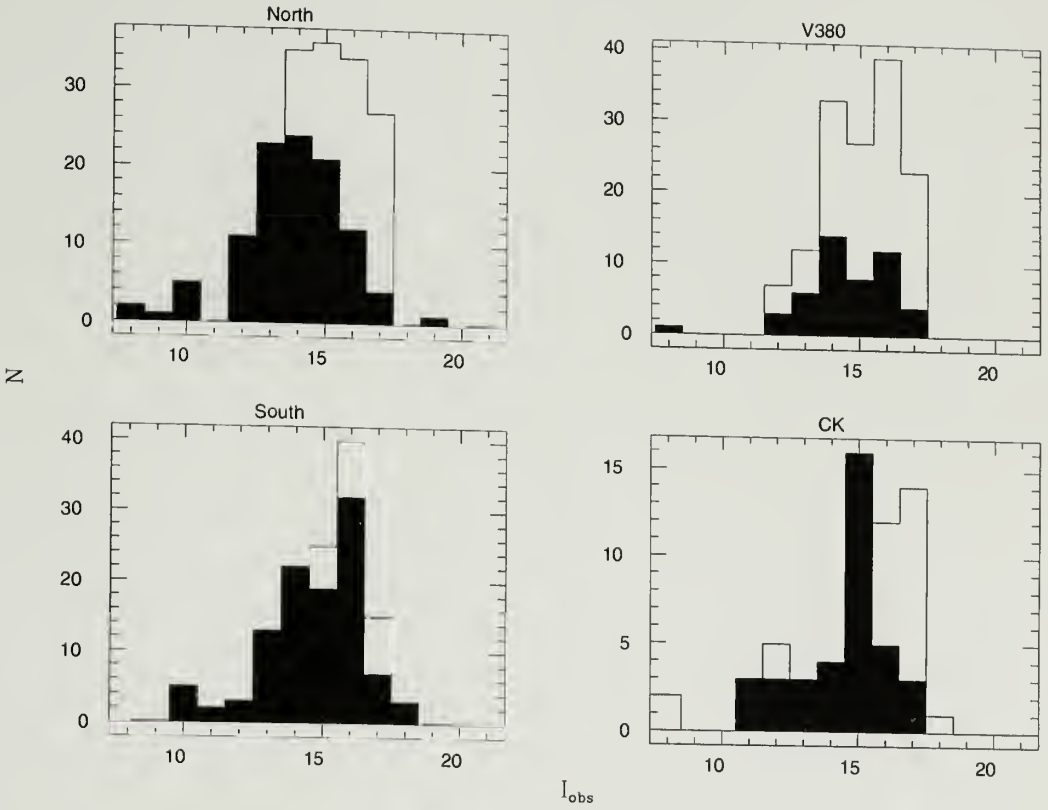

Figure 2.2. Observed I magnitudes, in the photometric sample (open histogram), and the spectroscopic sample (solid histogram). Magnitude distributions are shown for stars within the $R-$ and $I-$band completeness limit, and having photometric errors in *all five* bands (R, I, J, H, K) of 10% or less.

2.4 ^{12}CO and ^{13}CO Spectral Line Imaging

The regions covered by our spectroscopic survey were mapped in both ^{12}CO(J=1-0) and ^{13}CO(J=1-0) (115.271203 GHz and 110.201370 GHz, respectively) in 1993 November through 1994 February using QUARRY, the 15 element focal plane array on the Five College Radio Astronomy 14-m telescope. The half-power beam width of the 14-m telescope is 45″ at 115 GHz, and 47″ at 110 GHz. Maps were Nyquist sampled, for a beam spacing of 22.5″.

A quasi-optical sideband filter and cryogenic Schottky diode mixer receivers were used with 32 channel spectrometers at a resolution of 250 kHz per channel. Integration times were 15 sec in ^{12}CO and 30 sec in ^{13}CO, for an rms noise level of 0.2 to 0.4 K. Each spectrum had a first order, linear baseline removed. Spectra were reduced using FCRAO's SPA software package. Intensity and optical depth maps were transformed to images using IRAF.

The resulting maps of ^{12}CO and ^{13}CO emission were combined in a standard LTE analysis to produce a map of the ^{13}CO column density. Assuming an abundance in CO of $H_2 = 0.5 \times 10^6 \cdot (^{13}CO)$, and a standard relation between gas column density and extinction of $A_v = 10^{-21} N(H_2)$ (Dickman and Herbst 1990), extinction maps were made for each of the three regions. These are superposed on $K-$band images in Figures 2.3- 2.6.

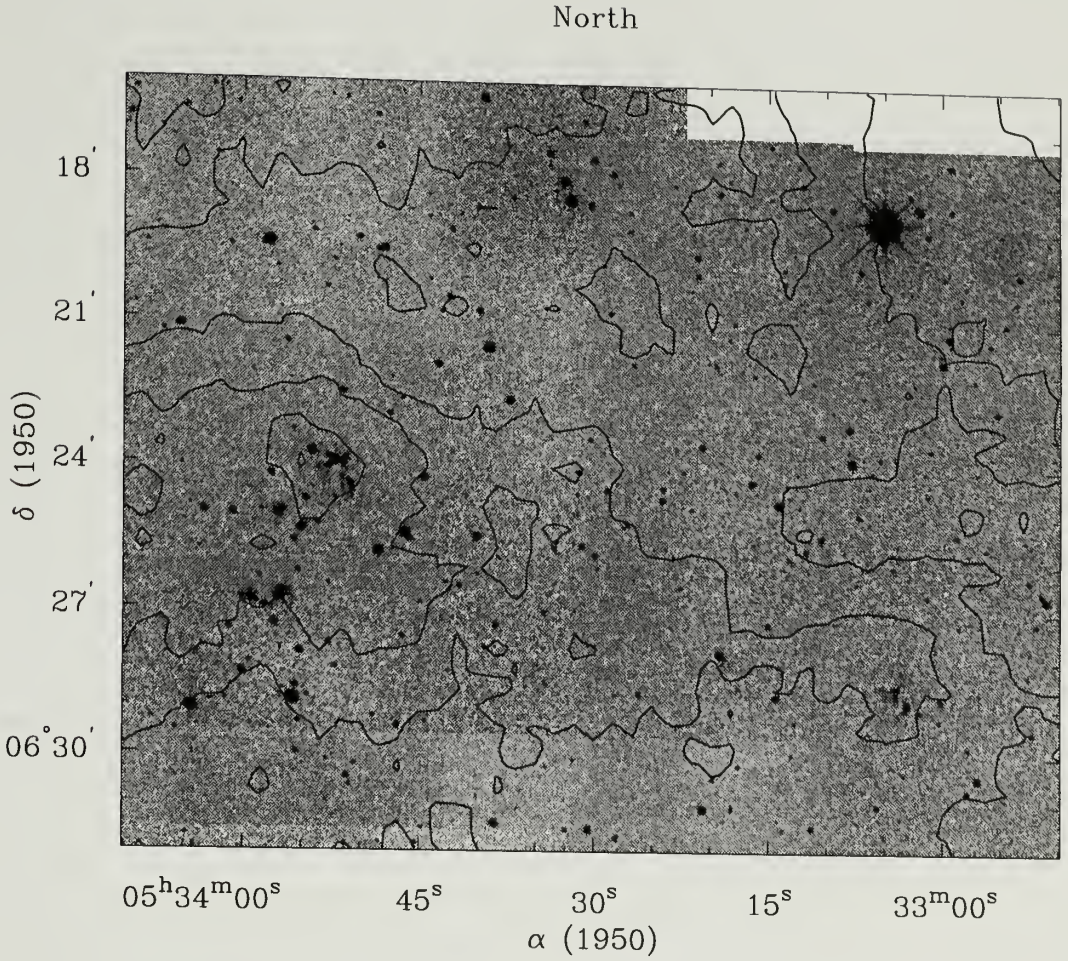

Figure 2.3. K-band image of L1641 North with extinction contours overlaid. Contours begin at $A_v = 4$ and are in intervals of $4A_v$.

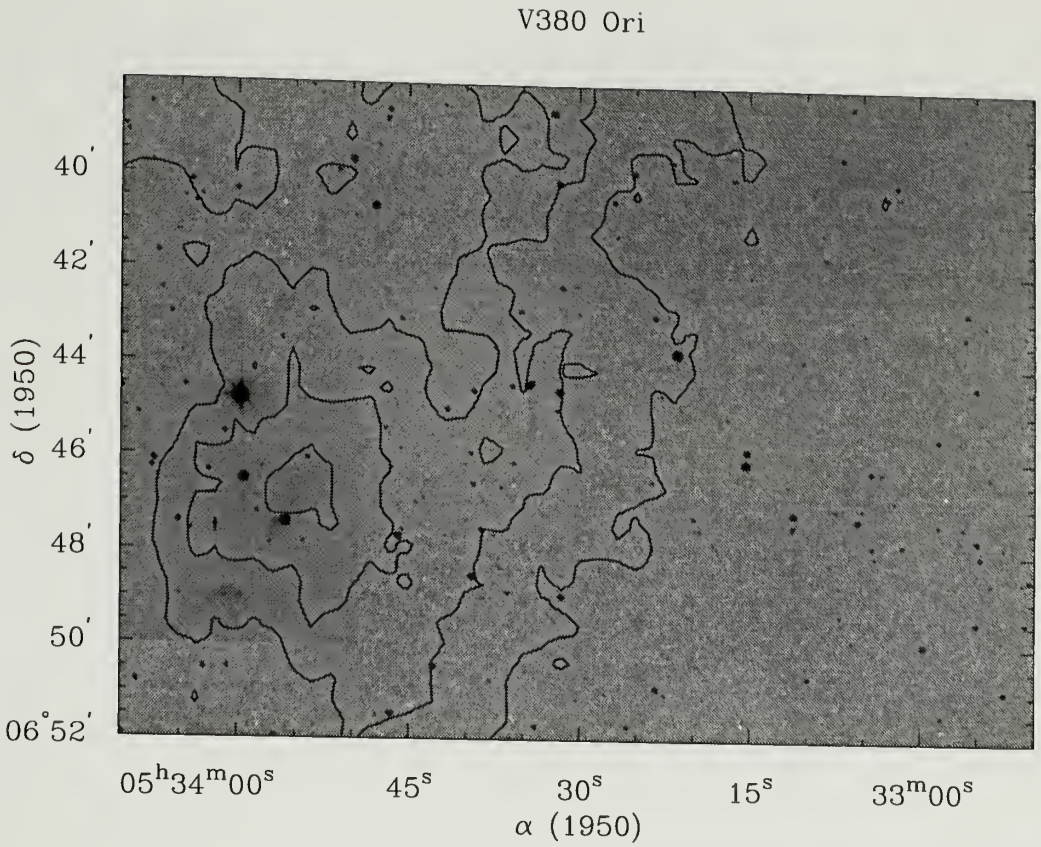

Figure 2.4. K-band image of the V380 region with extinction contours overlaid. Contours begin at $A_v = 4$ and are in intervals of $4A_v$.

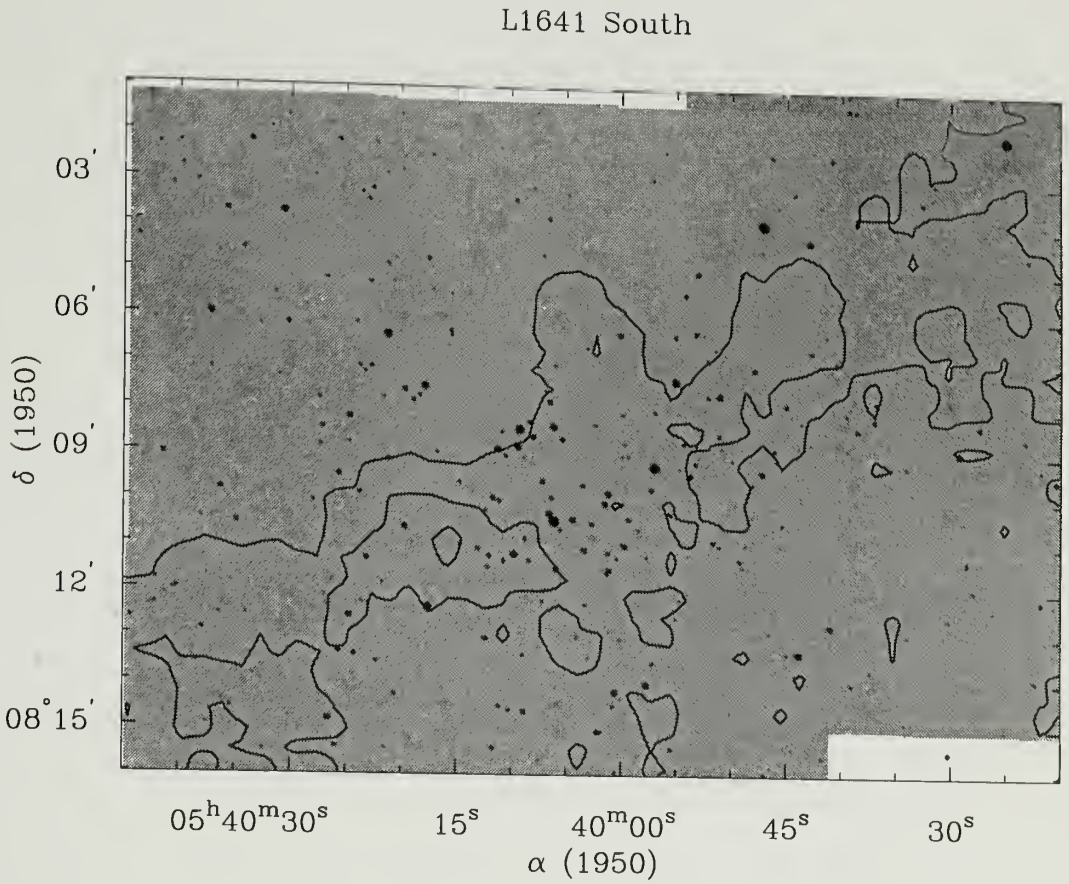

Figure 2.5. K-band image of the L1641 South region with extinction contours overlaid. Contours begin at $A_v = 4$ and are in intervals of $4A_v$.

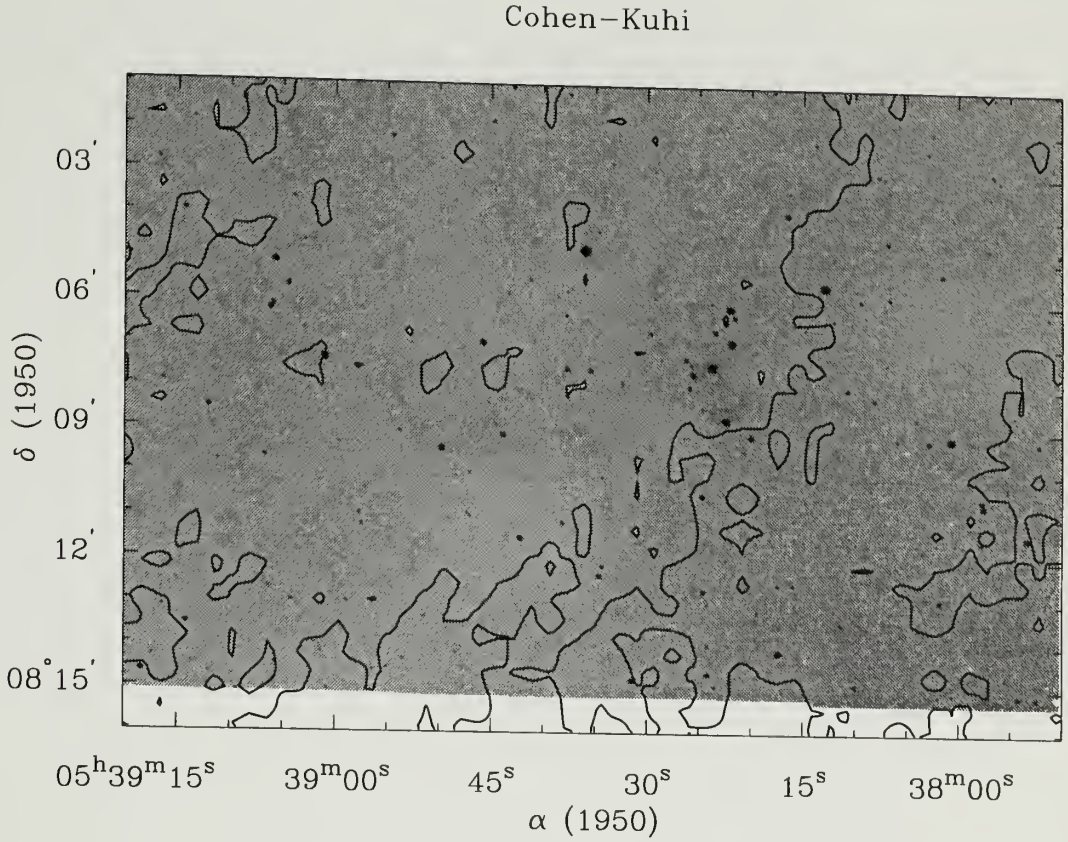

Figure 2.6. K-band image of the Cohen-Kuhi Group region with extinction contours overlaid. Contours begin at $A_v = 4$ and are in intervals of $4A_v$.

Chapter 3

Stellar Aggregates in L1641

In this chapter we define our spectroscopic sample in terms of stellar aggregates and a distributed population of stars. We investigate the stellar surface density (number of stars per square arcminute) in the surveyed regions, and compare the distribution of stars with our defined aggregates. Then we briefly examine the relationship between the stellar aggregates and the molecular gas.

3.1 Definition of Stellar Aggregates

In their IR survey, SSM defined aggregates in L1641 as regions of apparently enhanced stellar surface density, centered on signposts of recent star formation. The SSM aggregate (R=1/3pc) boundaries are shown in Figures 3.1 - 3.3, superposed on the $K-$band images.

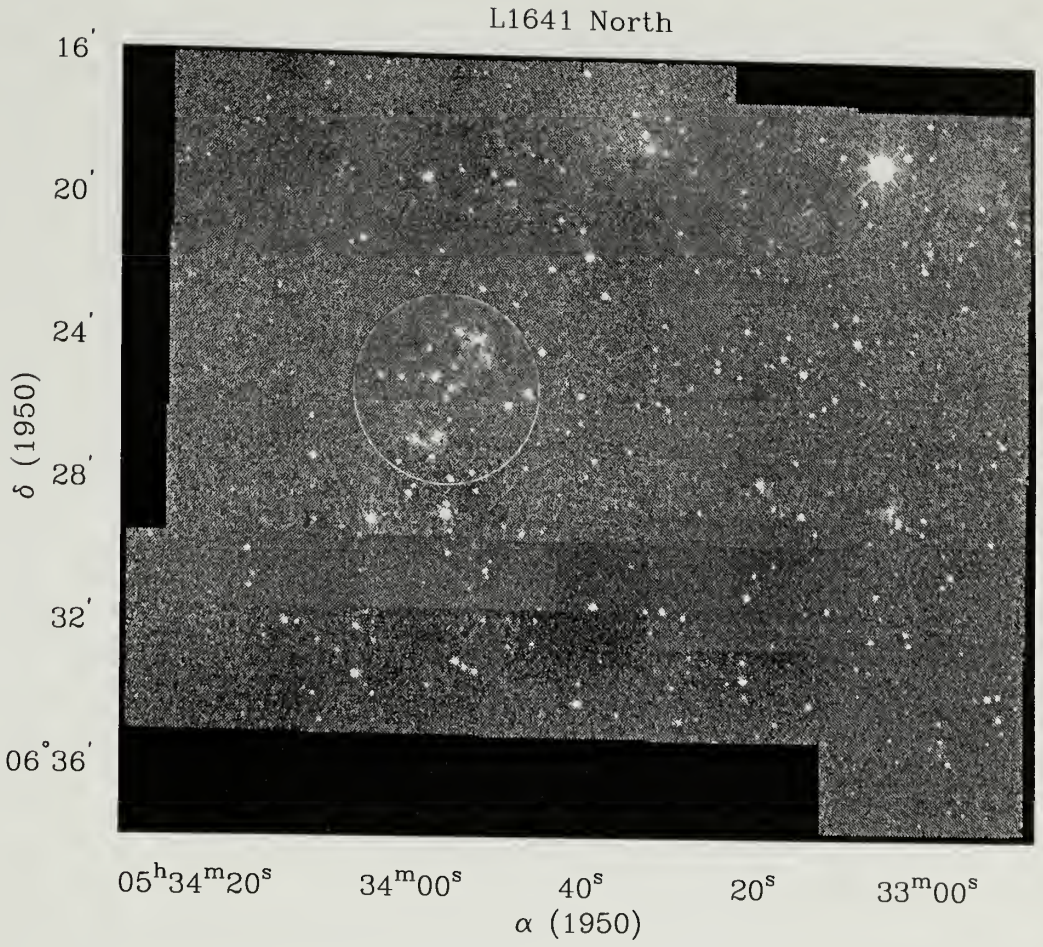

Figure 3.1. $K-$band mosaic of the L1641 North region showing the aggregate boundary, of radius 1/3 parsec.

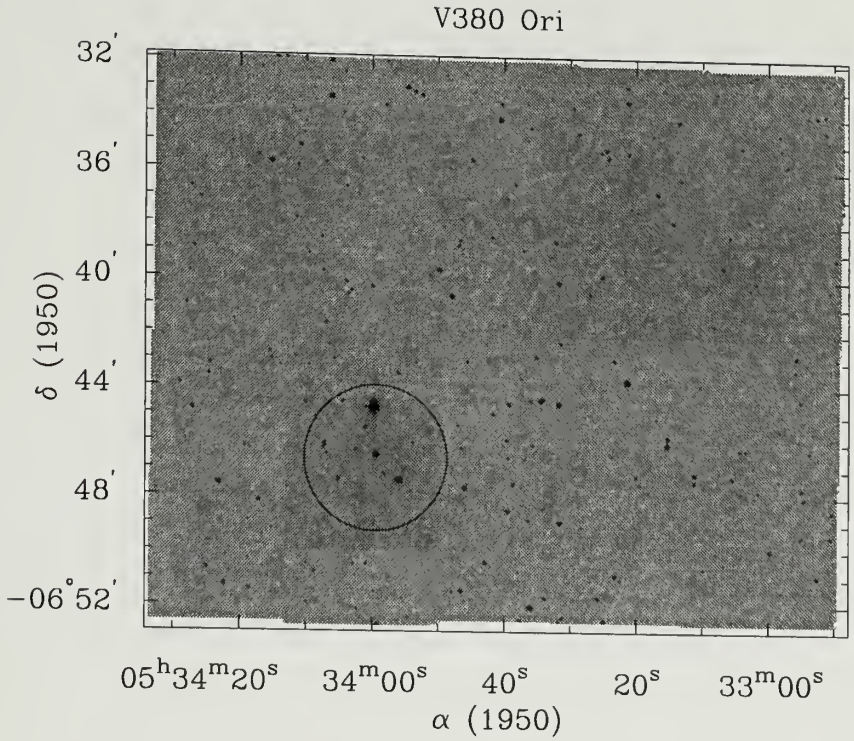

Figure 3.2. $K-$band mosaic of the V380 region showing the aggregate boundary, of radius 1/3 parsec.

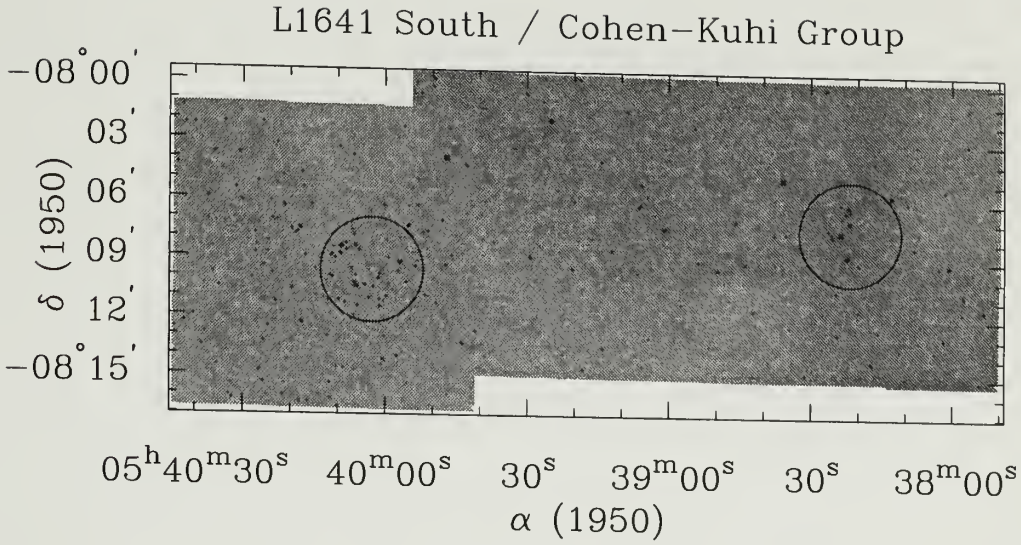

Figure 3.3. $K-$band mosaic of the South and Cohen-Kuhi regions showing the aggregate boundaries, each of radius 1/3 parsec.

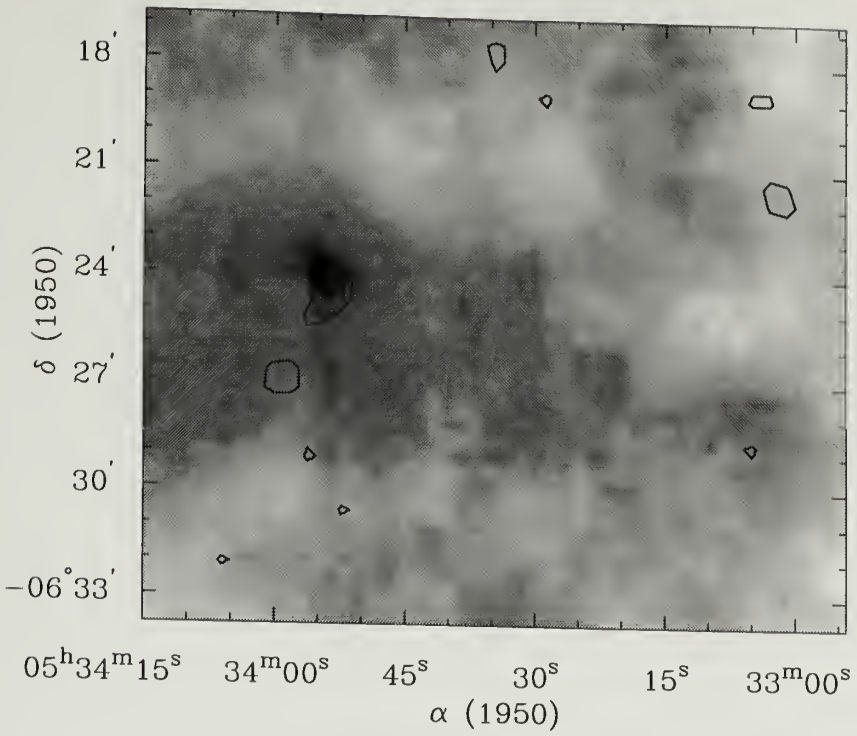

Figure 3.4. Contours of the stellar surface density (black lines) superposed on a grayscale map of the gas column density for L1641 North. The lowest stellar surface density contour level is 3σ above the average star density in the field, and higher contour levels are at 2σ intervals. Gas column density is expressed in units of A_v, over the range 1-20 A_v.

In order to test whether our eyeball-estimates of aggregate locations represented true surface density enhancements, we calculated the stellar surface density in each of the 4 fields, for all stars in the magnitude range $K \leq 14.5$, using a 60″ square aperture and 30″ sampling. The results are shown in Figures 3.4 - 3.6.

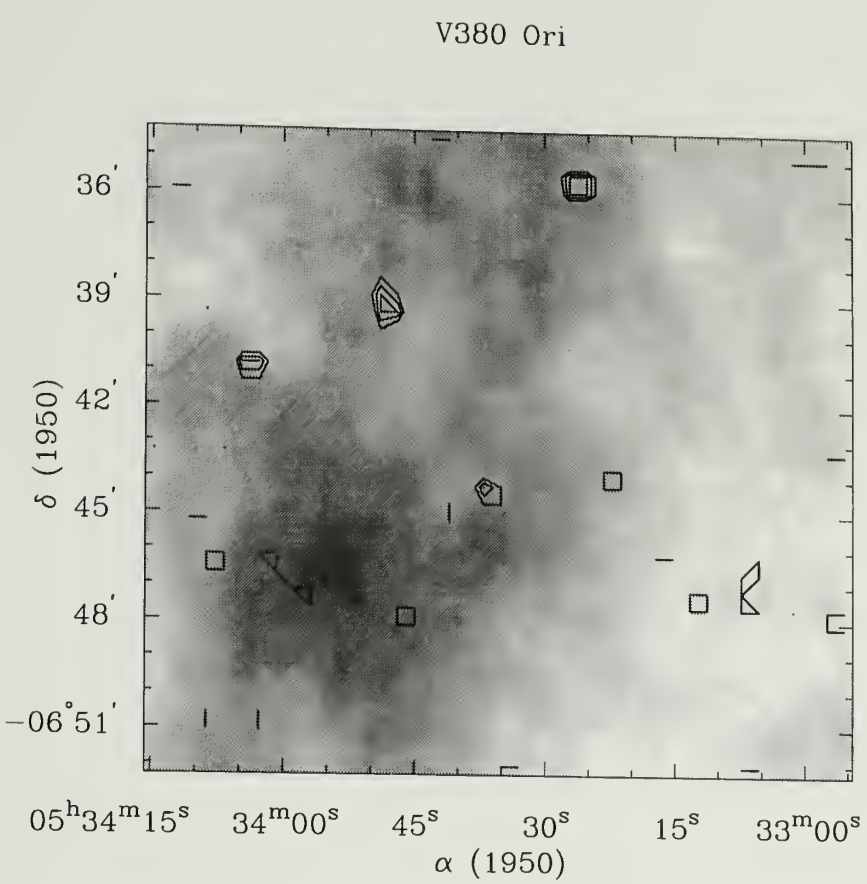

Figure 3.5. Contours of the stellar surface density (black lines) superposed on a grayscale map of the gas column density for the V380 region. The lowest stellar surface density contour level is 3σ above the average star density in the field, and higher contour levels are at 2σ intervals. Gas column density is expressed in units of A_v, over the range 1-20 A_v.

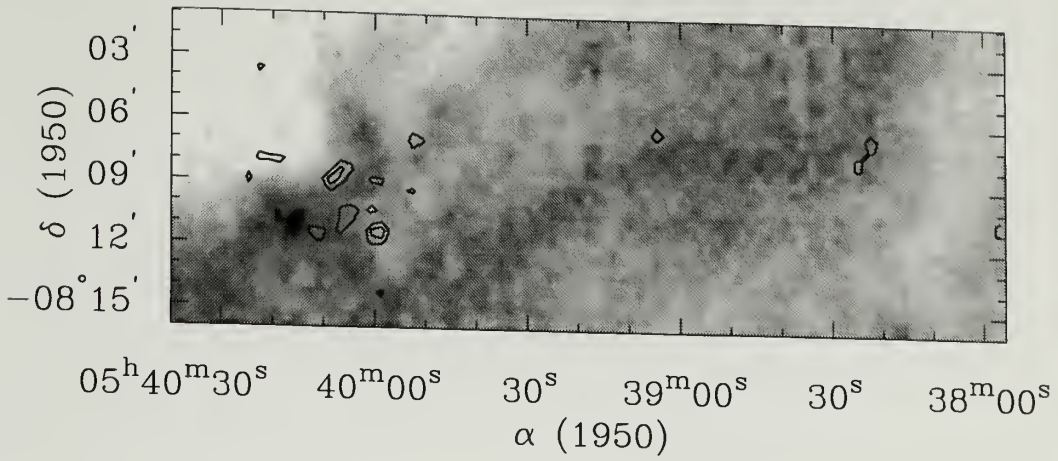

Figure 3.6. Contours of the stellar surface density (black lines) are drawn on grayscale maps of the gas column density for the South and Cohen-Kuhi regions. The lowest stellar surface density contour level is 3σ above the average star density in the field, and higher contour levels are at 2σ intervals. Gas column density is expressed in units of A_v, over the range 1-10 A_v.

In the North, South, and Cohen-Kuhi regions, the aggregates each coincide with the peak in the stellar surface density distribution in their respective fields. In the V380 field, no well-defined peak in the stellar surface density emerged. These results are in agreement with an independent analysis by D. Wall (1994) in which the two-point correlation function was used to quantify the degree and extent of clustering in L1641.

3.2 Aggregate Environments

The molecular environments of the aggregates are varied, as Figures 3.4 - 3.6 illustrate. For instance, the North aggregate is projected on the highest column density in the field, while in both the South and the CK Group, the aggregates are located adjacent to, but not coincident with, local peaks in the ^{13}CO column

Table 3.1. Average Extinctions (A_v)

Region	CO		E(R-I)	
	R< 1/3 pc	R> 1/3 pc	R< 1/3 pc	R> 1/3 pc
North	11	<5	10	2
Cohen-Kuhi	5	<5	3	3
South	6	<5	4	2

density. In Table 3.1, we list the average molecular gas column density both inside and outside the aggregate boundaries, expressed in terms of A_v. The morphologies in Figures 3.4 - 3.6 suggest that in the North, the aggregate is still closely associated with its parent molecular core, whereas in the South and CK Group, the aggregates have had time to disperse some distance from their natal cores.

Extinctions were also calculated for each star in the spectral survey, using the star's intrinsic colors (according to spectral type), and the measured colors at R and I. They, too are tabulated in Table 3.1, and their distributions are shown in Figure 3.7.

The mean extinctions calculated from CO and from $E(R-I)$ are in good agreement. Both show that the aggregates are more embedded than their surrounding distributed populations.

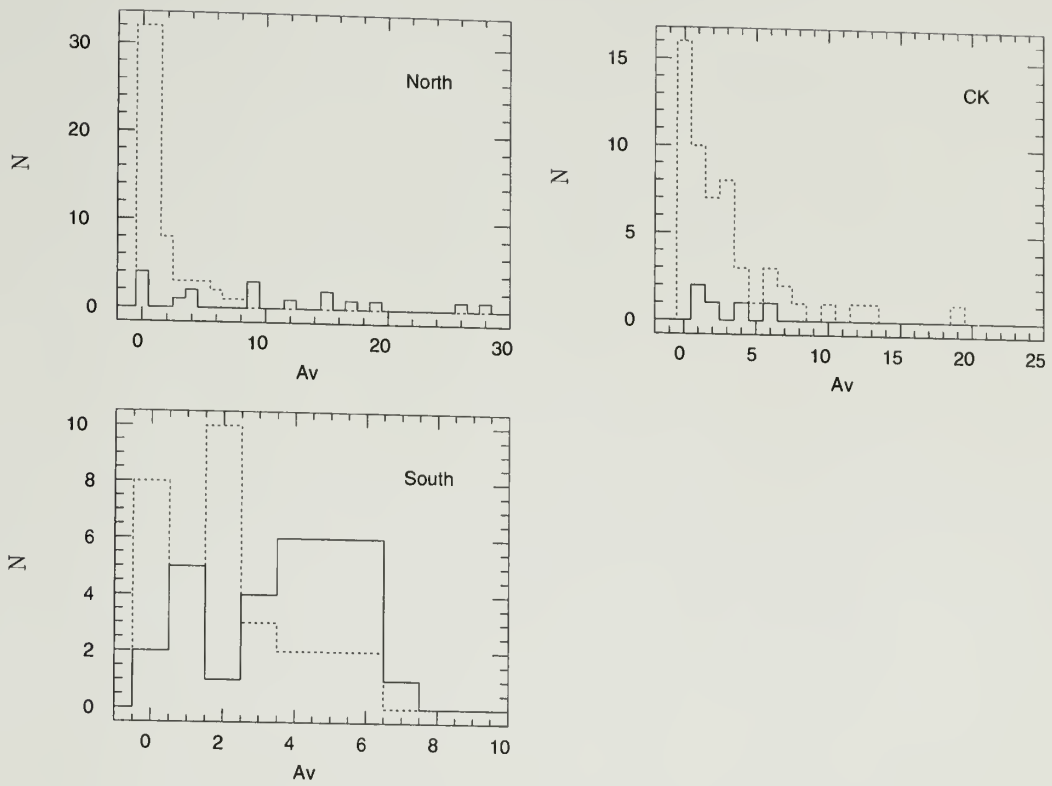

Figure 3.7. Distributions of measured extinctions for the aggregate (solid line) and distributed (dashed line) stars.

Chapter 4

Construction of H-R Diagrams

In order to place stars in the H-R diagram we must first determine their effective temperatures and luminosities. In this chapter we describe how the imaging and spectroscopic data are combined to calculate T_{eff} and L_*. Then we present H-R diagrams for the four regions surveyed in L1641.

The basic procedure for calculating T_{eff} and L_* is as follows: T_{eff} is determined from spectral type, while L_* is calculated from an extinction-corrected monochromatic flux, a bolometric correction, and of course, correction for distance.

4.1 Spectral Classification

Stars were classified by comparing their red [$\lambda\lambda 5500 - 9000 \AA$] spectra with the grid of spectral standards, compiled from observations of main sequence and giant stars in open clusters and in the field (Allen & Strom 1995) and listed in Appendix A. Both quantitative methods (e.g. measurement of equivalent widths) and qualitative means (i.e. visual comparison) were employed. A standard relation between spectral type and effective temperature (Bessel 1991) was used to translate spectral type to T_{eff}.

4.1.1 Effective Temperature

A preliminary classification of each of the L1641 spectra was made simply on the basis of visual comparison with spectroscopic standard stars. A quantitative classification was made according to a) line equivalent widths (for spectral types B-G), or b) narrow-band molecular band indices (for spectral types K and M). An

example of a quantitative classification index is that used for spectral types M0 and later; a plot of two narrow band molecular indices containing TiO absorption features at λ7140Å and λ7800Å. The ratios are defined as:

$$\mathrm{TiO}(7140\text{Å}) = \frac{\mathrm{C}_1\,(\lambda\lambda 7020 - 7050\text{Å})}{\mathrm{T}_1\,(\lambda\lambda 7125 - 7155\text{Å})}$$

and

$$\mathrm{TiO}(7800\text{Å}) = \frac{\mathrm{C}_2\,(\lambda\lambda 7485 - 7515\text{Å})}{\mathrm{T}_2\,(\lambda\lambda 7785 - 7815\text{Å})}$$

where C_1 and C_2 denote continuum fluxes, and T_1 and T_2 are the fluxes in the TiO absorption features (Figure 4.1).

Figure 4.2 shows the dependence of spectral type on the TiO flux ratios, for dwarf stars. The stars plotted in Figure 4.2 were taken from our standards survey in Praesepe and from the survey of Kirkpatrick *et al.* (1991).

Estimated uncertainties in the spectral classification are: for spectral types K2 and later, approximately 1 subclass; for earlier types, 2-3 subclasses. The resulting uncertainty in log T_{eff} is $+.03/-.04$ for spectral types M1-M4.

4.1.2 Luminosity Class

At a distance of ~480 pc, a typical surveyed area (~20′ in diameter) subtends a significant volume in space. Thus, we can expect at least some contamination by foreground dwarfs (10-20 for a typical field in our survey). If mistaken for cloud members, the luminosities of foreground main sequence stars will be overestimated, and their computed location in the H-R diagram (above the main sequence) will be indistinguishable from that of true pre-main sequence stars.

Contamination by background stars is also a concern; visual extinction maps constructed from CO maps yield extinction estimates of 1-20 A_v across the surveyed regions. While this is likely a *lower limit* to the actual extinction, and while the molecular ISM is undoubtedly clumpy on a size scale unresolved by the

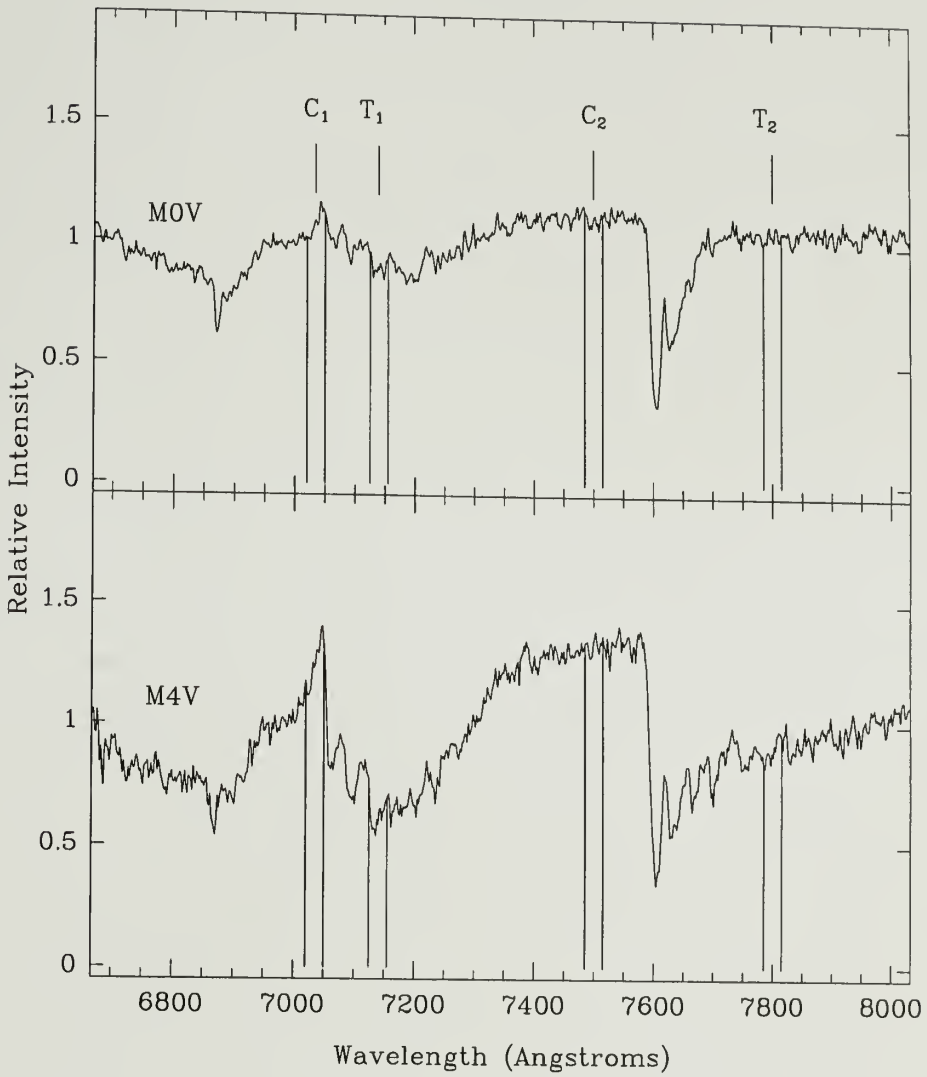

Figure 4.1. The bands used to compute TiO indices at λ7140Å and λ7800Å, shown superposed on an M0 and an M4 spectrum. The light shaded regions represent the continuum bands, and the dark shaded regions indicate the bands containing the TiO features.

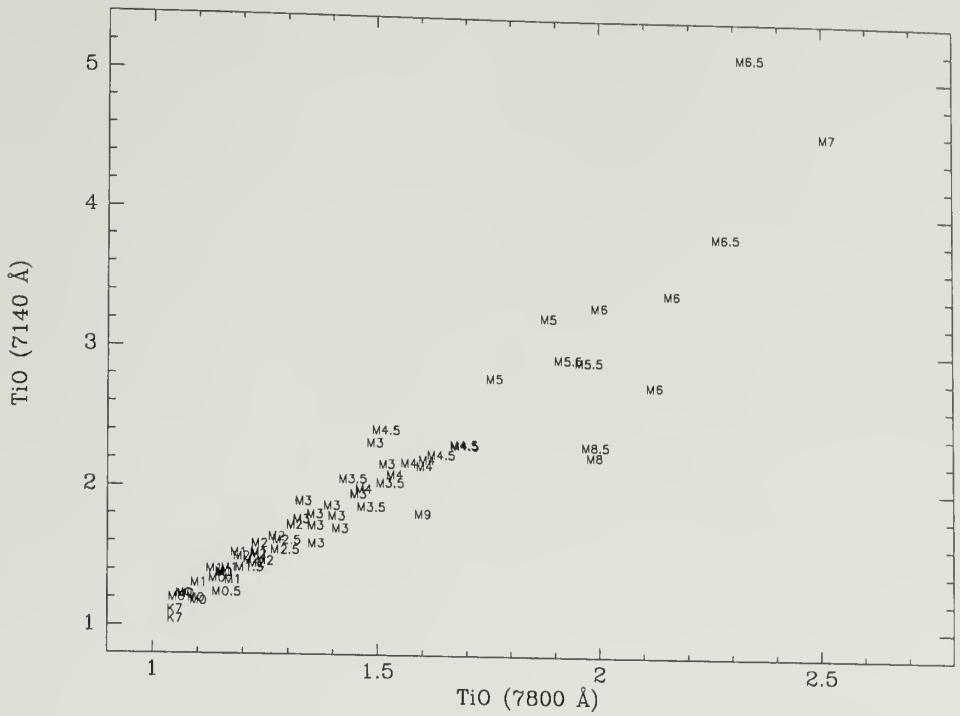

Figure 4.2. Plot showing the dependence of spectral type, for dwarf stars, on the flux ratios containing TiO absorption features at λ7140Å and λ7800Å.

FCRAO 45″ beam, the beam-averaged A_v serves as an approximation, and suggests the absence of an extremely high (A_v=50) uniform extinction screen across the field.

Fortunately, the R–band spectra offer some clues as to the luminosity class of the star, since this spectral region contains at least one feature which is sensitive to surface gravity. Pre-main sequence stars, because they are still contracting, have surface gravities intermediate to those of dwarfs (high) and giants (low). The metal hydrides provide an important indicator of a star's luminosity class, because unlike atomic neutral lines, hydride lines grow stronger (deeper) with increasing surface gravity, hence the hydrides are stronger for dwarfs than for giants. As long as six decades ago, it was recognized that at least two of the light metal hydrides

(MgH and CaH) were strongly present as absorption bands in M dwarfs, but absent in M giants (Öhman 1936). Thus we define a CaH spectral index (Figure 4.3), which is proportional to the depth of the absorption feature, as

$$\mathrm{CaH}(6975\text{Å}) = \frac{\mathrm{C_1}\,(\lambda\lambda 7020 - 7050\text{Å})}{\mathrm{CaH}\,(\lambda\lambda 6960 - 6990\text{Å})}$$

A plot of the CaH index against the TiO index defined above shows the potential of the CaH/TiO ratio to provide a luminosity discriminant for late-type stars (Mould & Wallis 1977). Dwarfs and giants of spectral type M0 and later are shown in Figure 4.4. How well can we distinguish stars with PMS gravities from foreground dwarfs and background giants? In part, the answer to this question depends on stellar age. The youngest ($\sim 10^5$ yr) optically visible stars have typical surface gravities of $\log g = \sim 3.5$, and increase to $\log g = \sim 4.5$ by the age of 10^7 yr. By comparison, the surface gravity of a typical M giant star is 1.0, while that of a typical M dwarf is 4.5. In Figure 4.4, we plot the location of a sample of PMS stars in the CaH/TiO plane. Clearly, there is no difficulty in distinguishing PMS stars from background giants, for all stars later than K7. However, our ability to distinguish PMS stars from foreground dwarfs depends on age; the older the pre-main sequence star, the more similar its gravity to that of a star on the zero-age main sequence.

To quantify this dependence, we plot in Figure 4.5 the distance of a star from the CaH dwarf locus (δ[CaH]) against the distance of the star above the main sequence ($\delta[\log L_*]$), where

$$\delta\mathrm{CaH}(6975\text{Å}) = \mathrm{CaH(dwarf\ locus)} - \mathrm{CaH(measured)}$$

and

$$\delta(\log L_*) = L_*(\mathrm{measured}) - L_*(\mathrm{main\ sequence})$$

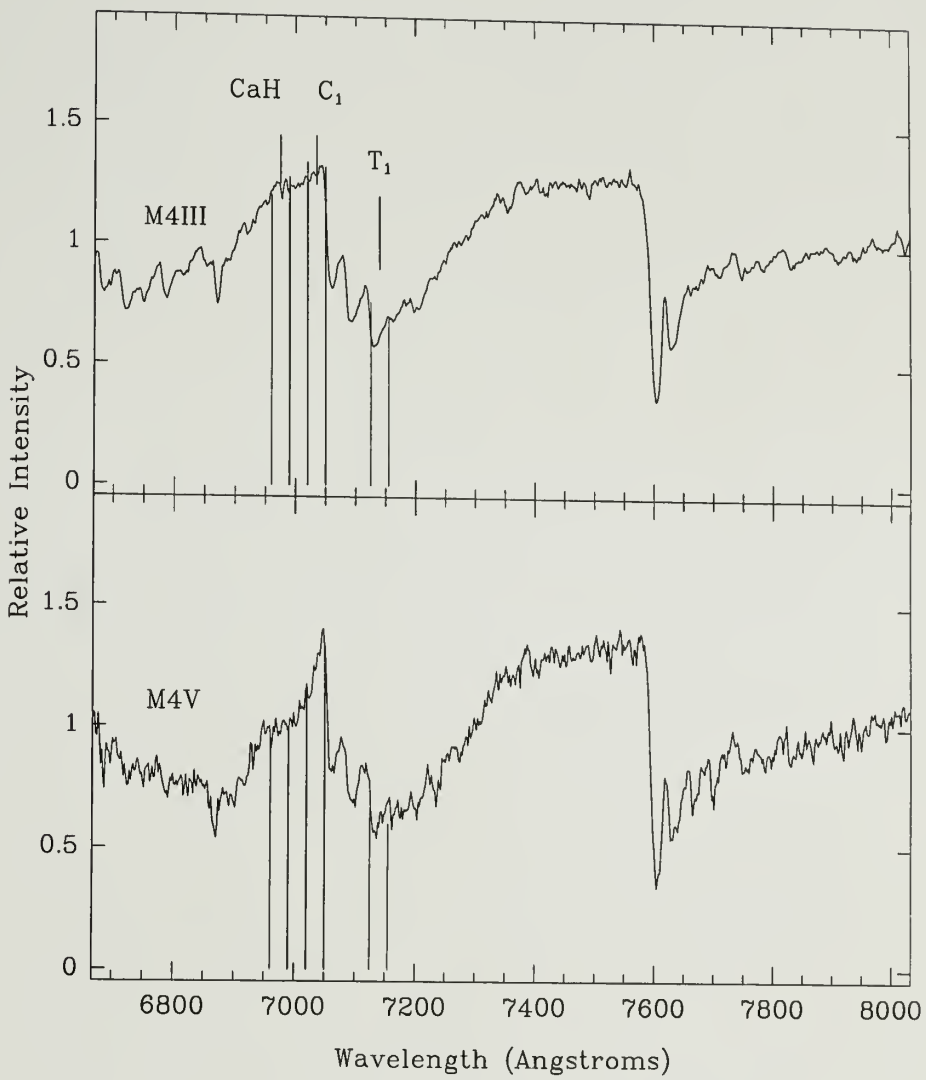

Figure 4.3. The bands used to compute the CaH index at λ6975Å shown for two M stars. The light shaded region represents the continuum band, and the dark shaded region indicates the band containing the CaH feature.

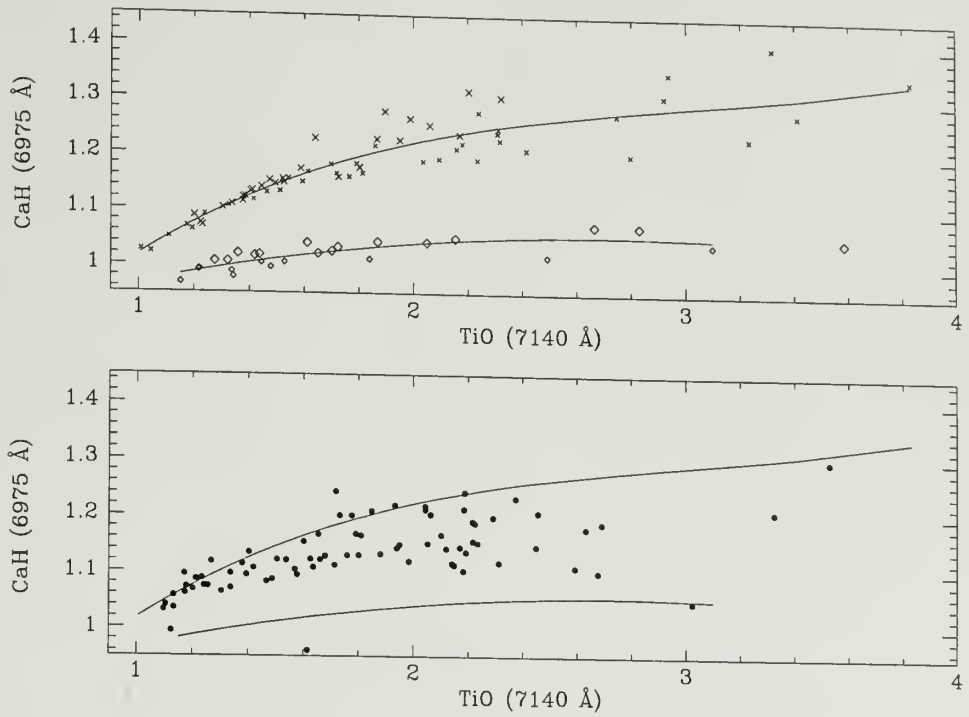

Figure 4.4. Luminosity discriminant for late-type dwarfs, giants, and pre-main sequence stars. *Upper:* The dependence of stellar luminosity on the flux ratios containing CaH and TiO absorption bands at λ6975Å and λ7140Å. The dwarfs (x's) have higher surface gravities than the giants ($\diamond$'s), as reflected in the strength of the CaH band. Large symbols are our data, small symbols are from Kirkpatrick *et al.* 1991. Solid lines represent the best fits to the dwarf and giant loci. *Lower:* The fits to the dwarf and giant loci from the top panel, plotted with the indices computed for M stars in L1641N.

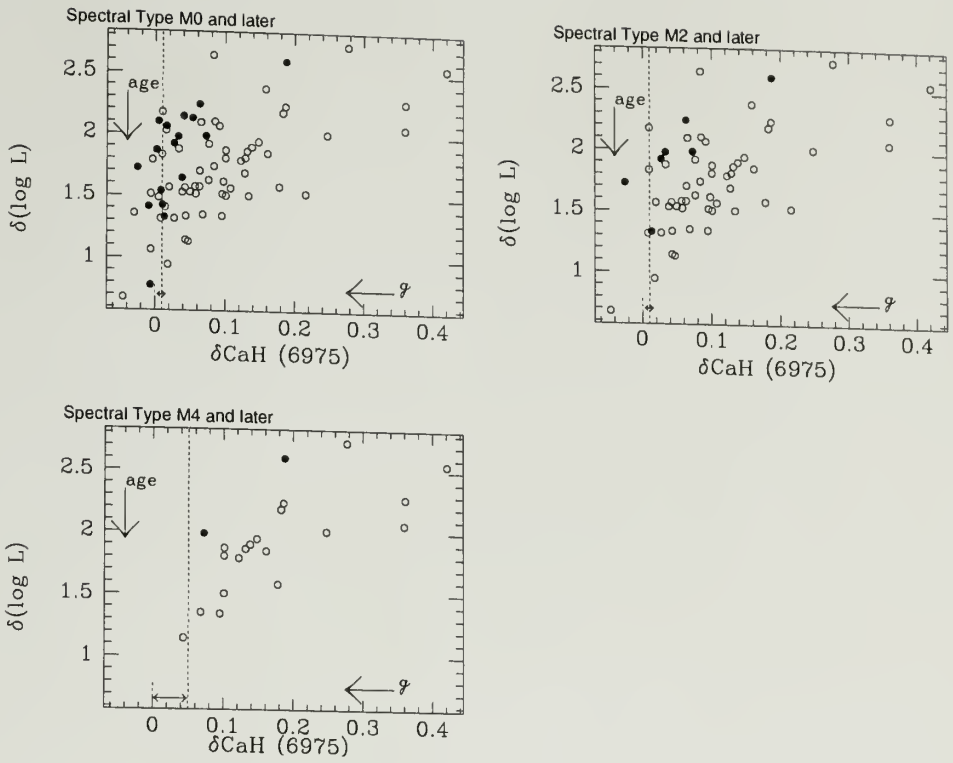

Figure 4.5. The dependence of the luminosity discriminant on age. δ(log L) vs. δCaH(6975Å) for stars in L1641N. The filled symbols represent stars with infrared excess in the (H-K), (R-I) plane. Young stars with low (giant-like) surface gravities would be in the upper right of the diagram, main sequence stars in the lower left. The dwarf locus in the previous fig is at δCaH(6975Å)=0. The dashed line indicates the maximum deviation from the mean locus defined by the dwarf standards.

Note that δ(CaH) and $\delta(\log L_*)$ are inversely proportional to surface gravity and age, respectively. Figure 4.5 shows δ(CaH) vs. $\delta(\log L_*)$ for various ranges in spectral type. Assuming that all stars with infrared excess are pre-main sequence stars rather than foreground dwarfs (see Chapter 6 for details on determining IR excess), we see that for the latest type stars, the distinction between cloud members and foreground dwarfs is apparent to $\delta(\log L) = 1.2$, which corresponds to an age (for M4 and later type stars) of $\sim 3 \times 10^6$ yr. For earlier spectral types, the segregation of dwarf and pre-main sequence stars is not clear at any age. Thus, unambiguous identification of early M-type foreground stars based solely on the

CaH index is not effective. However, the index can be used to identify *candidate* foreground stars, and combined with extinction measurements and a Galactic model, statistical corrections for foreground populations can be made.

Using the CaH/TiO indices, we identified 1 to 2 giant stars in each of the surveyed fields, and as many as 15 candidate foreground dwarfs. Each of the dwarf candidates was further considered, and those having $A_v < 1$ and no infrared excess were taken to be foreground stars. In this way, 8 to 10 stars in each field were designated "foreground".

4.1.3 Effects of Extinction

Some of the pre-main sequence stars, being more deeply embedded in the molecular cloud, will have higher extinctions than others. How will the reddening of the spectra affect our spectral classification? In principle, because the spectra are normalized to the continuum before the classification indices are calculated, smooth changes in the shape of the spectrum should not affect classification. In practice, experience shows that the normalization of M stars can vary, even when care is taken to keep the continuum fit uniform from spectrum to spectrum.

Thus we consider the effects of interstellar extinction on our classification indices, by taking an unreddened spectrum of an M star (from the Praesepe standards sample) and reddening it by 5 A_v (using the extinction law of Rieke and Lebofsky 1985). The initial and reddened spectra are shown in Figure 4.6. Shown also is the difference after normalizing both spectra and subtracting the initial spectrum from the reddened spectrum. The residual over the relevant wavelength range (6900$\AA$-7900$\AA$) is small $\pm 5\%$, and will not affect the spectral classification.

4.1.4 Effects of Veiling

Similarly, we have investigated the effects of nonstellar optical excess continuum emission (the main contribution to veiling) on our classification indices.

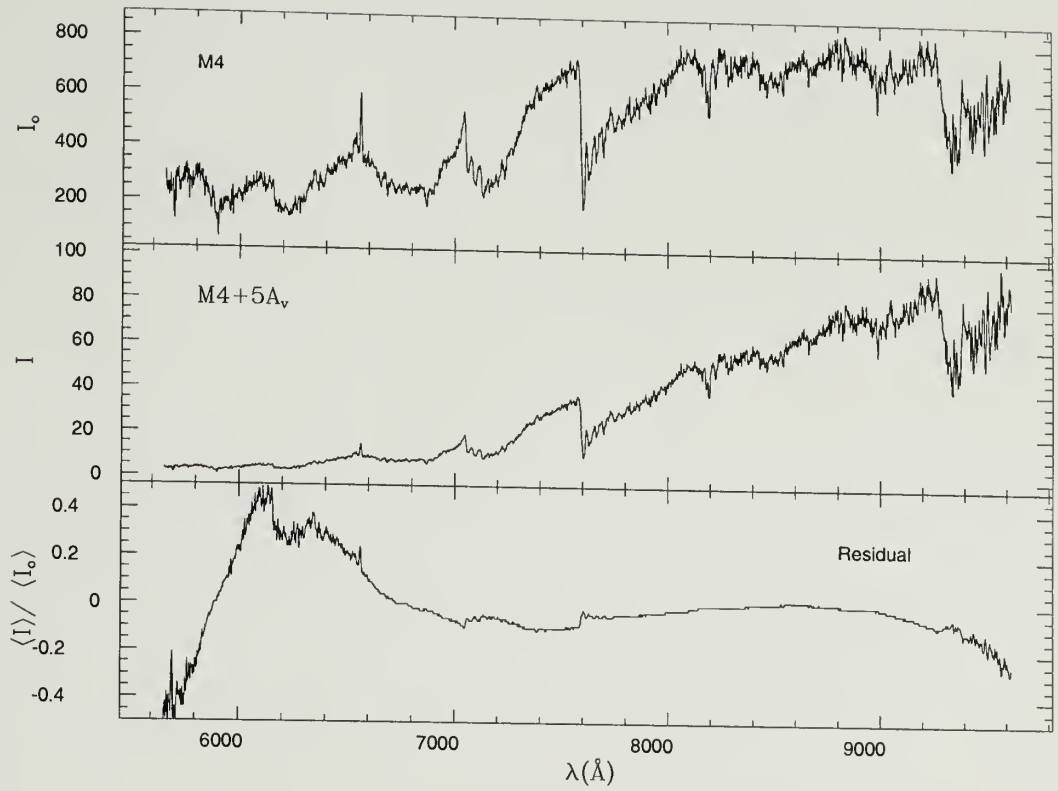

Figure 4.6. The effects of extinction on spectral classification. *Upper:* An unreddened M4 dwarf from Praesepe. *Center:* The same spectrum, but reddened by 5 A_v. *Lower:* The difference between the normalized reddened spectrum and the normalized initial spectrum.

This excess emission from cTTs is attributed to accretion processes, which either liberate energy in the disk itself (producing an infrared excess), or in hot spots (T~10,000 K) on the surface of the star where disk matter accretes onto the star (producing excess optical continuum radiation which "veils" photospheric absorption spectra). Our simple test for the effects of veiling consist of comparing the contribution of veiling to the measured brightness at 7140 $\AA$ and 7800 $\AA$, the wavelengths at which our TiO classification indices are found. We model the veiling as a 10,000 K blackbody, and calculate its effect on stars of various T_{eff}, and for various values of the veiling parameter r, where $r_\lambda = F_\lambda(\text{excess})/F_\lambda(\text{stellar continuum})$, after Hartigan *et al.* (1992). A typical value of the veiling paramater at $\lambda = 5700\,\AA$ is 0.5 (Hartigan *et al.* 1991). We show results for an extreme case, $r_{5700} = 1$, for a star with $T_{eff} = 3500$ K (M2) in Figure 4.7.

First, we note that the veiling at 7140 $\AA$ is less than half that at 5700 $\AA$. For the extreme case of $r_{5700} = 1$, the veiling at 7140 $\AA$ is therefore less than 0.5, which means that less than 25% of the photons measured originate in the accretion-related "hot spot", rather than the stellar photosphere. The actual change in the spectral index can be calculated from the relation between equivalent width and r_λ,

$$(EW)_v = \frac{(EW)_o}{1 + r_\lambda}$$

so that the change in the TiO(7140 $\AA$) index is $\Delta(EW) = (EW)_o/1.4 = 0.7(EW)_o$, and at 7800 $\AA$, $\Delta(EW) = (EW)_o/1.3 = 0.8(EW)_o$. The effect of $r_{5700} = 1$ is therefore to move a star down and to the left in Figure 4.2, by 0.3 and 0.2 units, respectively, which is enough to change the spectral class from M2 to M1. Since most cTTs are likely to be less veiled than the example shown here, the net effect will be to spread the relation given by Figure 4.2 by a few tenths in the vertical dimension, and less so horizontally. Thus, spectra which fall below the standard

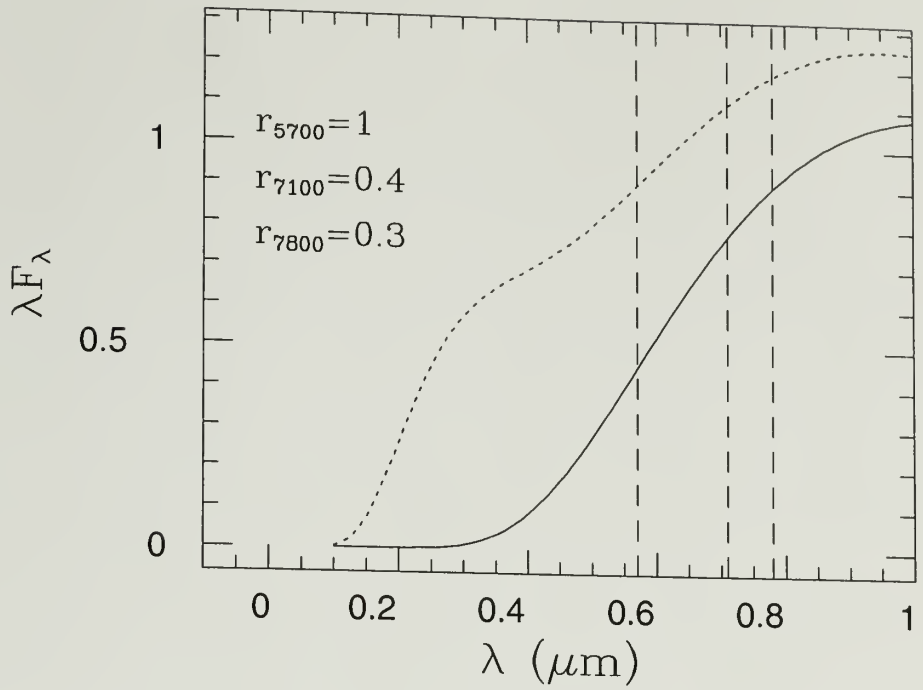

Figure 4.7. The effects of veiling on spectral classification. The intensity of a 10,000 K blackbody (dotted line), and a 3500 K blackbody (solid line) for $r_{5700} = 1$. Dashed vertical lines mark $\lambda = 5700\,\AA$, $\lambda = 7140\,\AA$ and $\lambda = 7800\,\AA$.

relation in Figure 4.2 are re-examined visually, and classification is based on pattern recognition, which depends not only on band strength but also on the shapes of temperature sensitive bands and blends.

4.2 Stellar Luminosity

Stellar luminosity is calculated by dereddening a monochromatic flux, correcting for the distance, and applying a bolometric correction. We use J band fluxes, m-M=8.4 (d=480 pc), and the (T_{eff}, BC_J) relation compiled by Hartigan, Strom, & Strom (1994; hereafter HSS). J band fluxes are dereddened using measured R and I fluxes and the intrinsic $(R-I)$ color for the determined spectral type, according to the extinction relation from Cohen *et al.* (1981): $A_J = 1.66 \times E(R-I)$.

Our selection of J as the wavelength for computing L_* is based on the examination of spectral energy distributions (0.5 to 60 μm) for a large sample of solar-type pre-main sequence stars surrounded by circumstellar accretion disks and spanning a wide range of accretion rates (Hartigan *et al.* 1992; Hartmann & Kenyon 1990). The region between 0.9 and 1.2μm is least affected by accretion-related excess emission (driven by energy liberated in the disk itself or in a boundary layer), and thus provides the most reliable measure of the true photospheric luminosity.

The uncertainty in L_* is dominated by the possible presence of unresolved binary companions, which could result in an overestimation of the luminosity by as much as a factor of 2 (0.3 dex). Other sources of error in L_* are:

1) Excess emission (veiling) at J due to disk accretion. Hartigan et al. (1992) adopt a color temperature of 10^4 K for the excess emission and show that for an M0 star, the ratio of excess flux to stellar flux at 1.25μm is $r_J = 0.08 r_V$. Based on their sample of $\sim$25 T-Tauri stars, the average r_V is $\approx$1, so $\sigma(r_J) \sim 0.08$ mag.

2) Photometry. Photometric errors are $\sigma \leq 0.10$ mag.

3) Bolometric corrections (BC_J). HSS have compiled bolometric corrections at the $J-$band magnitude from a variety of sources, and estimate the uncertainty in the BC to be $\sim$0.04 mag.

4) Extinction. Comparison of the different extinction laws derived in the literature suggests that the uncertainty in A_V is about 30%. Thus, $\sigma(A_J) \sim 0.08$ mag.

5) Distance. The distance to the Orion GMC complex is uncertain by about 10%, but since all of our sample lies at approximately the same distance, the effect is less relevant to our results.

6) Variability. We do not have the data to estimate source variability, but HSS observed a mean value of ΔH=0.12 mag for their sample of 39 pre-main sequence binary pairs. Assuming that the $J-$band magnitude varies by about the same amount, we adopt this value.

Noting that an error in magnitude transforms to an error in luminosity according to $\sigma(\log L_*)=0.4\times\sigma(\mathrm{mag})$, and adding all the errors in quadrature, we calculate $\sigma(\log L_*) = \pm 0.3$ for a star of type M0. For a representative 1 Myr old M0 star, this translates to an error in log (Age) of $\sim$0.8.

4.3 H-R Diagrams for Individual Regions

Following the procedures described above, we constructed H-R diagrams for each of the 4 regions in our L1641 survey. The diagrams are presented here, along with brief, descriptive comments. Analysis of the H-R diagrams is contained in the next chapter(s). The photometric and spectroscopic data are presented in Appendix B.

4.3.1 L1641 North

Figure 4.8 shows the H-R diagram for the $\sim$100 stars within field 1 (Figure 2.1), for which we have obtained optical and infrared photometry as well as classification spectra. An additional 13 stars from the $K-$band spectroscopic study by Hodapp and Deane (1993; hereafter HD) are also plotted in Figure 4.8. These stars were classified on the basis of their K-band spectra, and were placed on the H-R diagram using the K-band spectral types given by HD and the RIJHK photometry of our surveys.

A comparison of spectral types based on the Hodapp and Deane K-band spectra with those based on our R-band spectra for the 8 sources included in both

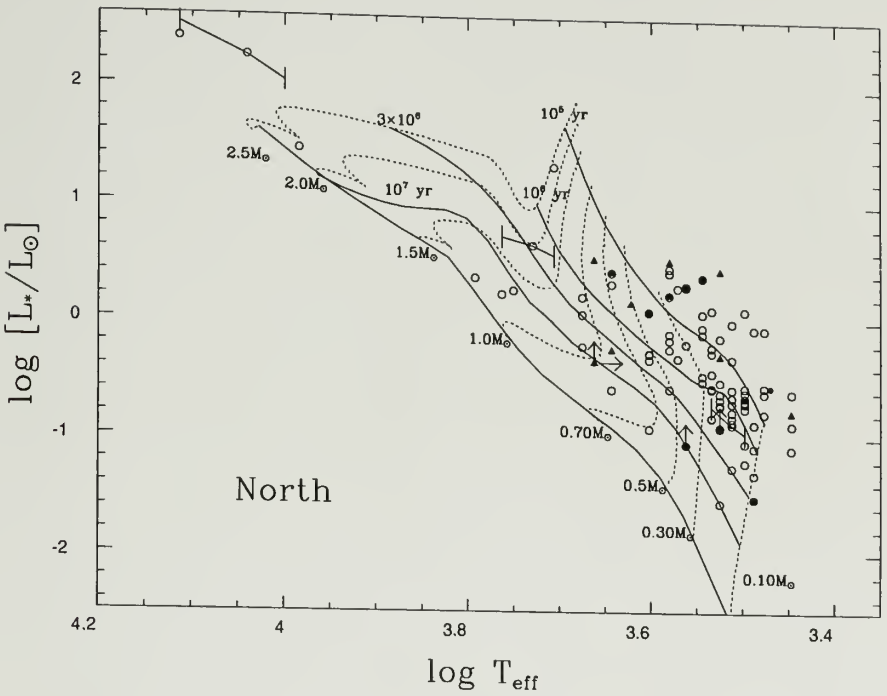

Figure 4.8. H-R diagram for the L1641 North region, showing aggregate and distributed populations. Also plotted are the model evolutionary tracks from D'Antona and Mazzitelli (1994). Filled symbols are "aggregate members", stars within a 1/3 pc radius of the defined aggregate center. Triangles are from the 2μm spectral survey of Hodapp and Deane (1993). Representative errorbars are shown for stars of spectral type B8, G8, and M3.5.

studies indicates that the classifications in the two bands are consistent (within one subclass), with the exception of two sources, for which our optical spectral types are significantly later (5-7 subclasses) than those assigned by HD. In one of the two cases (N128 = HD#6), the S/N of the K-band spectrum is reportedly low, and in the other case (N265 = HD#23), the S/N of the R-band spectrum is low ($\sim$3).

The stars range from less than 10^5 yr to more than 10^7 yr old, and span the mass range of 0.1 to 3.5 $M_\odot$.

4.3.2 Cohen-Kuhi Group

In Figure 4.9, 47 stars in the Cohen-Kuhi Group region (field 4, Figure 2.1) are plotted. This group has a very large spread in age.

4.3.3 L1641 South

This cluster is in field 3 in Figure 2.1. 72 stars are plotted on the H-R diagram. It appears that this group has the largest proportion of older stars (t> 1 Myr).

4.3.4 V380 Ori

Figure 4.11 shows the H-R diagram for 50 stars in field 2 (Figure 2.1). These stars appear to be somewhat older, on average, than those in the North. Although this region was originally treated as an aggregate by SSM, it does not fit the definition in Chapter 3. Therefore, it is treated here as a representative cloud region.

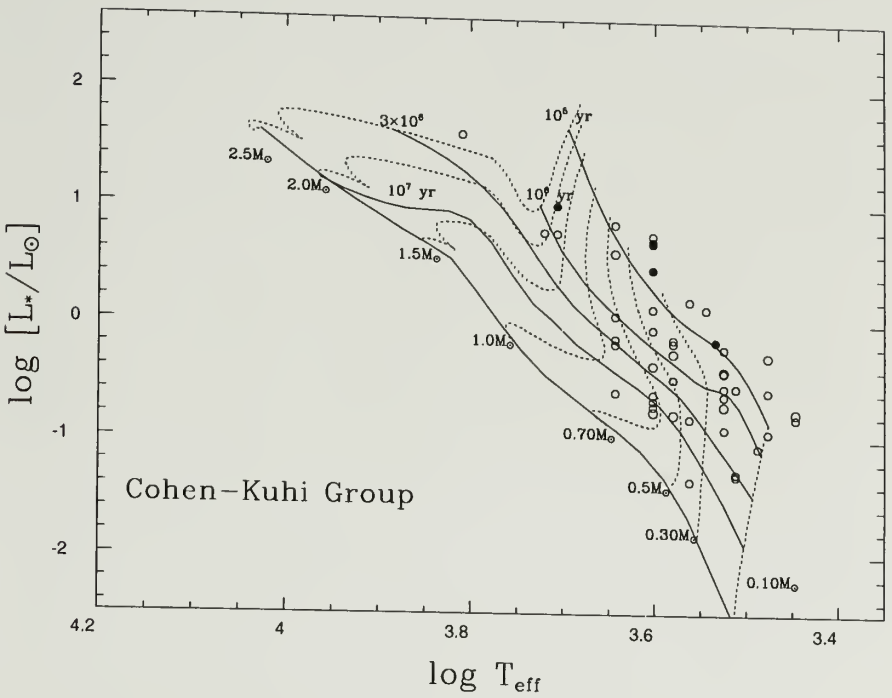

Figure 4.9. H-R diagram for the Cohen-Kuhi Group region, showing aggregate and distributed populations. Filled symbols are "aggregate members", stars within a 1/3 pc radius of the defined aggregate center.

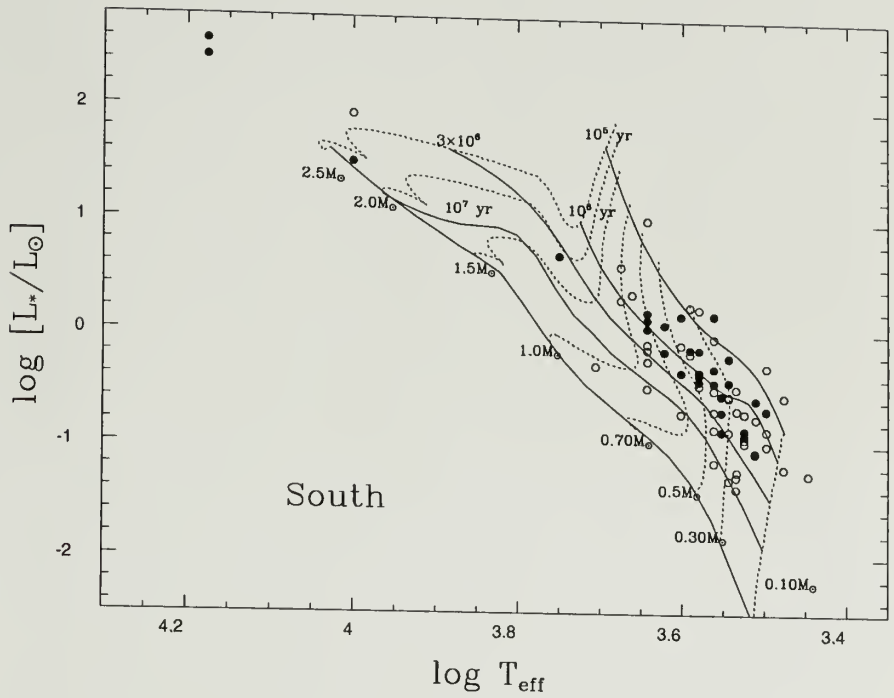

Figure 4.10. H-R diagram for the L1641 South region, showing aggregate and distributed populations. Filled symbols are "aggregate members", stars within a 1/3 pc radius of the defined aggregate center.

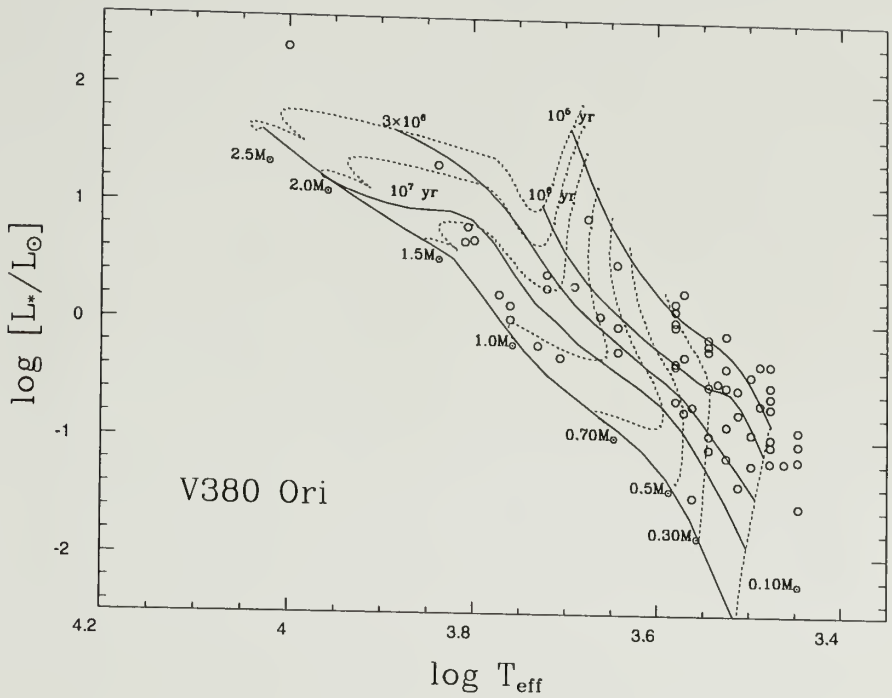

Figure 4.11. H-R diagram for the V380 Ori region.

Chapter 5

Interpretation and Analysis of H-R Diagrams

In this chapter, we determine the spatial and temporal nature of star formation and the mass functions of recently formed stars in the L1641 GMC. Our goals are to determine 1) if there are differences in the ages and masses of stars inside and outside the defined aggregate boundaries, 2) what fraction of all recent star formation has taken place in the aggregates, and 3) whether the observed mass spectra in L1641 are consistent with the solar neighborhood IMF. Our strategy is to examine the distributions in age (N[t]) and mass (N[m]) of stars in and among the aggregates and the surrounding distributed population. We compare the observed N(t) with a simple model for star formation as a function of time, and N(m) with standard IMFs.

5.1 Completeness of the Spectroscopic Samples

Our spectroscopic survey is not complete. More importantly, because brighter stars were targeted first the incompleteness is a function of age and mass. Age dependence of the sample completeness results from the fact that pre-main sequence stars become fainter as they evolve toward the main sequence, and mass dependence because for a give age, low-mass stars are fainter than high-mass stars. In addition, low-mass stars far outnumber high-mass stars in the region. As seen in Figure 2.2, the fraction of stars for which classifiable spectra were obtained is high among the bright stars ($I \leq 15$) in the photometric survey, however the completeness of the spectroscopic sample decreases with increasing magnitude, and thus with increasing stellar age and decreasing stellar mass.

We can evaluate the completeness of the spectroscopic sample using an $I, (R-I)$ color-magnitude diagram and the reddening-corrected colors of the stars. In Figures 5.1– 5.3 the evolutionary tracks from Figure 4.8 have been transformed to the I_o, $(R-I)_o$ plane. Dereddened values of I, $(R-I)$ are plotted for the photometric (open circles) and spectroscopic (filled) samples. Sources have been dereddened according to $A_v = 6.25 \times (R-I)_c$, where for each source A_v was estimated according to the star's location in the $(J-H)$, $(H-K)$ plane. Developed and coded by M. Meyer (1996), this dereddening procedure works in the following way: stars which fall within the reddened main sequence zone in the $(J-H)$, $(H-K)$ diagram are dereddened along the reddening vector in the J, $(J-H)$ plane until they intersect with a mean isochrone, corresponding to the mean position of the pre-main sequence isochrones from 0.1-3.0 Myr. Dereddening to this mean isochrone instead of any individual isochrone results in an uncertainty in the estimated A_v of no more than 1.25 mag (Meyer 1996), which translates to 0.75 mag at I, or a Δt of a few million years. Stars which fall outside the reddening vectors in the $(J-H)$, $(H-K)$ plane, but within the zone typically occupied by classical T-Tauri stars, are dereddened to the cTT locus (defined by dereddened cTT stars of known spectral type). Stars which fall redward of the cTT zone are not dereddened.

The fraction of stars in the photometry survey observed spectroscopically is listed by region in Table 5.1, as a function of age. In the North and South regions, the spectroscopic samples represent 66% and 70%, respectively, of the photometric samples, for stars of type K5 and later and age 1 Myr and less. The completeness fraction in the CK group is less; only 55% of stars with $t \leq 1$ Myr have spectra. The spectroscopic completeness should be the same inside and outside the aggregates, as there was no bias toward either aggregate or distributed populations in the observing procedure. Thus, the comparison of aggregate with distributed

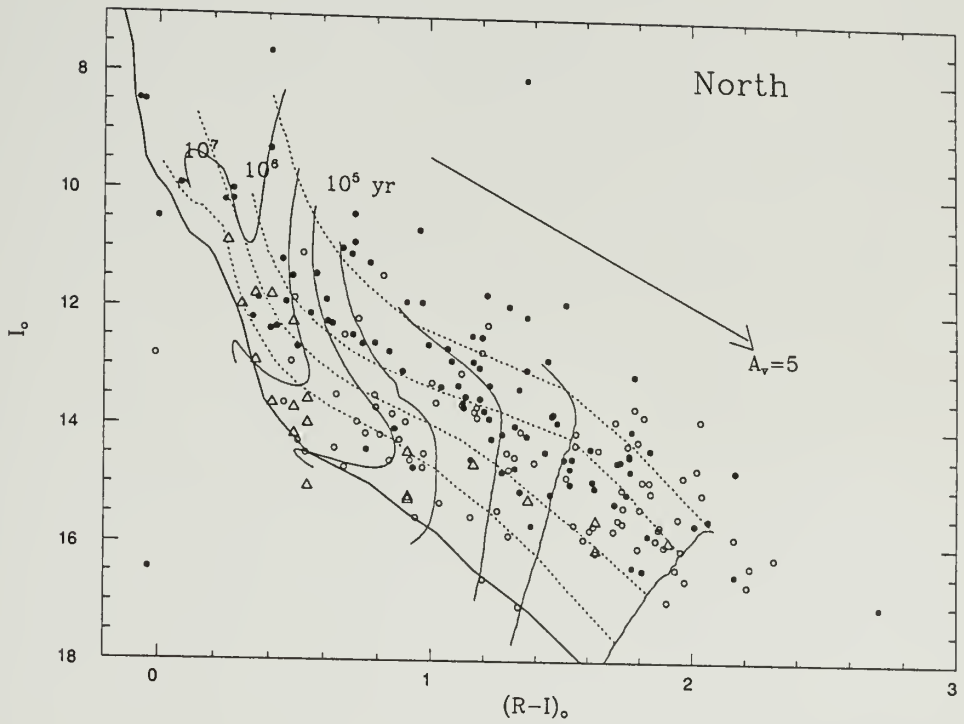

Figure 5.1. Optical color-magnitude diagram for L1641 North. Shown are the dereddened I magnitude and $(R - I)$ color for the photometric (open circles) and spectroscopic (filled circles) samples. Triangles represent predicted foreground dwarfs. Dotted lines are 10^5, 10^6, 3×10^6, and 10^7 yr isochrones (top to bottom) from DM, solid vertical lines are mass tracks for 2, 1, .7, .5, .3, .2, and .1 $M_\odot$ stars (left to right)

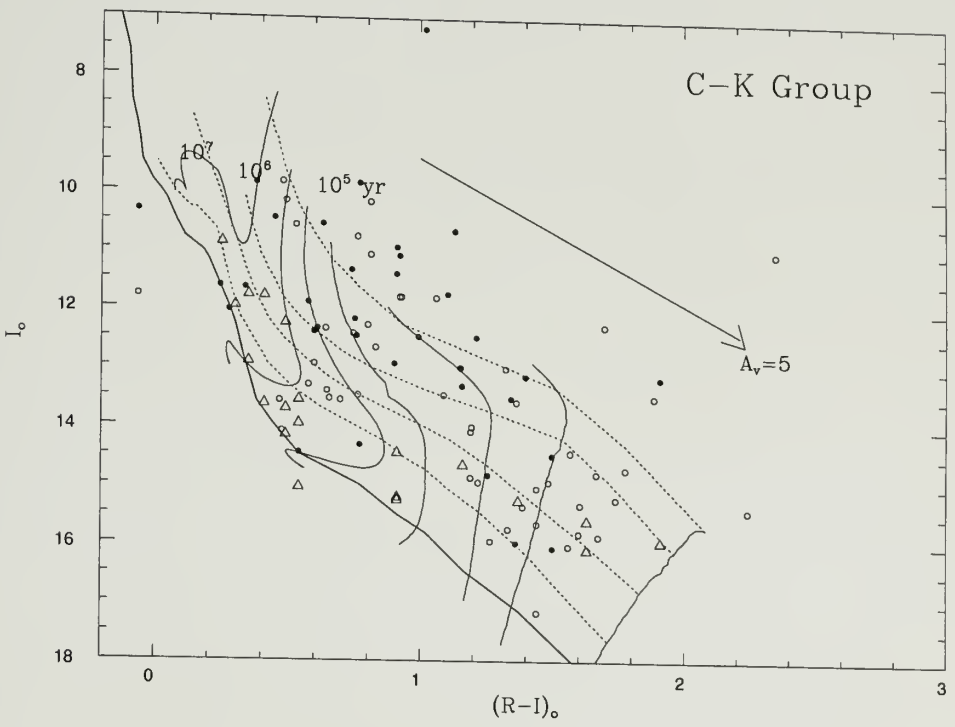

Figure 5.2. Optical color-magnitude diagram for the Cohen-Kuhi Group. Symbols and curves same as in previous figure.

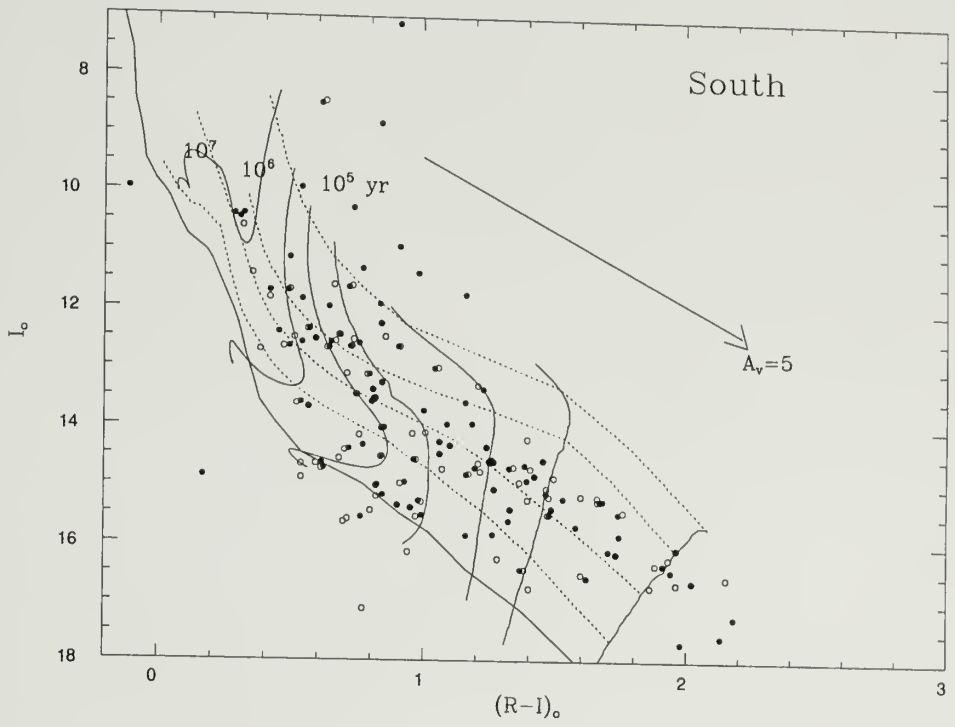

Figure 5.3. Optical color-magnitude diagram for L1641 South. Symbols and curves same as in previous figure.

Table 5.1. Completeness Fractions of Spectroscopic Sample

Region	t<1Myr	1Myr<t<3Myr	3Myr<t<10Myr
North	58/88 (54/82)	26/55 (23/52)	2/22 (5/14)
	67% (66%)	47% (44%)	54% (36%)
South	22/33 (20/30)	42/62 (38/54)	18/27 (16/24)
	67% (70%)	68% (70%)	67% (67%)
Cohen-Kuhi	23/43 (21/38)	2/13 (2/13)	4/15 (3/14)
	53% (55%)	15% (15%)	27% (21%)

Numbers in parentheses are for spectral types K5 and later only

stars should be unaffected by sample completeness fractions.

Of the three regions summarized in Table 5.1, the South spectroscopic survey covers a larger fraction of the photometric survey among older stars. (The South survey extended to fainter magnitudes because there are fewer stars there, so the spectra we obtained reached a deeper magnitude limit, and slightly more spectra were obtained.) Given these incompleteness factors, we proceed in the following sections to compare the age distributions for both the aggregate members and the distributed population. We first note that, although the completeness of the spectroscopic sample depends on age and mass, it does not depend on location; hence, the incompleteness at a given age is the same for both the aggregate and distributed populations, and a direct comparison of their observed age distributions can be made.

5.2 Aggregate vs. Distributed

As we saw in the previous chapter, aggregate boundaries were chosen to enclose regions of apparently recent star formation, containing embedded IR sources and molecular outflows, and (with the exception of V380) they correspond

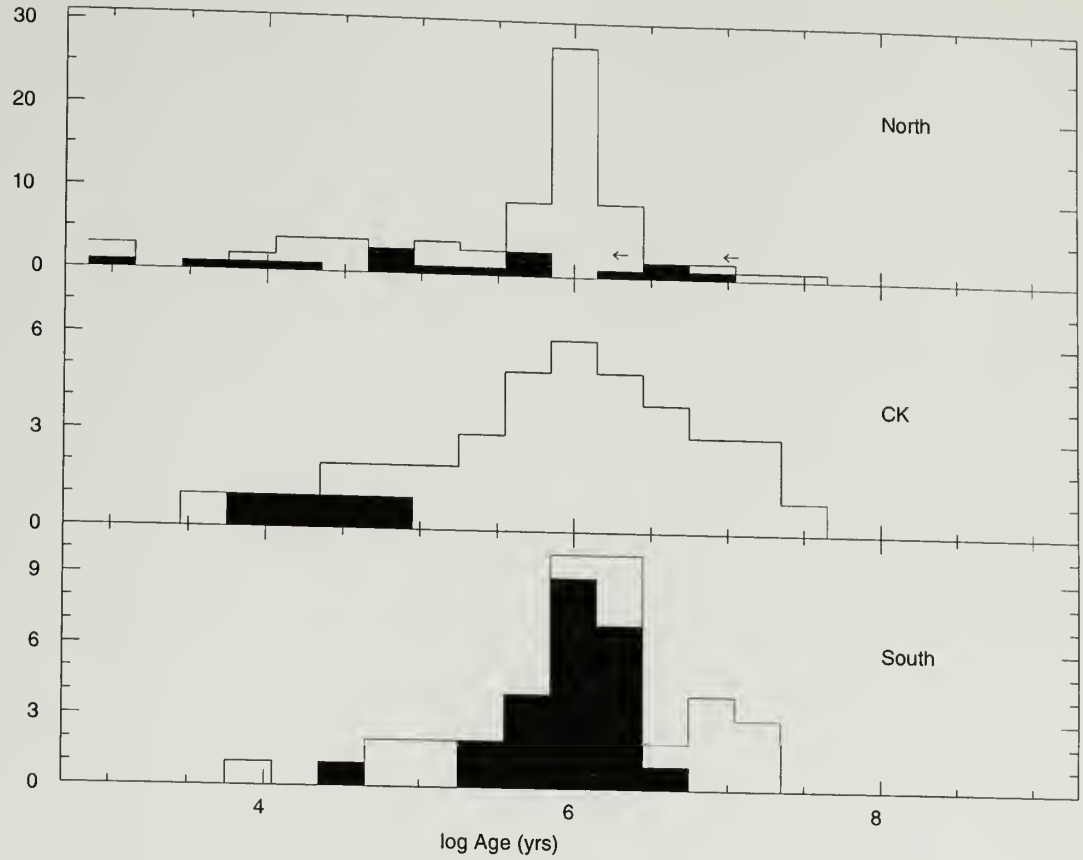

Figure 5.4. Distributions in log Age for the spectroscopic sample. Aggregate members are plotted in solid. Only stars with spectral type K5 and later are included.

to regions of enhanced stellar surface density. How do their properties compare with those of the distributed population?

Age distributions for the two populations in each of the three regions are shown in Figure 5.4. Because the ages of intermediate and high-mass stars are highly uncertain, we have excluded stars of spectral type earlier than K5 from Figure 5.4. For stars of earlier spectral type than about K5, the "stellar birthline" (a unique mass-radius relationship which depends on the initial stellar accretion rate;

Stahler 1983; Palla and Stahler 1993) crosses theoretical isochrones, making high mass stars appear older relative to low mass stars of the same age. However, for later spectral types ($M < 0.5\,M_{\odot}$), the theoretical birthline runs parallel to the conventional isochrones. Observational support for this is provided by the Trapezium cluster, where star-formation is believed to have been triggered (and therefore coeval). For stars of spectral type K5 and later, the "empirical" birthline, defined by the upper envelope of stars in the H-R diagram, runs parallel to the 10^5 yr isochrone (Hillenbrand 1995). Thus, we restrict our analysis to stars of type K5 and later.

We see from Figure 5.4 that the aggregates (solid histograms) contain a higher fraction of younger stars, relative to the distributed populations (open histograms). Statistically, we can test the hypothesis that the distributed and aggregate stars are drawn from the same distribution; in the North and the Cohen-Kuhi region that hypothesis is ruled out at the 99% probability level, in the South at the 90% level. We have not attempted to correct the aggregate samples for "contamination" by the distributed population. Such a correction would make the aggregates even younger, proportionally, than the distributed population.

If the aggregates are dispersing on a timescale of 1-2 Myr (as expected, given typical velocity dispersions of $\sim$1 km/s), it is not surprising to find that they are younger than the distributed population. It is conceivable that the distributed population originated in aggregates and over the time of a few to 10 Myr has spread through the cloud. Alternatively, the distributed stars may have formed in isolation. We can assess the fraction of stars formed in aggregates and in isolation by comparing the number of young stars in each spatial group.

In the North, 30% of the young stars ($t \leq 1$ Myr) are found within the defined aggregate. Similarly, 25% of the young stars in the Cohen-Kuhi Group region are found within the aggregate. In the South, the concentration of young stars is

higher: 50% lie within the aggregate. Each of the aggregates comprises only 6% of the surveyed area in its region; thus, surface densities of young stars are 3-30 times higher in the aggregates than in the distributed population.

The aggregates are responsible for 25–50% of the recent star formation. What about the other 50–75% of the young stars? Approximately half of the very youngest stars ($t \sim 10^5$ yr) are located more than a parsec from the center of any defined aggregate. Given that a typical dispersion velocity of 1 $km\,s^{-1}$ would carry a star approximately 1 pc from its birthplace in 10^6 yr, it is unlikely that these stars are associated with the defined aggregates, unless their ages, given by the evolutionary tracks, are in error by a factor of ten. Nor are they associated with other visible, yet unconsidered aggregates, since there there is no apparent clustering outside the aggregates (at the K=14.5 mag limit).

These young stars could be associated with *invisible* aggregates or clusters, groups of stars still deeply embedded in the molecular cloud and detectable only at longer wavelengths. To test this hypothesis, we compared the spatial distribution of the youngest stars with that of the deeply embedded (no optical or near-IR counterparts) IRAS sources (Strom *et al.* 1989), in Figure 5.5. Outside the aggregates, only 1 of the 6 IRAS sources is spatially associated with a young star. We conclude that these stars are truly isolated from other star-formation activity and, unless they have unusually high velocities, must have formed in isolation.

5.3 The Star Formation History of L1641

We can investigate star formation over time, using the completeness fractions listed in Table 5.1 to correct our sample statistics. The resulting distribution of stellar ages for the entire sample (North, South, and Cohen-Kuhi) is shown in Figure 5.6. To illustrate how the observed age distribution can be used to explore possible star formation histories of the cloud, imagine the simplest possible model,

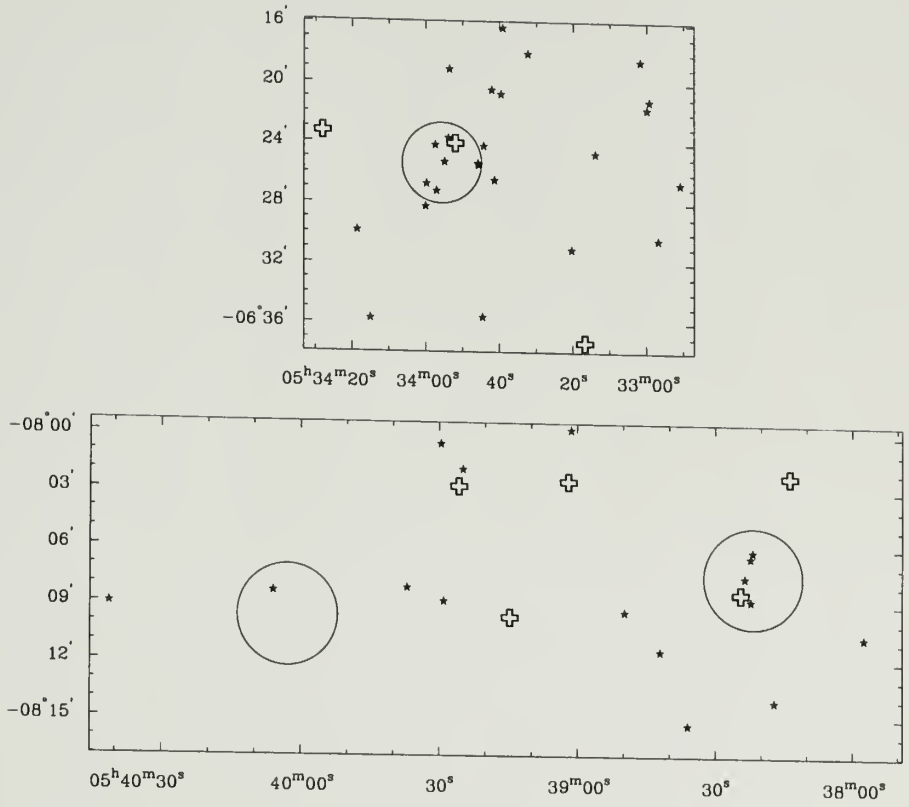

Figure 5.5. The distribution on the sky of young stars. Positions are plotted for stars 10^5 yrs old or younger (stars), and the IRAS sources (crosses) in L1641 North (upper), South (lower left), and the Cohen-Kuhi group (lower right). Circles indicate the defined aggregates.

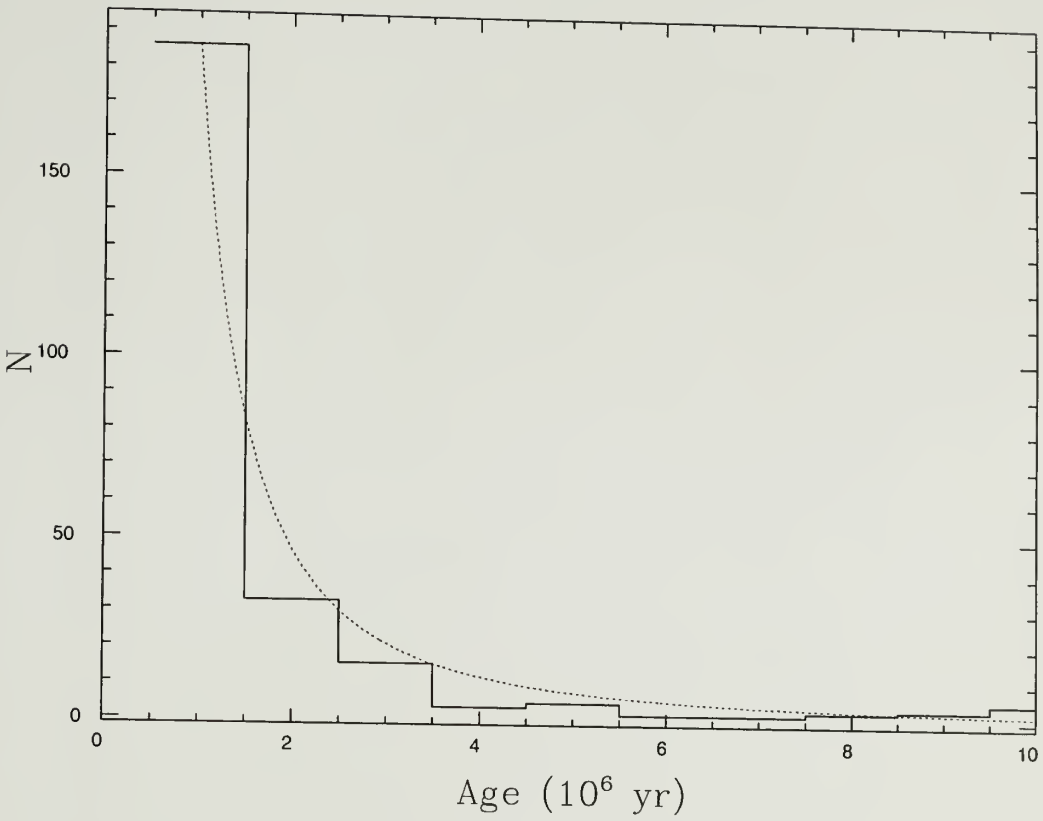

Figure 5.6. The observed age distribution (number of stars as a function of age) in L1641. The dashed line shows a $1/t^2$ distribution.

in which a spherical cloud of radius ~1 parsec forms stars in its center at a constant rate, and the stars, not bound to the cloud, drift off at a constant velocity v. At $v = 1\,km\,s^{-1}$, a star would travel approximately 1 parsec in 10^6 yr, leaving the cloud after a few to several million years. A survey of stellar ages, centered on the cloud but smaller in size than the entire cloud, will compile a $1/t^2$ distribution (where t=age). If L1641 as a whole followed this simple picture, we would conclude that the star formation rate was constant over the past 10 Myr.

Such a picture, while consistent with the observed distribution (Figure 5.6) is certainly an oversimplification. Instead of a spherical cloud with a central star-forming region, L1641 is a clumpy, fragmentary cloud with multiple star-forming sites scattered throughout, as evidenced by the aggregates. A given field within the cloud will therefore contain both stars which recently formed within that field, and stars which formed in other areas of the cloud and have drifted into view. Age distributions within the individual regions are shown in Figure 5.7. The steep age distribution in the North suggests that the most vigorous recent star formation activity of the three regions has taken place there, while the South cluster is represented by a broader distribution between 1 and 3 Myr. A realistic model for the star formation history of the cloud will have to take into account the multiple star-forming sites, their spatial separation and the characterstic timescale between star-forming events. However, without further consideration of a detailed model, we can reach some conclusions. We know that 1) the current star formation rate is given by the youngest observed stars (~200 stars/1 Myr), and 2) L1641 has been forming stars for at least 3×10^7 yr, as this is the age of the oldest observed pre-main sequence stars.

Assuming that L1641 has been forming stars at a constant rate (given by the current rate), we can estimate the maximum lifetime of the cloud. According to Figure 5.6, 186 stars have formed in the past 1 Myr. Recalling that we have

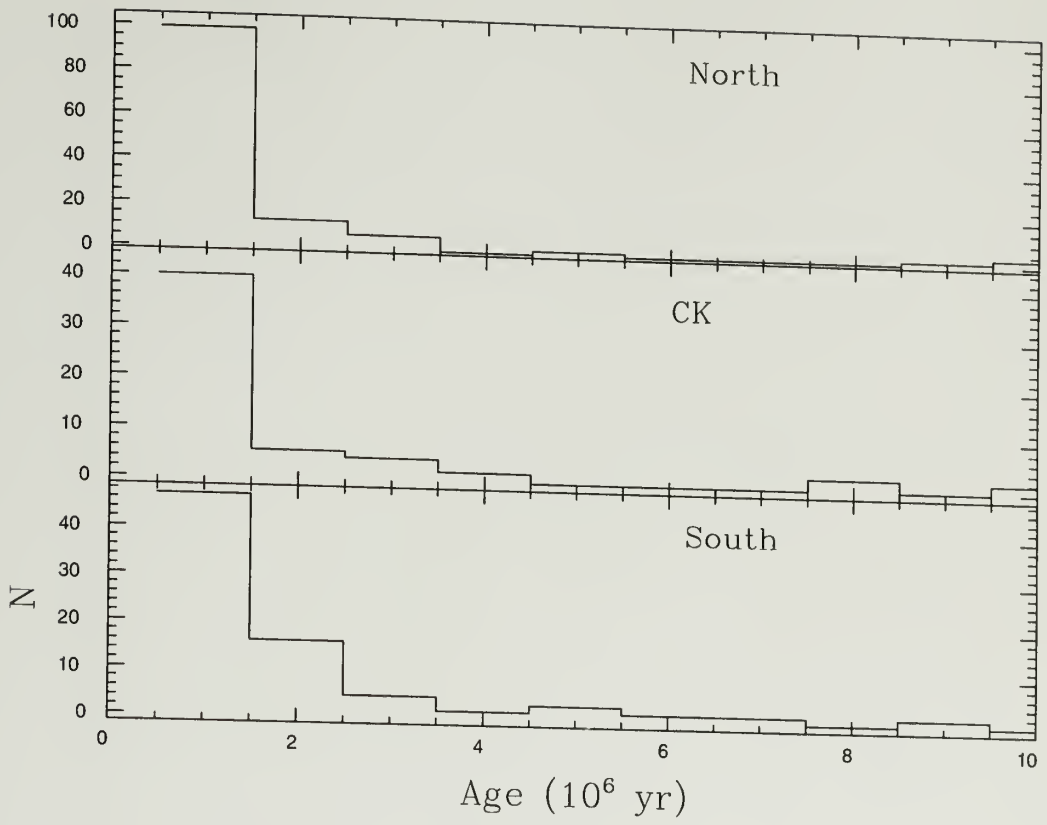

Figure 5.7. The observed age distributions in individual regions.

spectral types (and therefore masses) for 55%-70% of these stars (Table 5.1), we will assume that the remaining stars have a similar mass distribution, and will therefore take the average mass per star as being in the range 0.2-0.3 $M_\odot$ (see following section for mass distributions). Thus the average mass consumed in the production of stars in a 1 Myr period is $\sim 50 M_\odot$, in a surveyed area of $\sim 3 \times (2.5\,pc)^2$. The total molecular mass of L1641, excluding the Orion Nebula cluster, is $\sim 4 \times 10^4\, M_\odot$ (Bally *et al.* 1987), and has a total area of $\sim 130\,pc^2$. The gas depletion timescale of the cloud, given the current gas consumption rate, is therefore $\sim 10^8$ yr.

The effective star-forming lifetime of L1641 (3×10^7 yr), implies that there should be a significant population of pre-main sequence stars *outside* the cloud (for

it is only a few parsecs in width). Assuming an isotropic dispersion, approximately 2/6, or 1/3 of the stars formed in the cloud should traverse its half-width (only ~5/2 parsec) in ~3 Myr. The number of stars off the cloud is then given by the total number older than 3 Myr times 1/3, or approximately 10,000 stars. How many of these stars are detectable as pre-main sequence stars? Statistics for circumstellar disks indicate that 1-10% of PMS stars with accretion disks retain them beyond 3 Myr (see Chapter 7 for a discussion of the Hα–disk connection). Thus, there should be 100–1000 Hα stars near L1641, and their spatial distribution should fall off smoothly with distance from the cloud.

Large-scale Hα objective prism surveys of L1641 and its immediate surroundings show that the Hα stars are heavily concentrated within the cloud proper, while fewer than 50 are found off the cloud (Brand & Wouterloot 1991). The Hα surveys have all been made at a variety of depths. However, a typical survey limit is $V = 17$ (Parsamian & Chavira 1980), which for a star of spectral type M2 corresponds to $I \sim 15$, and an age (if the star is unreddened) of several million years (see Figure 5.1). Thus, in principle, all 3 Myr old Hα emitting stars lying off the cloud should have been detected.

More sensitive methods of searching for "old" PMS stars have recently become, or will soon become, available. They all exploit the ability to survey large regions on the sky. The simplest is to image the cloud surroundings in the near-infrared (J, H, K) and identify stars with near-infrared excesses characteristic of circumstellar disks. The Two Micron All Sky Survey (2MASS) will make such a search possible. Similarly, a recent large-scale survey for x-ray emitting stars in the vicinity of L1641 identified a large number (~1000) of possible pre-main sequence stars well outside the cloud (Sterzik *et al.* 1995). Candidate PMS stars should be observed spectroscopicaly, using one of the multi-fiber optical spectrometers, as was done for this thesis, to confirm their PMS nature and to determine their ages.

5.4 The IMF in L1641

We will confine our analysis of the stellar initial mass function (IMF) to samples for which our data are representative. Using the same approach which resulted in the tabulated completeness as a function of age, we examine the completeness of the spectroscopic sample as a function of mass. We find that, for stars of age $t \leq 1$ Myr and mass $M \geq 0.2 M_{\odot}$, the North spectroscopic sample is $\geq 80\%$ complete. In the South, the spectroscopic sample is $\geq 70\%$ complete, over the same range of mass, but to an age of $t \leq 3$ Myr. Thus, we select from the North all stars of age $t \leq 10^6$ yr and mass $M \geq 0.2 M_{\odot}$, and from the South, all stars of age $t \leq 3 \times 10^6$ yr and mass $M \geq 0.2 M_{\odot}$. Their distributions in log $(M/M_{\odot})$ are shown in Figure 5.8. Our "completeness" limit of 0.2 $M_{\odot}$ precludes detection of a different turnover mass at the low mass end. However, a K-S test finds that the samples are drawn from different distributions at the $> 99\%$ confidence level.

Do either of the observed mass spectra resemble the solar neighborhood IMF? All but a few of the stars in Figure 5.8 have masses $< 1 M_{\odot}$, so we will compare the data with mass functions only over the range $0.2 < (M/M_{\odot}) < 1.0$. The simplest analysis is a direct comparison of observed mass distributions with analytical forms of the IMF. We assume a power-law form for the mass function of

$$\xi(M) \propto M^{-(1+x)}$$

where (following Mateo 1988) we will refer to x as the slope of the IMF. This is equivalent to the form used by Miller & Scalo (1979), $\xi(log\, M) \propto M^{-x}$. In our formulation, the slope corresponding to the Miller-Scalo IMF between 0.1 and 1 $M_{\odot}$ is $x = 0.4$, and to the modified Salpeter IMF it is $x = 0.25$ (Mihalas & Binney 1981).

The K-S test was applied to the cumulative mass distributions shown in Figure 5.9. If we demand a relatively conservative confidence level of 95%, then

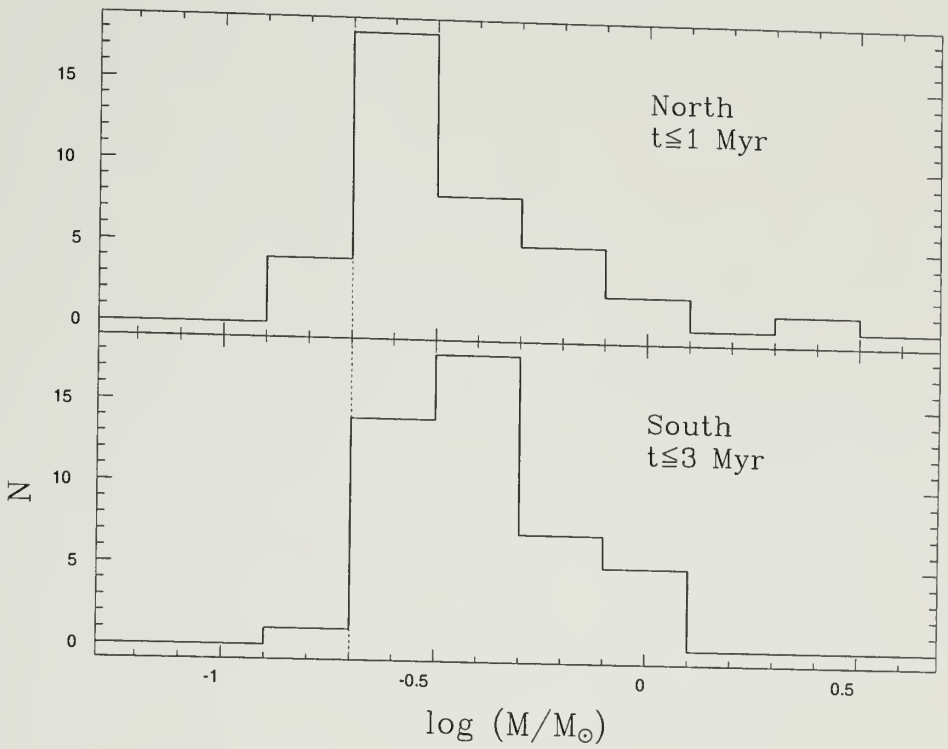

Figure 5.8. Distribution in log mass for stars in L1641 North, $t \leq 10^6$ yr, and L1641 South, $t \leq 3 \times 10^6$ yr. The dashed line marks the lower limit for which our data are "complete".

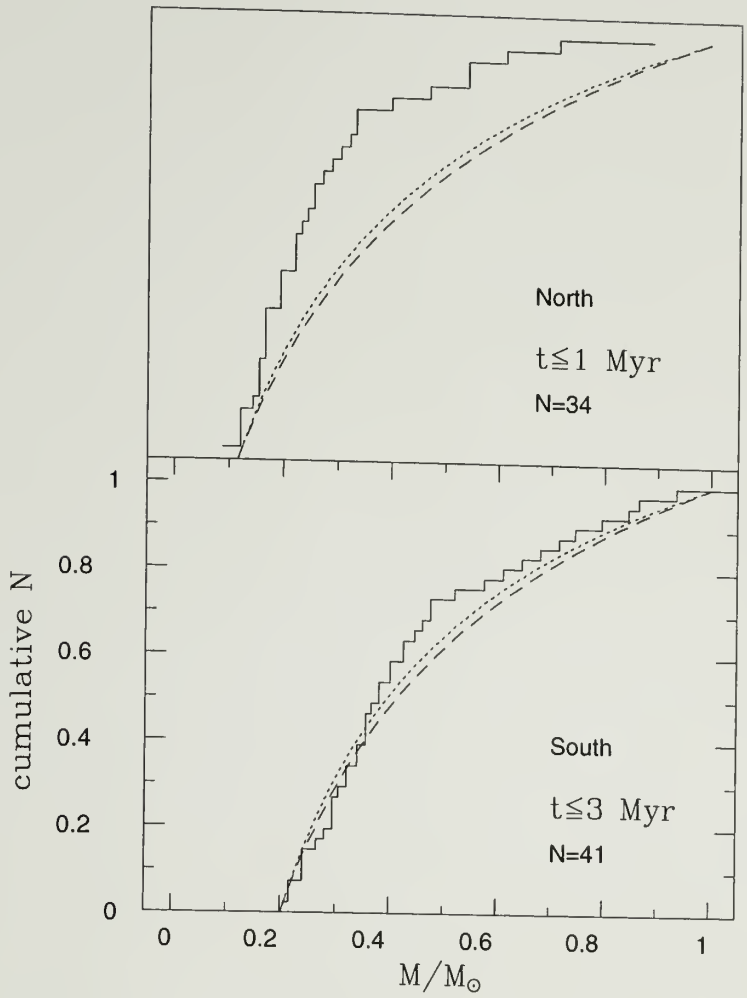

Figure 5.9. Cumulative mass distributions, in L1641 North and South. Masses range from 0.2-1.0 $M_{\odot}$ in L1641 North (upper) and L1641 South (lower). Solid line is the observed mass distribution, short-dashed line is the Miller-Scalo IMF, and the long-dashed line is the Salpeter IMF.

both the Miller-Scalo and the Salpeter IMF can be ruled out in the North. As Figure 5.9 demonstrates, the North region contains more stars in the mass interval 0.2-1.0 $M_{\odot}$ than is consistent with either of the standard IMFs. In contrast, the mass distribution in the South is consistent with both the Miller-Scalo and the Salpeter IMF, at the 95% confidence level.

5.5 Model Dependence of Results

The stellar masses and ages discussed in this chapter were derived from a particular pre-main sequence stellar evolution model, of which there are currently several in use in the literature. Unfortunately, the models do not yield the same mass and age for a given L_*, T_{eff}. This doesn't affect the *relative* age distributions discussed earlier in this chapter, since we have used a single model in our analysis. However, the consequences for our mass distributions, since they were compared with the solar neighborhood IMF, are significant. In Figure 5.10 we plot selected mass tracks and the zero age main sequence for two contemporary models, one by D'Antona & Mazzitteli (1993; DM93), used in this thesis, and one by F. Swenson (1994;FJS).

Ages and masses derived from the two models, for stars in both the North and South regions are shown in Figure 5.11. The FJS tracks give systematically higher ages and masses relative to the DM tracks. Specifically, the masses at the low mass end (0.2 $M_{\odot}$) differ by a factor of two. Thus, our result in the previous section, that the North region is producing too many low-mass stars relative to the solar neighborhood IMF, must be qualified, until uncertainties regarding the transformation between (L_*, T_{eff}) and (mass, age) are clarified.

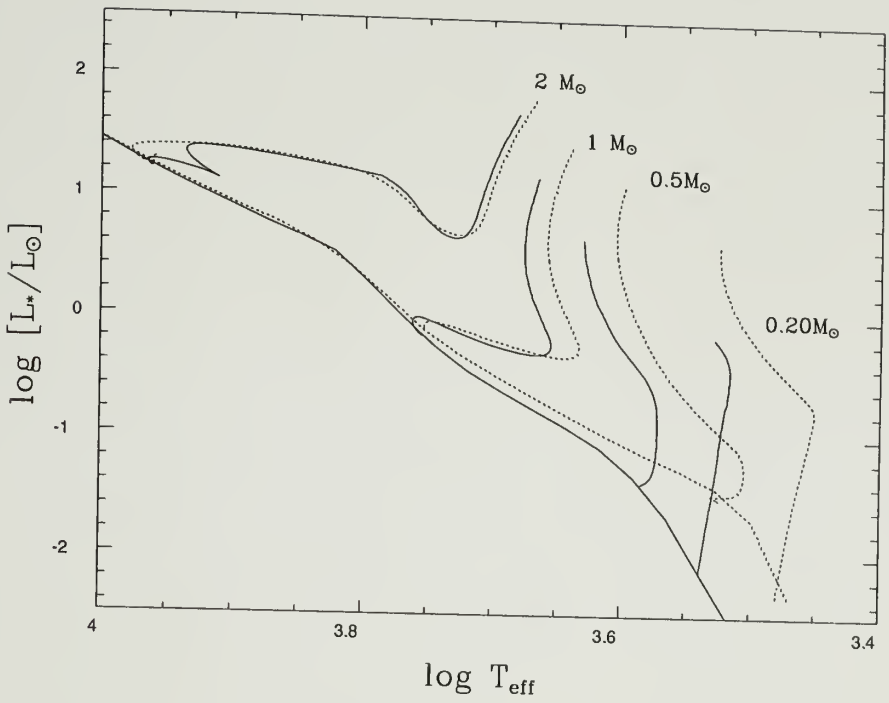

Figure 5.10. Comparison of two sets of evolutionary tracks. The D'Antona & Mazzitteli (1993) model (dashed line), and the Swenson (1994) model (solid line).

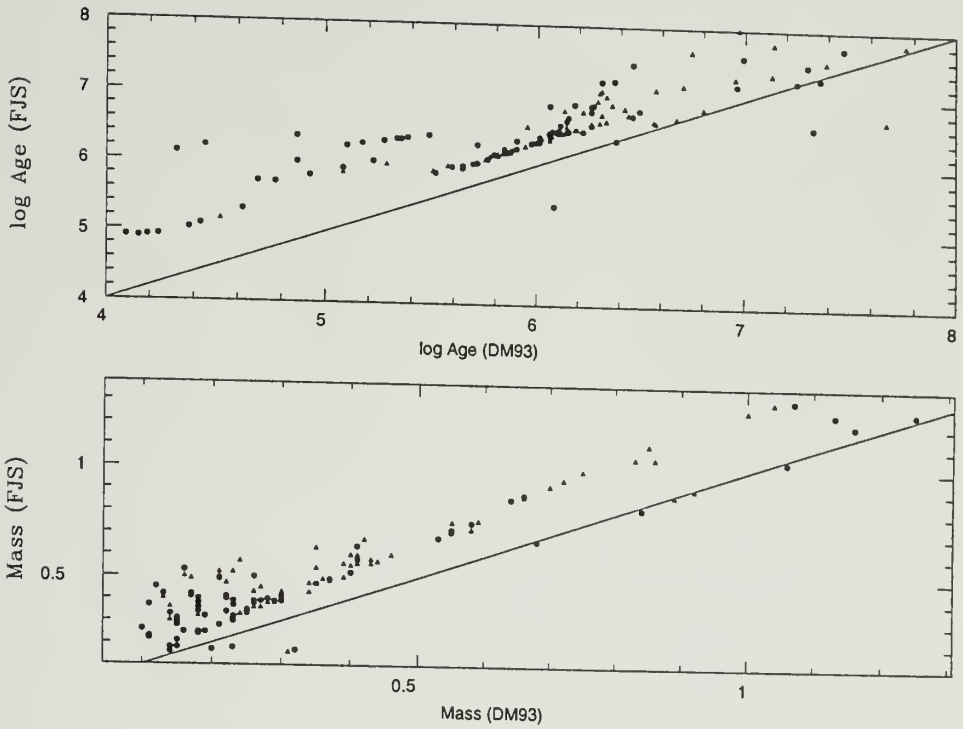

Figure 5.11. Comparison of stellar ages and masses derived from two evolutionary models. Stars in L1641 North are dots and stars in L1641 South are triangles. The diagonal line in each panel shows the one-to-one relationship.

Chapter 6

The Frequency and Lifetime of Circumstellar Disks in L1641

Most stars are surrounded by disks of dust and gas at birth (Strom *et al.* 1993). The two most compelling lines of evidence for disks are 1) observations of infrared, submillimeter, and millimeter continuum radiation in excess of the stellar photosphere, arising both from the reprocessing of stellar radiation in the disk and from accretion processes, and 2) observations of blueshifted broad forbidden line profiles, and the implied occultation of the redshifted component of the outflow by an optically thick disk 10-100 AU in radius.

In this chapter we investigate the frequency of circumstellar disks in L1641. We begin by identifying stars which have near infrared excess emission characteristic of circumstellar disks. Then we explore possible trends of the inferred disk frequency with stellar age and mass. Finally, we assess possible evolution of disk accretion rate with age by examining the variation of Hα luminosity (a surrogate indicator of accretion rate) with age for stars which show evidence of accretion disks via their infrared excesses.

6.1 Excess Near-Infrared Emission

The most effective surveys for disks are those carried out through near-infrared imaging. Although excess emission at near-IR wavelengths is the result of heated dust only from radii near the star (within 0.1 AU of the stellar surface), it provides an extremely reliable indicator of the presence of accretion disks. In a study of young stars in Taurus-Auriga, Hartigan *et al.* (1995) found that all but one of the

32 stars with infrared excess $(K - L)$ also have detectable optical veiling. Veiling emission is attributed to hot spots on the stellar surface, where material falls onto the star. In the current models, mass flows to the stellar surface from a truncated inner accretion disk along closed magnetospheric filed lines (Königl 1991). Although we do not have measurements at L, we can measure the near-infrared excess using $H - K$.

We define infrared excess as

$$\Delta(H - K) = (H - K)_o - (H - K)_*$$

where $(H - K)_o$ is the dereddened color of a star, and $(H - K)_*$ is the intrinsic color appropriate to the star's spectral type. We shall refer to "disked" stars as those which satisfy

$$\Delta(H - K) > 3\sigma(H - K) + 0.05 \tag{6.1}$$

where

$$\sigma(H - K) = \sqrt{\sigma^2(H - K)_{observed} + C^2\,\sigma^2\,(\mathrm{A_v})}$$

The value of the constant C is determined by the color index used in the calculation of $\mathrm{A_v}$. In most cases, $\mathrm{A_v}$ is calculated from $E(R - I)$, and $C = 0.30$. The 0.05 offset is our estimated minimum error in the dereddened color, taking into account uncertainties in the calibration, zero point, and airmass corrections of the photometry.

6.2 Timescales for Disk Evolution

Our conservative disk criterion excludes those stars with large uncertainties in their photometry, and is therefore biased toward the brighter (younger) stars. Before examining disk fraction as a function of age, we should account for this bias. To do so, we shall include in our analysis only those stars whose photometric

errors are comparable in magnitude to the errors of the youngest (brightest) stars, for which disks are detected. This corresponds to $\sigma(H-K) \leq 0.01$. With this restriction applied, H-R diagrams for the "disked" and "non-disked" stars are shown in Figures 6.1- 6.3. Note that few stars of mass $> 1 M_{\odot}$ have disks, and our requirement that $\sigma(H-K) \leq 0.01$ has eliminated all stars with $M < 1 M_{\odot}$ and $t > 3$ Myr. A robust estimate of disk fractions for stars of advanced age is therefore prohibited. However, if we discard the requirement that $\sigma(H-K) \leq 0.01$, we find 6 stars of age $t > 3$ Myr, which satisfy the infrared excess requirement of equation 6.1. Discovery of these stars was enabled by a relatively deep ($H \leq 15.8, K \leq 14.75$) survey over a wide area (0.77 degree^2) of the cloud. This suggests that another deep imaging survey with improved photometric accuracy ($\sigma(H-K) \leq 0.01$) be conducted, in order to quantify the fraction of old stars (3-10 Myr) with disks.

6.3 Accretion Evolution in Circumstellar Disks

An important conclusion of this work is that some circumstellar disks have lifetimes of up to 10 Myr. In principle, the existence of such old disks enable us to track secular changes in accretion rates as star/disk systems age. To do this, we examine accretion rates as a function of age, for the stars in our sample whose $\Delta(H-K)$ indicate the existence of accretion disks. Thus, we need an observable quantity which reflects the accretion rate. Although the $(H-K)$ excess is a good indicator of the presence of accretion disks, its magnitude does not correlate with the actual rate of accretion, for several reasons: (1) it is influenced by inclination, so that a disk seen face-on will contribute a larger excess than one seen edge-on, (2) it is affected by the size of the disk, and the radial distance of the inner disk from the stellar surface, (3) for geometrically flat, optically thick accretion disks

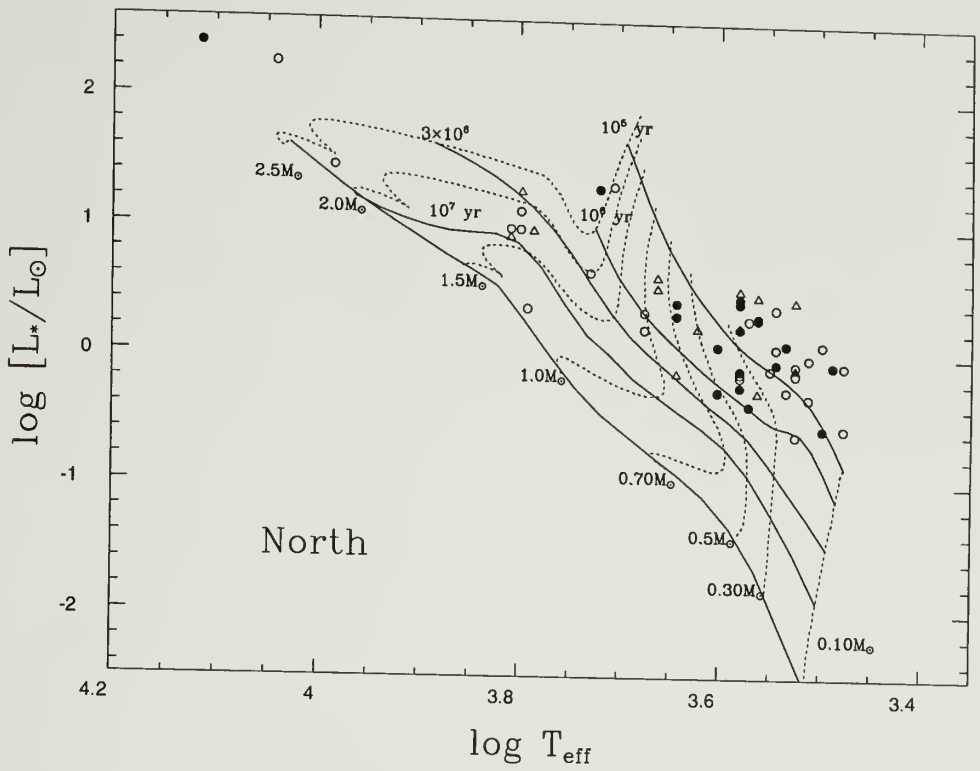

Figure 6.1. H-R diagram for L1641 North, showing stars with infrared excess emission. Filled symbols are stars having IR excesses characteristic of circumstellar disks.

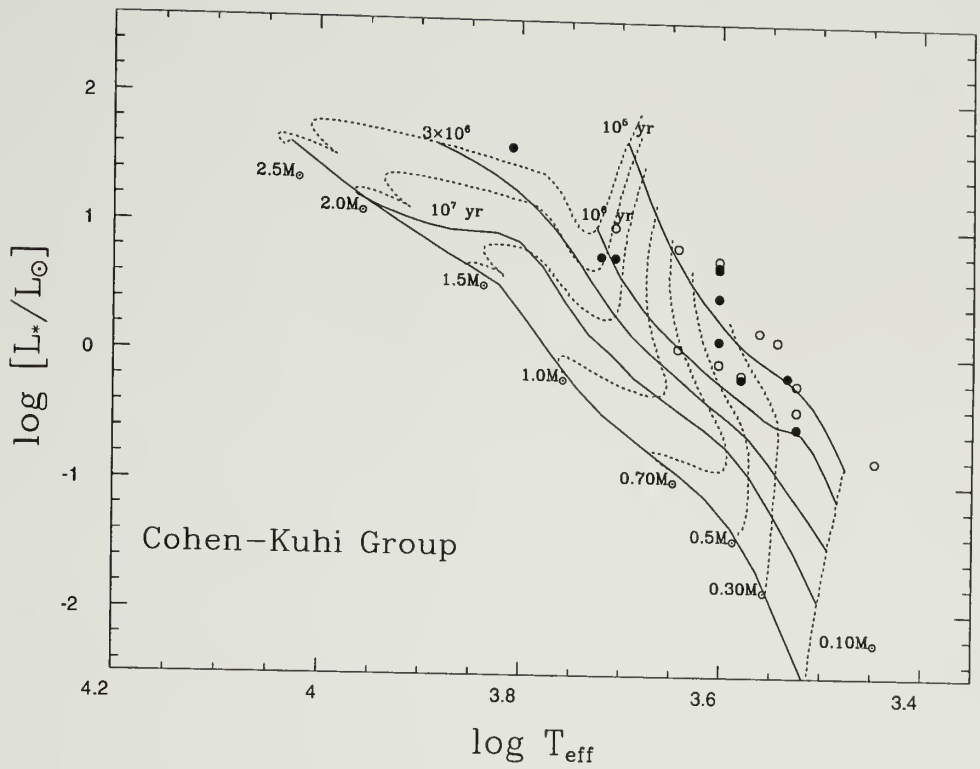

Figure 6.2. H-R diagram for the Cohen-Kuhi Group region, showing stars with infrared excess emission. Filled symbols are stars having IR excesses characteristic of circumstellar disks.

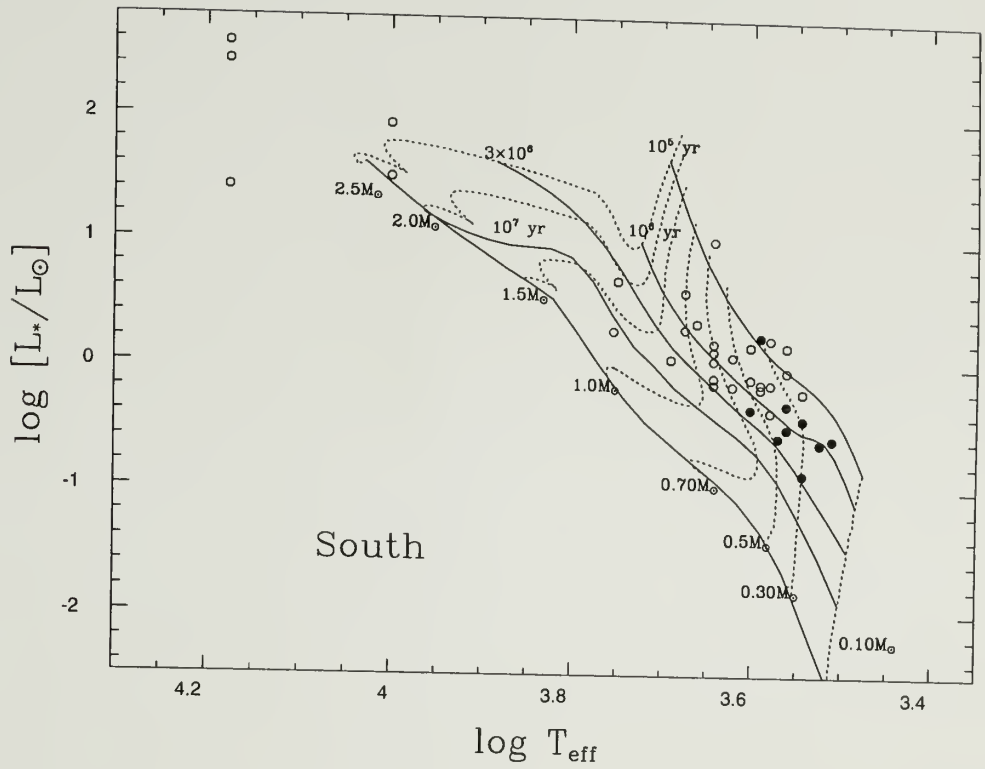

Figure 6.3. H-R diagram for L1641 South, showing stars with infrared excess emission. Filled symbols are stars having IR excesses characteristic of circumstellar disks.

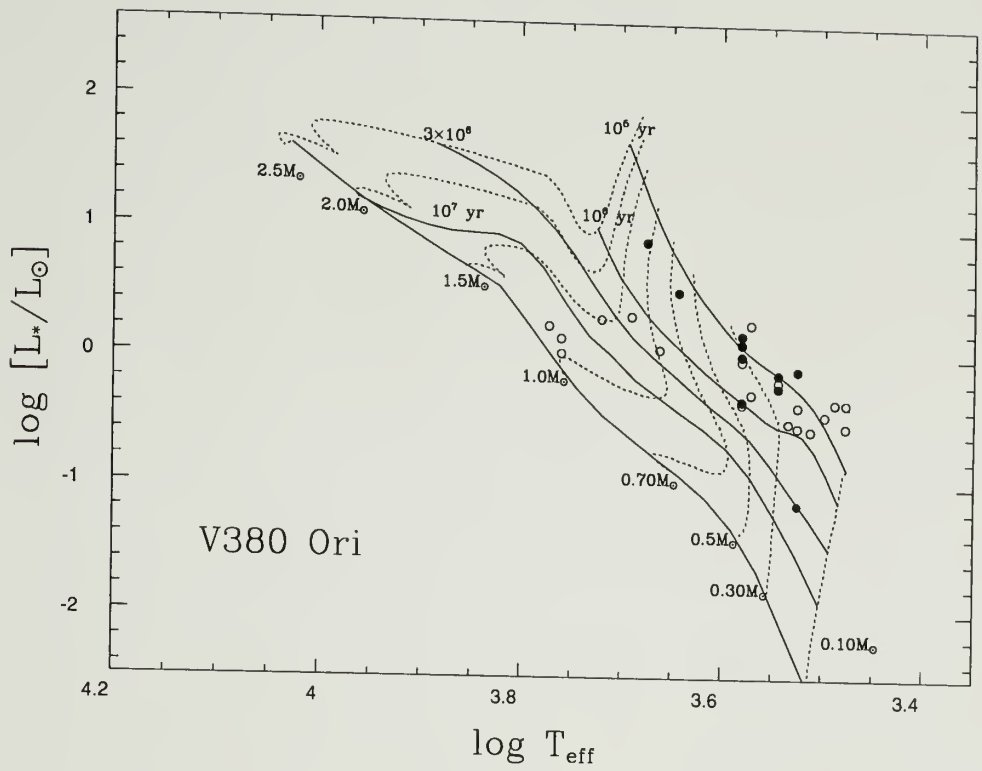

Figure 6.4. H-R diagram for the V380 region, showing stars with infrared excess emission. Filled symbols are stars having IR excesses characteristic of circumstellar disks.

($\lambda F_\lambda \propto \lambda^{-4/3}$), the excess emission over the stellar photosphere ($\lambda F_\lambda \propto \lambda^{-3}$) "saturates" at a value of 0.9, no matter how high the accretion rate.

As mentioned in §6.1, the best indication of accretion rate is provided by the optical veiling which measures the accretion luminosity produced by disk material landing on, and heating, the stellar photosphere. Unfortunately, the resolution of our spectra is insufficient to provide accurate estimates of the veiling. Since we cannot measure the accretion rate directly, we must use a surrogate, such as the Hα luminosity. Hartigan *et al.* (1995), following Cabrit *et al.* (1990), show that the Hα luminosity correlates with veiling and thus with accretion. Presumably, the Hα emission is dominated by emitting gas confined to the accretion columns, which transport material from the inner disk to the surface of the star. Although there may be some contribution to the Hα luminosity from the stellar photosphere, or from the stellar wind, the Hα luminosity is not little affected by inclination, nor does it saturate for high accretion rates. The Hα luminosity is calculated from

$$L(H\alpha) = F_o \times 4\pi d^2 \times EW(H\alpha) \times 10^{-0.4\,R_o}$$

where R_o is the dereddened R magnitude of the star and F_o is the flux at R for a zero magnitude star. The Hα luminosity, in units of log solar, are plotted in Figure 6.5, as a function of $\Delta(H-K)$.

Note that it is the luminosity, rather than the line equivalent width, which shows the correlation with infrared excess. About half of the non-excess stars in Figure 6.5 have *significant* (> 20) Hα equivalent widths. These could be disked stars viewed edge-on, or non-disked late-type stars with active chromospheres, whose Hα line emission is very bright in contrast to the faint stellar photosphere. The Hα luminosity takes into account the brightness of the star, thus eliminating some of the above ambiguity. In Figure 6.5 it is seen that approximately 80% of the stars meeting our IR excess criterion fall to the right of the line at

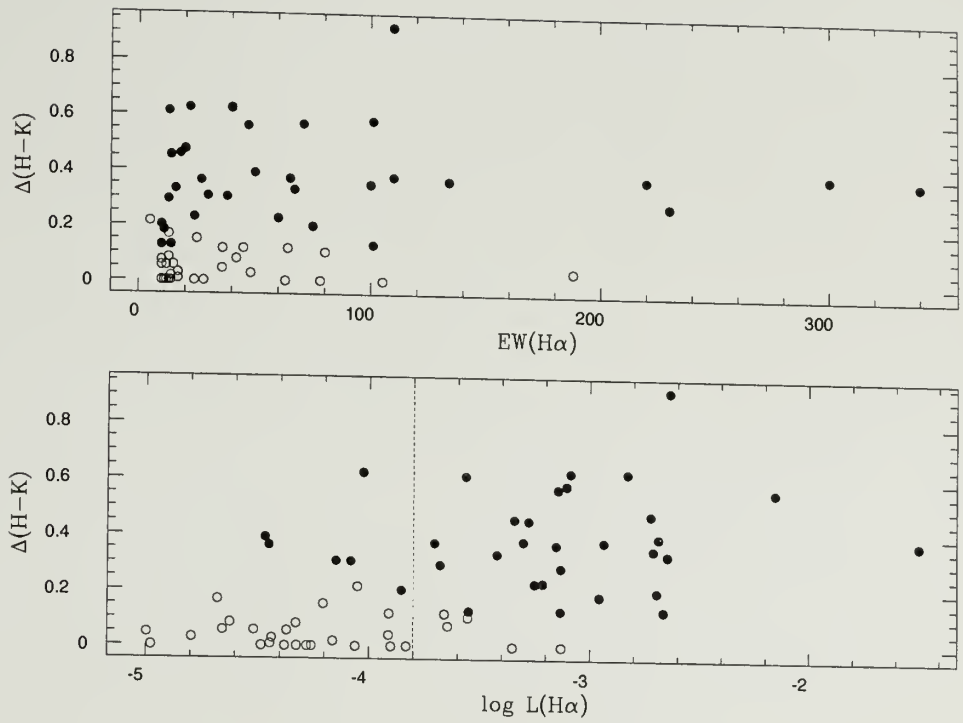

Figure 6.5. Hα equivalent width and luminosity as a function of infrared excess. Stars which satisfy our IR excess criterion are plotted as solid symbols.

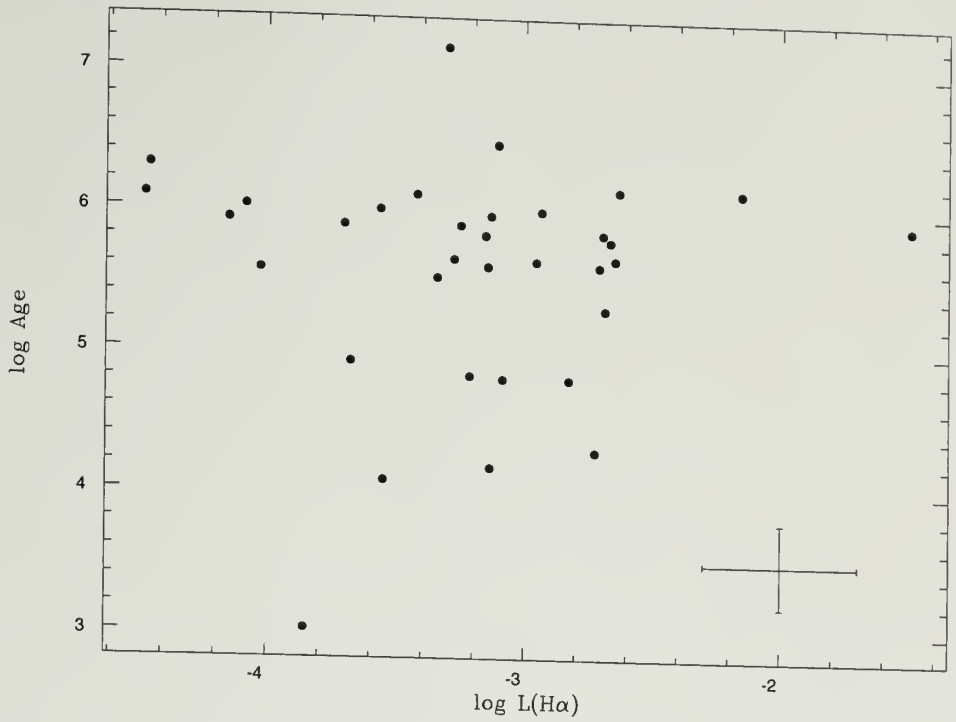

Figure 6.6. Hα luminosity as a function of age. All stars satisfy the infrared excess disk criterion in Equation 6.1. Representative errors are indicated.

$\log L(H\alpha)/L_{\odot} = -3.8$, while approximately the same fraction of non-excess stars fall to the left of the line.

In Figure 6.6, we plot the Hα luminosity against the age derived from our H-R diagrams, for all stars which satisfy our disk criterion. For this sample, Hα luminosity appears to be roughly constant with age. If Hα luminosity is indeed a measure of accretion luminosity, then we must conclude that on average, the mass accretion rate is roughly constant during the disk accretion phase. However,

Table 6.1. Disk Fraction as a function of Mass

Mass Range	North	V380	Cohen-Kuhi	South	Total(%)
$M > 1$ $M_\odot$	2/15	1/6	2/4	0/10	14%
$0.5 \leq M \leq 1.0$ $M_\odot$	3/7	1/2	0/2	1/10	24%
$M < 0.5$ $M_\odot$	13/32	8/21	6/13	8/18	42%

For stars with $\sigma(H-K) \leq 0.01$

the number of disked stars with ages >3 Myr is small, and future surveys, as mentioned in §6.2, should improve the sample statistics.

6.4 Disk Frequency as a Function of Mass

Examination of the H-R diagrams in Figures 6.1-6.4 reveals that the disk fraction tends to be higher among low-mass stars than among stars of 1 $M_\odot$ or more. We have tabulated the disk fraction below, for three mass ranges. The combined disk fraction as a function of mass is shown graphically in Figure 6.7. The trend, for a higher disk fraction with decreasing mass, is suggestive of the hypothesis that more massive stars may exhaust their accretion disks on a shorter timescale than less massive stars (Hillenbrand *et al.* 1992) It is especially noticeable in the South cluster, where stars are older, and may therefore have existed long enough for the high mass stars to lose their disks.

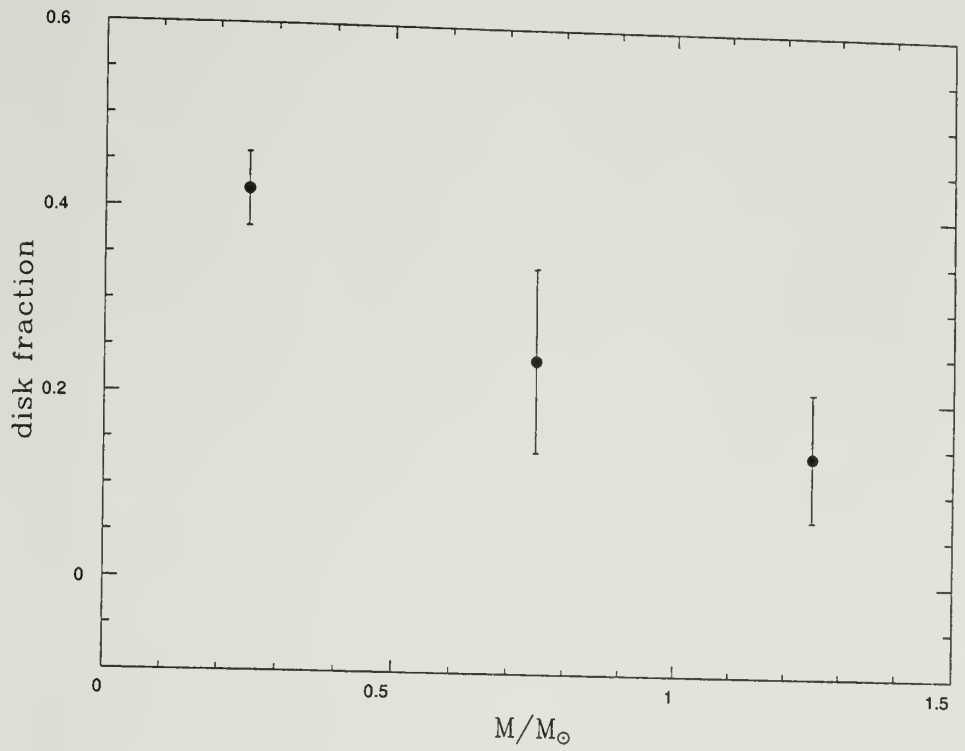

Figure 6.7. Disk fraction as a function of mass. The numbers plotted are from the "Total" column in Table 6.1, for stars with $\sigma(H-K) \leq 0.01$. Poisson errors are indicated.

Chapter 7

Discussion

7.1 L1641 and the Orion GMC Complex

In Chapter 6 we showed that the youngest stars are found both in small (R < 1/3pc, N∼10-50) aggregates and in isolation. Approximately 25% to 50% of the current star formation in L1641 occurs in aggregates, and the rest in isolation. These two "modes" are dominate the current star formation; the only evidence for "cluster mode" star formation is in L1641 South.

The distribution of ages as a function of position in the cloud indicates that the most vigorous star formation is is currently occurring at the northern end, in the region of the L1641 North aggregate, and that at least one rich (N>100) episode has occurred with the last 2-3 Myr at the southern end, where the South cluster is found. Stars spanning a wide range in age, from less than 0.1 Myr up to 15 Myr, are distributed randomly throughout the cloud.

These results confirm those of SSM, who, based on their $J, H, K-$band imaging study covering 0.77 deg^2 (49 pc^2) identified (1) a distributed population of ∼1500 stars spread throughout the cloud, (2) seven small aggregates comprised of 10-50 stars, with projected surface densities several times higher than that of the distributed population, and (3) a partially embedded cluster comprised of ∼150 stars (L1641 South). They concluded that, given the large number of stars in the distributed population, most stars in L1641 form either (1) in isolated random events throughout the cloud or (2) in unbound aggregates which disperse on time scales of a few million years. In this thesis, we were able to quantify that ∼50% of

the stars in L1641 are formed in aggregates, which may indeed disperse, while the remaining ~50% are formed in isolation.

A very different picture of star formation was presented by Lada *et al.* (1991), in a study of L1630, the northern Orion cloud which contains the clusters NGC 2024, NGC 2068, and NGC 2071. They concluded that the vast majority of stars in the surveyed area were formed in the three rich embedded clusters. However, their results are not directly comparable to ours since (1) Their survey depth was m_K =13 mag, while this work is based on a survey which reached m_K =14.5 mag, (2) They surveyed in the $K-$band only, and therefore did not have the color information which allows identification of stars with infrared excess, while this work uses J, H, and K, (3) The regions surveyed, while comparable in area to the L1641 survey, are predominantly centered on the rich clusters, and (4) They did not have spectroscopic information on the optically visible population, as we do, allowing placement in the H-R diagram and estimation of stellar ages. The distributed and aggregate populations found in L1641 could also be present in L1630, but were missed by Lada *et al.* for any of the reasons cited. We contend that a *direct* comparison of the young stellar populations in the two clouds will have to wait until a study similar to this one is done in L1630.

It is clear that star formation in "cluster mode" has recently occurred in L1630, as it has in the Trapezium and BN/KL regions, and has *not* in L1641. It has been argued by Blaauw (1991) and others that various subgroups of the Orion OB1 association are responsible for triggering the recently formed rich clusters in both Orion A and B. The general cometary morphology of both clouds, as shown in Figure 7.1, suggests an interaction between the subgroup 1a and the molecular gas. In addition, the ages of the subgroups and their projected spatial relation to the dense clusters is supportive of a "sequential" star formation hypothesis. Elmegreen (1992) lists three morphological signatures of sequential star formation,

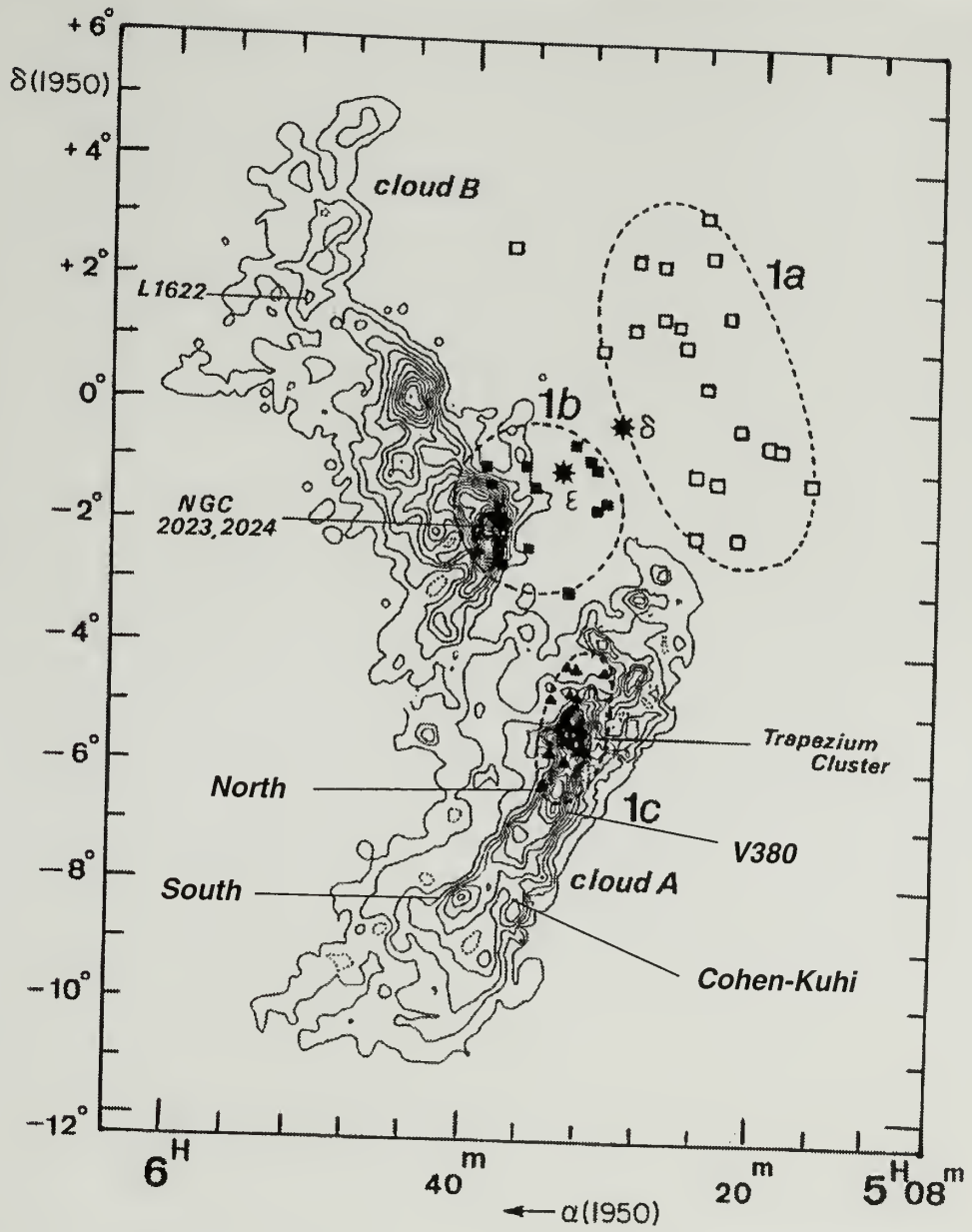

Figure 7.1. The Orion giant molecular cloud complex. Shown are clouds A and B (Maddalena *et al.* 1986), and their association with the Ori OB1 association subgroups a, b, and c. Subgroup d contains the Orion Nebula cluster, including the Trapezium stars. *Reproduced with permission from A. Blaauw.*

all of which are satisfied by Ori OB1: (1) regions of star formation with ages separated by several Myr and positions separated by 10-50 parsecs, (2) a substantial amount of molecular gas near or around the youngest cluster, with very little gas near the old cluster, and (3) a velocity difference of about 5 to 10 km s^{-1} between the old and the young regions.

The ages of the Ori OB 1 subgroups span the age of less than 1 Myr, to more than 10 Myr (Blaauw 1991; Warren & Hesser 1978; Brown *et al.* 1994). The oldest is 1a, which has an age of 8-12 Myr. The youngest is 1d, which contains the Orion Nebula cluster, and is less than 1 Myr old. Subgroups b and c are intermediate in age, although there is some disagreement over which is older (Brown *et al.* 1994). It is believed that the 1b and 1c subgroups are responsible for triggering current star formation in NGC 2024 and the ONC. If so, then 1c may also have influenced star formation in the L1641 North region.

It is unlikely that star formation in the southern extent of L1641 is related to the 1c subgroup, since (1) the projected separation is large (15 parsecs), and (2) the L1641 South cluster is older than the stars in the north, where triggering is believed to have occurred, and (3) the South cluster and the Cohen-Kuhi group are approximately the same distance from 1c, as seen in projection, but are not the same age. Thus, the age distributions of stars in L1641 rule out a sequential propagation of star formation from the northern end to the southern end of the cloud.

7.2 Comparison with the Taurus-Auriga Molecular Cloud

L1641 is by no means unique in its stellar population of young, predominantly low-mass stars. Indeed, low-mass pre-main sequence stars are found in all star-forming clouds, whether or not higher mass stars are present. The most extensively studied region of low mass star formation is the Taurus-Auriga

molecular cloud. Several optical and IR photometric and spectroscopic surveys of Taurus-Auriga were synthesized recently by Kenyon & Hartmann (1995). They concluded that the distribution in stellar ages is consistent with a constant star formation rate over the past few Myr. In spatial distribution, the young stellar population in Taurus resembles that of L1641: individual or small associations of stars distributed throughout a filamentary molecular medium, with visual extinctions of 5-10 A_v.

However, the optically visible, spectroscopically observed populations in the two clouds have different mass distributions. In Figure 7.2 we plot the distribution of spectral types for Taurus-Auriga, from Kenyon & Hartmann (1995), and for L1641, restricted to the age and mass ranges for which our spectroscopic sample is representative of the cloud population (see Chapter 5). There is less than a 0.03% chance that the two populations shown in Figure 7.2 are drawn from the same distribution.

Although we cannot evaluate the completeness of the Taurus-Auriga sample as we have for our L1641 study, Kenyon and Hartmann estimate that their sample is incomplete for masses less than 0.3 $M_\odot$, which corresponds, at t=1 Myr, to spectral types later than M2.5. If we restrict both samples to spectral types earlier than M2.5, there is a 2% chance that the spectral types are drawn from the same distribution.

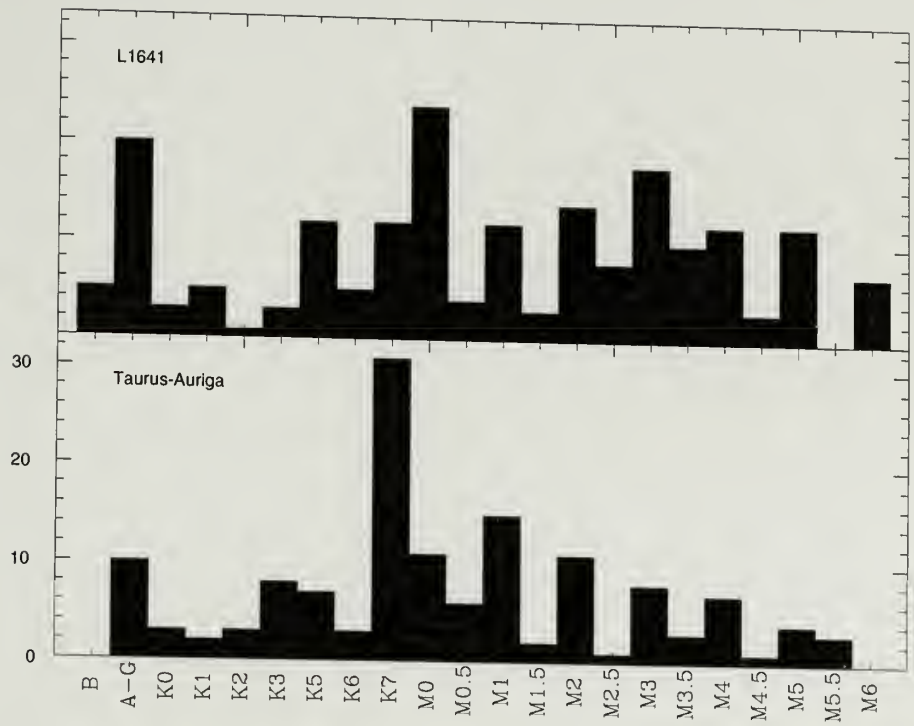

Figure 7.2. Comparison of spectral types in L1641 and Taurus-Auriga.

Chapter 8

Summary

We have undertaken a a study of the star formation properties and history of the L1641 giant molecular cloud. Combining spectroscopic and photometric data at visual and infrared wavelengths, we have developed a procedure for calculating stellar luminosities and effective temperatures of pre-main sequence stars. An important part of our procedure is spectral classification: because our program stars are reddened by dust (up to 20 A_v) in the molecular cloud, we utilize classification resolution spectra in the R, I bands, where ($A_I = 0.6A_v$).

Relatively little work has been done in this spectral range in the past, especially for late type stars, so we have constructed a grid of spectral standards at $\lambda\lambda$5500-9000$\AA$. A number of useful features, both atomic and molecular, were identified in this spectral range which enable both stellar effective temperatures and luminosity classes to be assigned.

Based on an analysis of 2.2μm images, we defined young stellar aggregates as local enhancements in the stellar surface density (3σ above the mean), and identified three such aggregates among the four regions surveyed. We placed ~300 pre-main sequence stars in the H-R diagram, and used current theoretical models to transform (T_{eff}, L_*) to mass and age.

Our analysis of the age, mass, and circumstellar disk properties of young stars in L1641 yielded these main results:

1. The aggregates contain a higher fraction of young stars than the distributed population.

2. The aggregates are responsible for 25% – 50% of all recent ($t \leq 1$ Myr) star formation in the surveyed area, even though they account for only 6% of the area.

3. 50% of very recent ($t \sim 10^5$ yr) star formation has occurred in isolation from any detected aggregate.

4. Star formation has occurred more recently (within the past 1 Myr) in the North and CK regions than in the South (within the past 2 Myr).

5. The oldest stars in L1641 are approximately 30 Myr old. If the molecular cloud has been forming stars at a roughly constant rate over the past 3×10^7 years, there should be on order 10,000 "old" pre-main sequence stars that have moved off the cloud, perhaps 10% of which are detectable (via their Hα emission) as pre-main sequence stars.

6. The recent star formation event in L1641 North produced more stars in the $0.2 - 1.0 M_\odot$ range than can be accounted for by a standard IMF. The mass spectrum produced by the less recent event in the South is statistically indistinguishable from either a Miller-Scalo or a modified Salpeter IMF.

7. The circumstellar disk fraction is a function of stellar mass, in the sense that low-mass stars have a higher disk frequency than do high-mass stars.

8. The Hα luminosity, a surrogate indicator for the accretion rate, shows no evidence for evolution with time, within our limited sample.

9. There exist a half dozen stars in the age range 3–10 Myr having infrared excesses characteristic of circumstellar disks, but more accurate photometry is needed to determine the true fraction of old disked stars.

10. The distribution of stellar masses in L1641 and Taurus-Auriga are inconsistent with having been drawn from the same population.

Appendix A

Spectroscopic Standards

A.1 The Sample

Our standards sample is drawn primarily from the open clusters M67 and Praesepe. We chose cluster stars because it is an efficient use of the multi-object spectrometer used in our pre-main sequence star program; we could obtain spectra for a large number of stars having a substantial range of spectral types simultaneously. While cluster members' common age, metallicity, and distance offer some advantages in forming a spectral sequence, they also present some limitations in its use; for example, the variation in line strength with metallicity cannot be investigated. Likewise, since Praesepe is believed to be similar to the Hyades in composition and M67 is thought to have solar metallicity, this spectral sequence may not be appropriate for the classification of very metal-poor stars.

We observed o y those stars which have a high probability (based on proper motion studies) of cluster membership. In Praesepe, 74% of our sample have a 90% or higher probability of membership (Jones and Stauffer 1991; hereafter JS), and in M67, 71% of our sample are members at or above the 90% probability level (Girard et al. 1989). Color-magnitude diagrams for the two cluster samples are presented in Figure A.1. In order to extend our sample coverage to late-type luminous stars, we also obtained spectra of several isolated giants (types K7-M7 III). These are listed in Table 3.

A.2 Classifying the Standards

Since both the distance and the amount of interstellar reddening to the two clusters are well determined, the stars were ordered both according to their

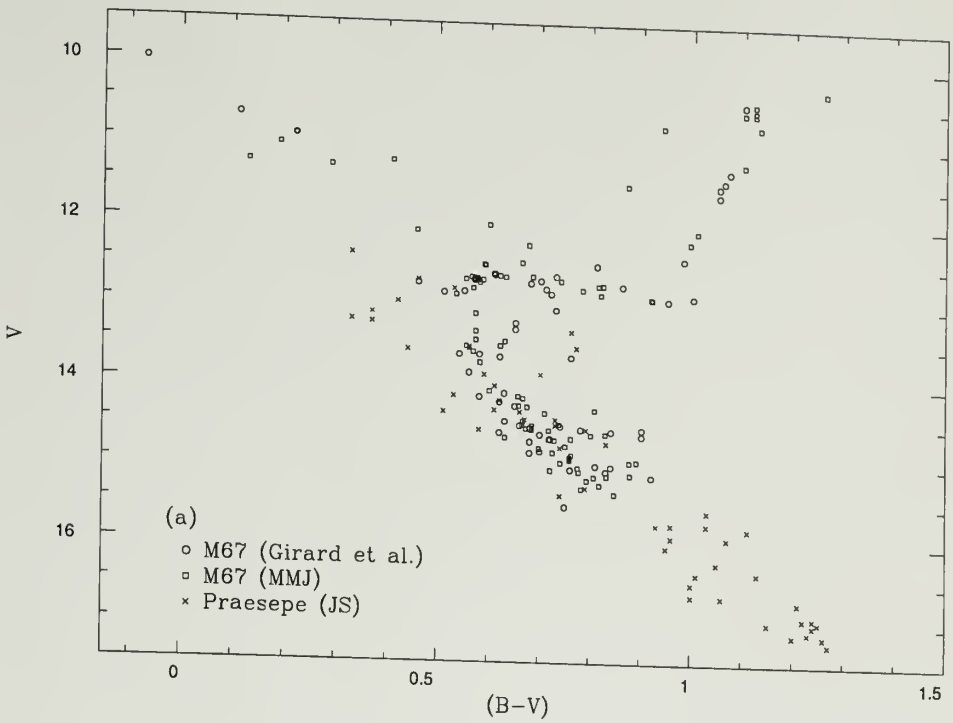

Figure A.1. Color-magnitude diagrams for stars observed in Praesepe and M67. (a) V vs. $(B-V)$, (b) V vs. $(V-I)$. Praesepe's distance modulus has been shifted by 3.4 magnitudes to match that of M67.

absolute magnitudes and their extinction-corrected colors. To convert M_v to spectral type, we used the main sequence M_v/spectral type relation given by Schmidt-Kaler (1982) for dwarfs earlier than type K7, and the relation given by Bessell (1991) for types K7-M5V. $(B-V)_o$ and $(V-I)_o$ colors were converted to spectral types using, for dwarfs of type F0 and later, the $(B-V)$ and $(V-I)$/spectral type relations of Bessell and Brett (1988), Schmidt-Kaler (1982), and Bessell (1991), as compiled by Hartigan et al. (1994). For earlier type dwarfs, we used the $(B-V)$/spectral type relation given by Schmidt-Kaler (1982). For giants we used the $(V-I)$/spectral type relation of Bessell (1991).

A.2.1 Praesepe

We used BVI photographic photometry from the proper motion study of JS, distance modulus as determined by Upgren et al. (1979) of $(m - M) = 6.20 \pm 0.05$ mag. (174 ± 4pc), and zero reddening (Johnson, 1952). In Table 1 we list the stars observed in Praesepe. Designations, coordinates, BVI photometry, and probability of membership are from JS, spectral types are those assigned by us. Previously published spectral types are listed in the "Notes" column. Spectroscopic binaries are indicated by "SB", and stars which are probable binaries according to their location in color-magnitude diagrams are indicated by "PB". Cross-identifications of the star numbers in Table 1 with other Praesepe numbering systems are given by JS.

Our adopted spectral types are inferred from M_v, since 1) color measurements are not available for all the stars in our sample, and 2) the estimated σ of the V magnitudes (0.05 mag.) is less than that of the $(B - V)$ colors (0.1 mag.; JS). For main sequence stars of spectral class B through M, an error in M_v of 0.05 mag. translates to an error in spectral type of $\sim$1 subclass, while an error in $(B - V)$ of 0.1 mag. translates to an error of 3–4 subclasses. We note that spectral types inferred from M_v and from $(B - V)$ differ by approximately one subclass, while types inferred from M_v and from $(V - I)$ are in closer agreement.

Because we assigned spectral types on the basis of photographically determined V magnitudes, it is useful to compare them with magnitudes determined photoelectrically. We compared the magnitudes in Table 1 with photoelectric V magnitudes from Johnson (1952), Upgren et al. (1979), Weis (1981), and Stauffer (1982). Excluding two known binaries (JS407 & JS431) and four probable binaries (JS179, JS280, JS336, & JS428), there were 56 measurements in common for 41 sources. The mean in the distribution of

V(photographic)$-V$(photoelectric) is -0.008 ± 0.08 mag., which corresponds to a difference in spectral type of 0.0 ± 1 subclass.

Finally, we compared our adopted spectral types in Table 1 with spectral types from the literature. The largest overlap is with Corbally and Garrison (1986), who classified nine stars (F5-K0V) in our sample, using spectra in the range $\lambda\lambda 3800 - 5000$ Å. For all but two of the nine sources, our spectral types agree with theirs to within one subclass, which in this spectral range constitutes a difference in stellar effective temperature of $\sim$0.01 dex.

A.2.2 M67

In M67, modern CCD photometry is available, and the $(B-V)$ and $(V-I)$ colors are equally reliable. We used the BVI photometry of Montgomery, Marschall, and Janes (1993; hereafter MMJ) when available, or the BV photometry of Murray et al. (1965) and Murray and Clements (1968), as compiled by Girard et al. (1989). The relative difference between MMJ's photometry and the photometry from Girard et al.'s Table 1 is shown in Figure A.2. The magnitudes and colors from the two databases agree to within 0.1 mag. We assumed a distance modulus for M67 of 9.6 and uniform reddening of $E(B-V) = 0.05 \pm 0.02$ (MMJ).

Subgiants were classified according to their Hα equivalent widths, following the empirical W(Hα)/(B-V) relation observed by Danks and Dennefield (1994) for a sample of Southern Hemisphere MK standards. Similarly, a relation between W(NaI λ5896) and (B-V) was used to classify the giants. The blue stragglers were classified according to the W(Hα)/spectral type relation given by Didelon (1982).

In Table 2, the observed M67 stars are ordered by their Sanders (1977) designations. The first character under "Notes" is coded for the source of the photometry (1= Murray et al. (1965) or Murray and Clements (1968), as compiled

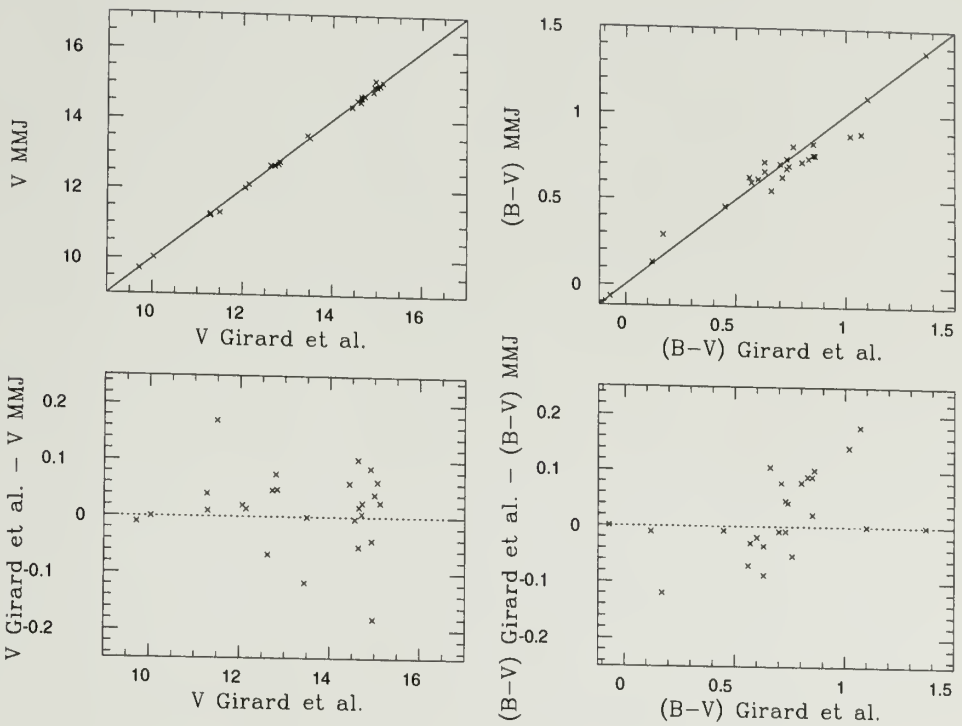

Figure A.2. Comparison of the two sources of photometry for M67 stars. Upper: V magnitudes and (B-V) colors from Montgomery, Marschall, and Janes (MMJ; 1993) vs. those compiled by Girard et al. (1989). Lower: Residuals as a function of Girard et al.'s V and (B-V).

by Girard et al.(1989), 2=MMJ) and is followed by cross-identifications with other numbering systems, as well as previously published spectral types. Coordinates and probability of membership (based solely on proper motion) are from Girard, et al. (1989).

A.3 The Standard Grid

Representative spectra for types B8V–M5V, G8III–M7III, and F5IV–K0IV are plotted in Figure A.3. The spectra have been normalized by a third order spline fit to the continuum, and shown in two wavelength sections in order to exclude the very deep atmospheric B-band absorption feature at λ7600 Å. Included in Figure 3(c) is the spectrum for the M5V star W9282B, obtained with Hydra on the KPNO 4-m telescope on 3 January 1994 by Lynne Hillenbrand.

We have scrutinized these spectra and produced a list of useful classification features, presented in Table 4. Note that, while there are many more identifiable features than those listed in the table (especially molecular bands in the late-type stars; *cf* Kirkpatrick et al. 1991), we list only those which have proved to be the most sensitive in our program to classify pre-main sequence stars.

Figure A.3. Representative spectra for types B8V–G9V, K0V–K8V, M0V–M5V, F5IV–K0IV and K0III–K2III, and M0III–M7III. The normalized spectra are displayed in two parts in order to avoid the deep telluric atmospheric absorption feature at λ7600 Å.

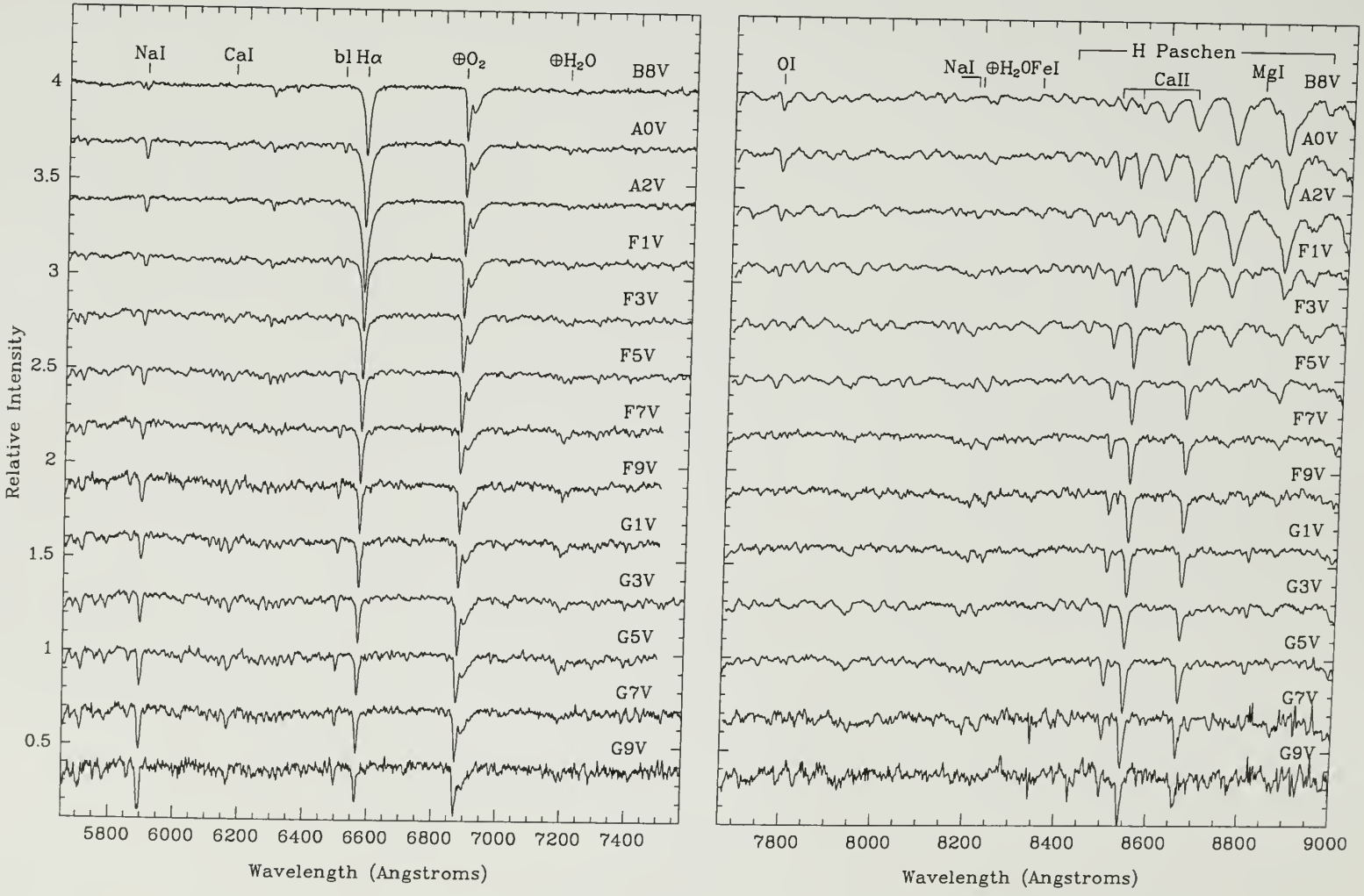
NaI
CaI
blHα
⊕O2
⊕H2O
B8V
A0V
A2V
F1V
F3V
F5V
F7V
F9V
G1V
G3V
G5V
G7V
G9V
Relative Intensity
4
3.5
3
2.5
2
1.5
1
0.5
5800 6000 6200 6400 6600 6800 7000 7200 7400
Wavelength (Angstroms)
OI
NaI ⊕H2OFeI
H Paschen
CaII
MgI
B8V
A0V
A2V
F1V
F3V
F5V
F7V
F9V
G1V
G3V
G5V
G7V
G9V
7800 8000 8200 8400 8600 8800 9000
Wavelength (Angstroms)

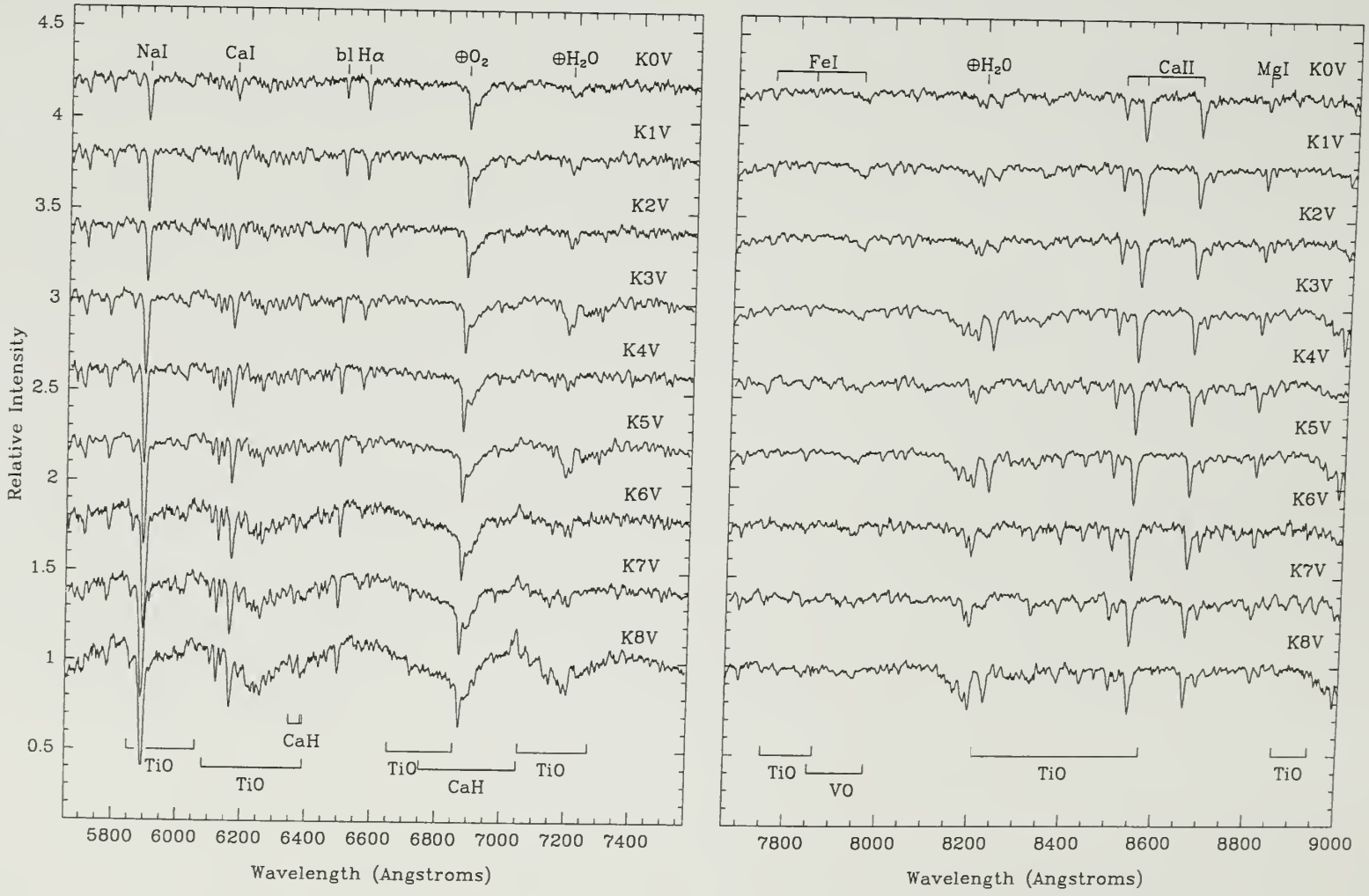
NaI
CaI
bl Hα
⊕O2
⊕H2O
K0V
K1V
K2V
K3V
K4V
K5V
K6V
K7V
K8V
TiO
CaH
TiO
TiO
CaH
TiO
Relative Intensity
4.5
4
3.5
3
2.5
2
1.5
1
0.5
5800 6000 6200 6400 6600 6800 7000 7200 7400
Wavelength (Angstroms)
FeI
⊕H2O
CaII
MgI
K0V
K1V
K2V
K3V
K4V
K5V
K6V
K7V
K8V
TiO
VO
TiO
TiO
7800 8000 8200 8400 8600 8800 9000
Wavelength (Angstroms)

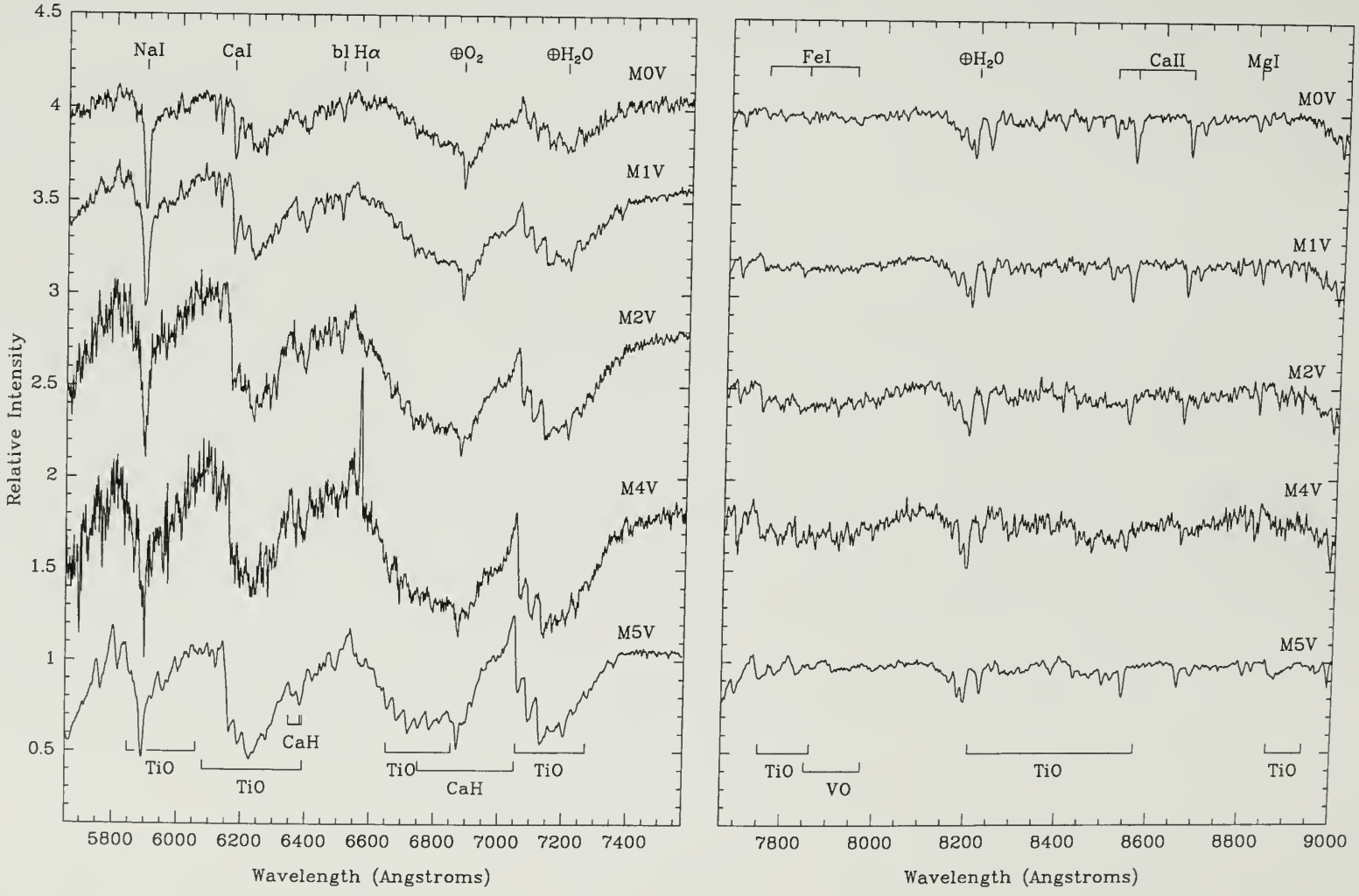
NaI
CaI
bl Hα
⊕O2
⊕H2O
M0V
M1V
M2V
M4V
M5V
TiO
TiO
CaH
TiO
CaH
TiO
Relative Intensity
4.5
4
3.5
3
2.5
2
1.5
1
0.5
5800 6000 6200 6400 6600 6800 7000 7200 7400
Wavelength (Angstroms)
FeI
⊕H2O
CaII
MgI
M0V
M1V
M2V
M4V
M5V
TiO
VO
TiO
TiO
7800 8000 8200 8400 8600 8800 9000
Wavelength (Angstroms)

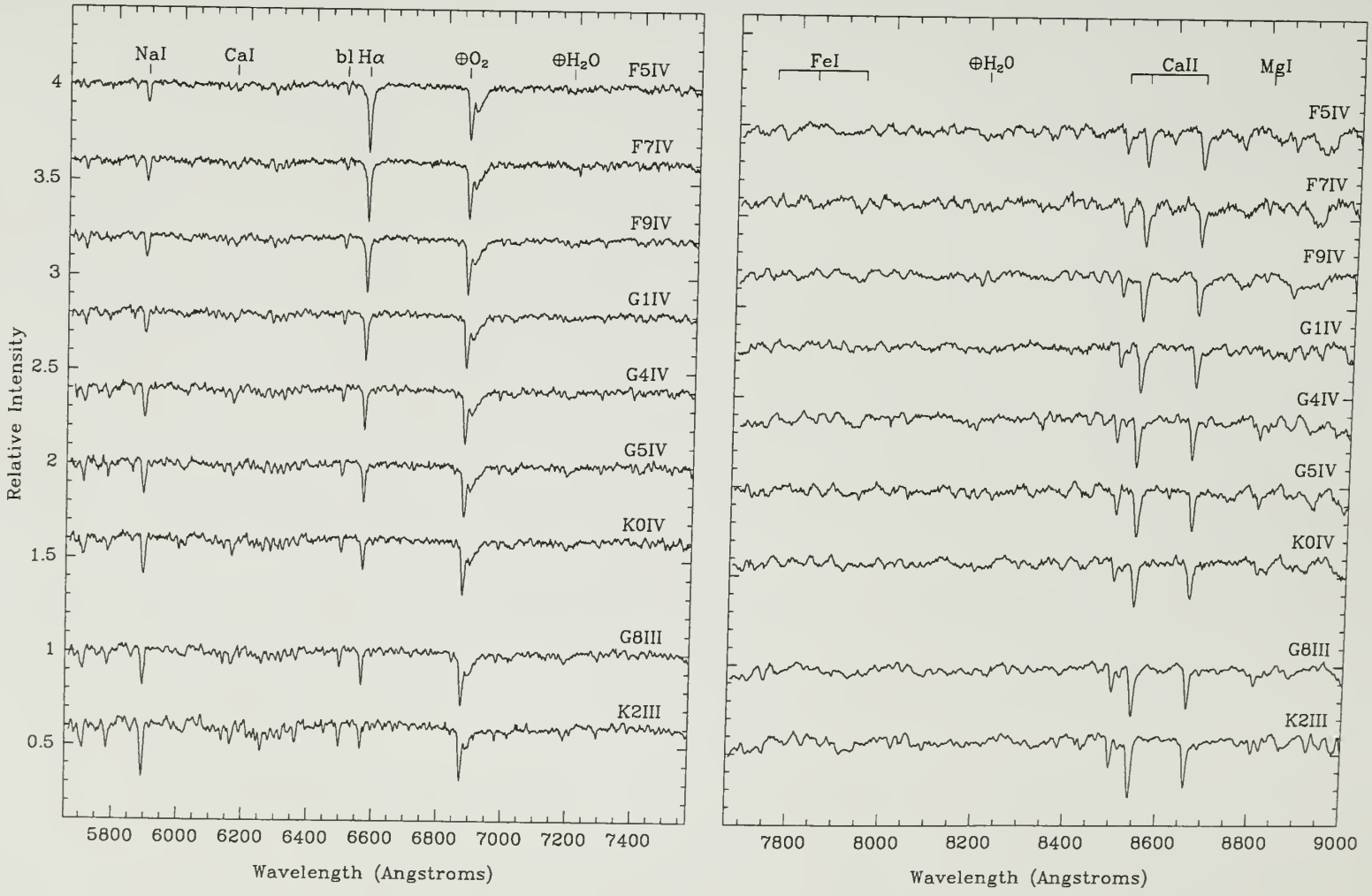
NaI
CaI
bl Hα
⊕O2
⊕H2O
F5IV
F7IV
F9IV
G1IV
G4IV
G5IV
K0IV
G8III
K2III
Relative Intensity
4
3.5
3
2.5
2
1.5
1
0.5
5800 6000 6200 6400 6600 6800 7000 7200 7400
Wavelength (Angstroms)
FeI
⊕H2O
CaII
MgI
F5IV
F7IV
F9IV
G1IV
G4IV
G5IV
K0IV
G8III
K2III
7800 8000 8200 8400 8600 8800 9000
Wavelength (Angstroms)

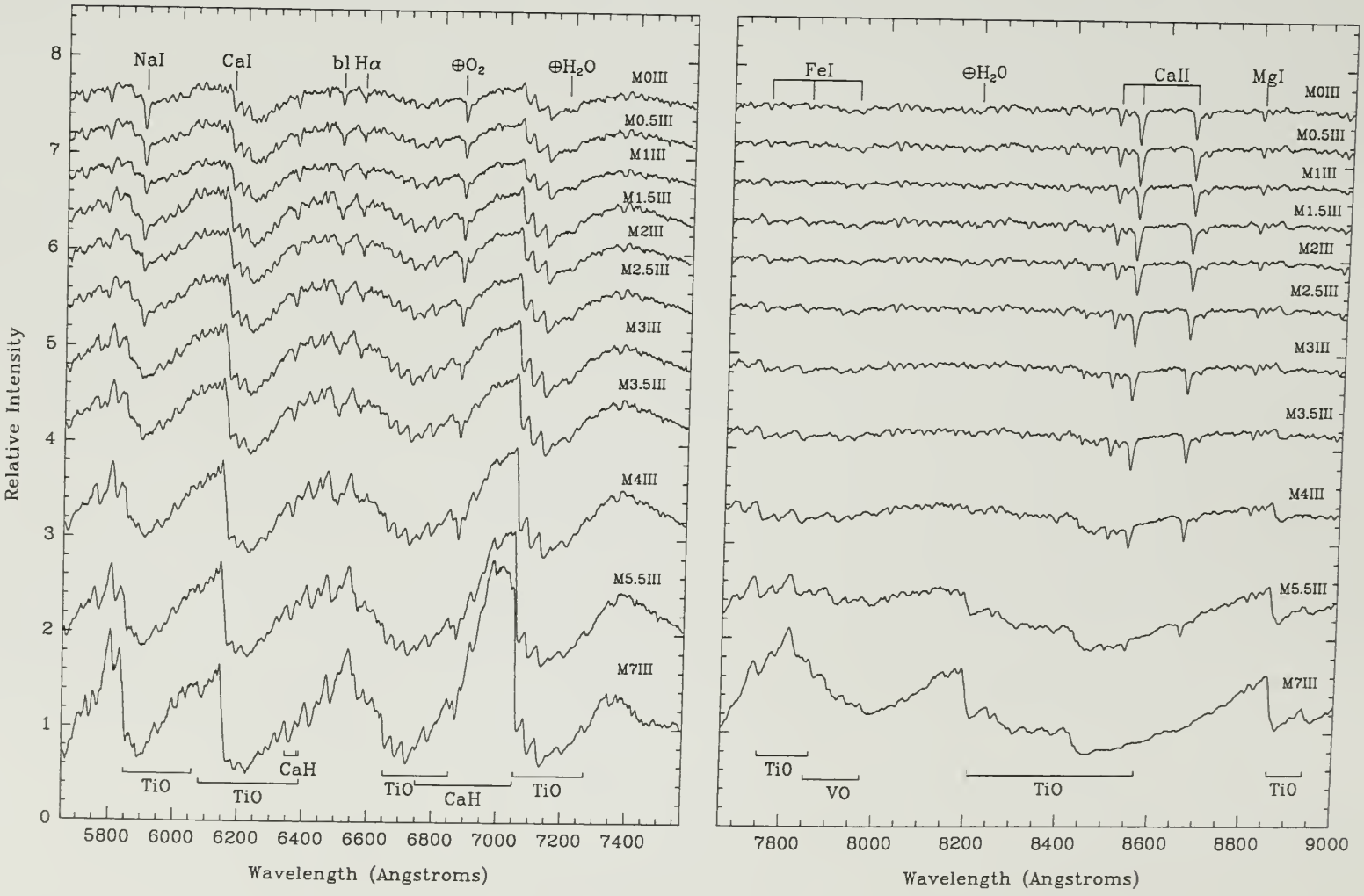
NaI
CaI
bl Hα
⊕O2
⊕H2O
M0III
M0.5III
M1III
M1.5III
M2III
M2.5III
M3III
M3.5III
M4III
M5.5III
M7III
TiO
CaH
TiO
TiO
CaH
TiO
Relative Intensity
Wavelength (Angstroms)
FeI
⊕H2O
CaII
MgI
TiO
VO
TiO
TiO
Wavelength (Angstroms)

Table A.1. Spectral Standards in Praesepe

ID[a]	α (1950)	δ (1950)	Adopted Sp. Type	m_V^b	B-V	V-I	%[c]	Notes[d]
127*	8:33:30.8	19:21:56	K2 V	12.41	1.11	–	92	
140	8:33:44.6	19:21:34	K7 V	14.48	–	1.56	82	
149	8:33:57.0	19:25:55	G4 V	11.18	0.79	–	96	
150	8:33:57.3	19:43:51	K6 V	13.96	–	1.66	97	
152	8:33:59.9	19:15:03	K6 V	14.01	–	1.51	98	
172	8:34:24.2	19:39:40	K6 V	14.07	–	1.52	57	
173*	8:34:26.0	19:52:26	G5 V	11.41	0.74	–	98	
179	8:34:34.3	19:39:43	K5 V	13.83	1.27	–	98	PB[St]
180	8:34:34.6	19:18:26	K7 V	14.72	–	1.70	98	
186	8:34:39.3	19:16:45	K6 V	13.99	–	1.54	93	
196	8:34:54.2	19:46:29	K1 V	12.36	0.96	–	93	
197	8:34:54.6	19:36:50	F9 V	10.65	0.61	–	87	
242	8:35:45.7	19:11:50	K5 V	13.74	1.26	–	98	
243	8:35:46.3	20:20:49	M3 V	17.23	–	2.60	73	
244	8:35:49.5	19:35:53	K7 V	14.61	–	1.68	96	
248*	8:35:54.9	19:40:38	F1 V	9.01	0.33	–	99	F4V[Bi],F1V[Ab],F2V[Re]
254*	8:36:01.4	19:44:52	K6 V	14.07	–	1.42	97	
255	8:36:02.4	20:23:45	M4 V	17.60	–	2.80	68	
259	8:36:04.5	20:21:29	K6 V	13.94	–	1.56	99	
263*	8:36:10.4	19:30:10	K1 V	12.36	1.03	–	98	
267	8:36:12.1	19:41:57	K5 V	13.71	–	1.20	97	
270	8:36:14.0	20:31:30	M2 V	16.20	–	2.26	90	
273	8:36:17.2	20:35:06	K6 V	14.19	–	1.43	77	
277	8:36:20.6	19:17:32	F9 V	10.50	0.70	–	98	
280	8:36:23.2	20:14:51	M0 V	14.77	–	1.80	98	PB[Up]
281	8:36:23.5	19:27:48	M2 V	16.82	–	2.57	52	
285	8:36:25.9	20:38:29	M2 V	16.42	–	2.22	57	
301*	8:36:44.5	19:39:46	M0 V	15.09	–	1.69	99	
302	8:36:44.7	19:26:15	K7 V	14.29	–	1.44	98	
306	8:36:46.4	19:37:05	K3 V	12.65	0.95	–	97	

Continued, next page.

Table A.1 continued

ID[a]	α (1950)	δ (1950)	Adopted Sp. Type	m_V^b	B-V	V-I	%[c]	Notes[d]
309	8:36:48.5	20:10:07	M0 V	15.29	–	1.80	98	
310	8:36:49.2	20:12:19	M1 V	15.72	–	2.05	95	
311	8:36:50.6	20:40:18	M3.5 V	17.99	–	2.94	56	
313	8:36:52.6	20:18:06	M3 V	17.49	–	2.92	68	
317	8:36:54.9	19:23:42	M1 V	15.63	–	1.86	98	
318	8:36:58.2	20:45:29	M2 V	16.23	–	2.45	64	
321	8:37:00.2	20:11:44	M3 V	17.68	–	2.75	74	
322*	8:37:00.6	19:29:24	F7 V	10.16	0.56	–	99	
324*	8:37:06.4	19:22:45	F3 V	9.44	0.53	–	99	F6V[Bi],F2V[Re],F5V[BB]
329	8:37:08.9	19:29:14	K8 V	14.50	–	1.68	99	
330	8:37:10.2	19:10:38	F6 V	9.96	0.76	–	99	F8V[Po],G1V[Ba],TX Cnc
332*	8:37:11.9	19:57:43	K0 V	12.01	0.74	–	99	K0.5V[CGa]
336	8:37:14.2	19:12:10	K1 V	12.53	1.07	–	57	PB[Up]
340	8:37:17.1	20:35:48	M1 V	15.49	–	2.13	91	
342	8:37:17.6	19:47:56	G9 V	11.91	0.79	–	99	K0V[CGa]
345*	8:37:20.2	19:49:02	F5 V	9.75	0.37	–	99	F5V[Re],F6IV[CGa]
349	8:37:23.6	19:38:11	K6 V	13.97	–	1.52	99	
350	8:37:26.3	20:22:11	K4 V	12.98	1.01	–	96	
352	8:37:28.5	19:06:18	M2 V	16.12	–	2.35	84	
353	8:37:29.3	20:49:07	K7 V	14.61	–	1.55	98	
354	8:37:29.7	19:21:34	K6 V	13.87	–	1.58	98	
357	8:37:33.6	19:39:13	F5 V	9.87	0.37	–	99	
359*	8:37:34.6	19:23:50	K3 V	12.84	1.05	–	91	
361*	8:37:35.7	19:27:21	G3 V	11.13	0.73	–	98	
363	8:37:35.9	20:16:32	M3 V	17.53	–	2.43	73	
364	8:37:36.9	19:06:50	M1 V	15.71	–	2.04	98	
365	8:37:38.2	20:06:39	M3 V	17.22	–	2.56	67	
373	8:37:45.1	20:30:59	M0 V	14.86	–	1.66	97	
377*	8:37:50.3	19:24:07	F9 V	10.51	0.59	–	98	G1V[Wi],SB[RS]
378	8:37:50.5	19:44:39	G4 V	11.20	0.58	–	86	G7V[CGa],G6V[CGb]

Table A.1 continued

ID[a]	α (1950)	δ (1950)	Adopted Sp. Type	m_V^b	B-V	V-I	%[c]	Notes[d]
379	8:37:51.4	20:39:00	K6 V	13.93	–	1.63	96	
384	8:37:54.0	20:39:11	M2 V	16.09	–	2.34	89	
385	8:37:54.4	19:29:16	F4 V	9.61	0.42	–	99	F2V[BB],F6V[Bi],F4V[Re]
387	8:37:55.9	19:50:14	G2 V	10.97	0.66	–	96	G5V[Wi],G7V[CGa],G7V[CGb]
388	8:37:56.0	20:06:00	G2 V	10.98	0.51	–	99	G3V[CGa],G3V[CGb]
390	8:37:59.5	20:07:12	M3 V	17.10	–	2.45	77	
391*	8:38:00.7	19:21:10	M4 V	17.43	–	2.87	81	
392	8:38:01.4	20:10:38	M2 V	16.77	–	2.62	82	
394*	8:38:02.0	19:33:26	M1 V	15.49	–	1.96	96	
405	8:38:12.4	20:39:07	M0 V	14.97	–	1.61	93	
406	8:38:15.4	19:37:32	K1 V	12.52	0.96	–	98	
407	8:38:15.9	19:14:59	F7 V	10.16	0.77	–	97	G1V[Wi],SB[Bo]
410	8:38:18.1	19:41:15	F7 V	10.21	0.44	–	99	F8V[CGa],F8V[CGb],F6V[Re]
419*	8:38:22.6	19:08:52	M2 V	16.44	–	2.44	89	
420	8:38:23.0	20:12:59	K6 V	14.26	–	1.46	98	
425	8:38:27.9	19:48:48	K5 V	13.56	1.25	–	99	
427	8:38:28.4	19:48:06	M1 V	15.81	–	2.01	97	
428	8:38:31.3	20:25:41	K7 V	14.44	–	1.76	99	PB[Up]
429	8:38:31.3	19:06:46	K3 V	12.96	1.13	–	94	
431	8:38:33.5	20:07:20	G0 V	10.78	0.53	–	98	G0V[CGa],SB1[CB]
433	8:38:36.0	19:27:23	M1 V	15.72	–	1.98	87	
435*	8:38:36.6	19:55:32	G1 V	10.95	0.61	–	98	G1.5V[CGa]
442	8:38:44.7	19:19:18	F2 V	9.33	0.46	–	99	F4V[Bi],F2III[Re]
445	8:38:45.5	19:41:58	K5 V	13.60	1.24	–	99	
448	8:38:47.4	19:26:41	K4 V	13.10	1.00	–	52	
451	8:38:51.4	20:08:28	K1 V	12.37	0.93	–	98	
453	8:38:53.9	19:26:47	F7 V	10.19	0.56	–	95	
455*	8:38:56.4	19:38:16	K5 V	13.69	1.23	–	96	
456*	8:38:57.8	19:22:32	K8 V	14.31	–	1.61	98	
463	8:39:02.8	19:26:12	G5 V	11.35	0.83	–	96	G5V[Wi]

Table A.1 continued

ID[a]	α (1950)	δ (1950)	Adopted Sp. Type	m_V^b	B-V	V-I	%[c]	Notes[d]
464	8:39:03.8	19:52:08	G2 V	11.06	0.73	–	99	G5V[SS]
466	8:39:06.4	20:17:12	K4 V	13.25	1.00	–	79	
472	8:39:19.9	19:27:24	K1 V	12.19	1.03	–	89	
473	8:39:20.8	19:23:35	K6 V	13.73	1.20	–	99	
474	8:39:21.3	19:26:50	K5 V	13.52	1.22	–	97	
478*	8:39:24.2	20:16:19	K7 V	14.10	–	1.47	98	
482	8:39:28.6	19:19:52	K5 V	13.51	1.24	–	97	
486	8:39:40.6	19:34:34	G2 V	11.06	0.67	–	97	
493	8:39:44.6	20:19:20	K6 V	13.88	–	1.23	98	
516	8:40:14.7	19:58:19	K5 V	13.67	–	1.25	98	
520*	8:40:16.3	19:53:37	K4 V	13.32	1.21	–	96	
526	8:40:22.9	20:14:46	K5 V	13.58	1.15	–	97	
531	8:40:28.2	19:56:59	G0 V	10.83	0.62	–	97	
554	8:40:59.7	20:05:41	K7 V	14.09	–	1.50	92	
556	8:41:04.8	19:54:24	K4 V	13.26	1.06	–	97	

* Spectrum plotted in Figure A.3

a ID numbers from Jones and Stauffer (1991).

b BVI photometry from Jones and Stauffer (1991).

c Probability of membership from Jones and Stauffer (1991).

d Previously published spectral types from:
[Ab]=Abt (1986), [Ba]=Barbier (1963),
[BB]=Boesgaard and Budge (1988), [Bi]=Bidelman (1956), [Bo]=Bolte (1991),
[CB]=Crawford and Barnes (1969), [CGa]=Corbally and Garrison (1986),
[CGb]=Corbally and Garrison (1983), [Jo]=Johnson (1952), [Po]=Popper (1948),
[Re]=Rebeirot (1966), [RS]=Randich and Schmitt (1994),
[SS]=Soderblom and Stauffer (1984), [St]=Stauffer (1982),
[Up]=Upgren et al. (1979), [Wi]=Wilson (1963).

Table A.2. Spectral Standards in M67

ID[a]	α (1950)	δ (1950)	Adopted Sp. Type	m_V^b	B-V	V-I	%[c]	Notes[d]
471	8:47:37.6	11:52:09	F6 V	13.660	0.580	–	96	1
611	8:47:54.5	11:57:51	K0 V	15.550	0.750	–	76	1
621	8:47:49.2	12:00:17	G1 V	14.490	0.630	–	87	1
711	8:48:09.2	11:42:36	F5 V	13.340	0.650	–	96	1
724	8:48:22.6	11:47:15	G2 V	14.570	0.680	–	93	1
744	8:48:03.1	11:54:10	F9 V	14.190	0.580	–	79	1
746	8:48:09.3	11:54:56	G0 V	14.380	0.709	0.800	94	2
748	8:48:15.6	11:55:24	G3 V	14.632	0.829	0.874	89	2
752	8:48:19.5	11:56:19	B9 V	11.320	0.290	0.379	99	2
753	8:48:08.2	11:56:19	G3 V	14.693	0.632	0.778	93	2
771	8:48:14.9	12:00:13	F6 V	13.557	0.554	0.684	96	2
777	8:48:03.9	12:00:57	G2 V	14.630	0.620	–	93	1
779	8:48:12.5	12:01:10	G3 V	14.700	0.720	–	85	1
785	8:48:15.7	12:02:29	G4 V	14.823	0.698	0.818	88	2
795	8:48:18.8	12:03:42	G5 V	14.997	0.741	0.852	62	2
799	8:48:11.5	12:04:11	G6 V	15.100	0.830	–	82	1
801	8:48:21.6	12:04:27	G6 V	15.094	0.721	–	87	2
807	8:48:02.1	12:05:46	F7 V	13.690	0.620	–	97	1
810	8:48:10.1	12:06:31	G7 V	15.160	0.920	–	71	1
814	8:48:17.4	12:07:32	G6 V	15.080	0.760	–	75	1
820	8:48:12.8	12:08:06	G6 V	15.040	0.840	–	77	1
829	8:48:14.2	12:10:55	G0 V	14.300	0.650	–	91	1
853	8:48:12.0	12:19:41	F4 V	13.270	0.650	–	98	1
943	8:48:44.7	11:49:49	G5 V	14.960	0.759	0.898	85	2
945	8:48:39.9	11:50:10	G2 V	14.528	0.665	–	93	2
951	8:48:26.8	11:51:08	G3 V	14.704	0.718	0.784	87	2
955	8:48:31.9	11:51:47	G4 V	14.860	0.700	–	74	1
958	8:48:30.3	11:52:26	G2 V	14.540	0.660	–	96	1

Continued, next page.

Table A.2 continued

ID[a]	α (1950)	δ (1950)	Adopted Sp. Type	m_V^b	B-V	V-I	%[c]		Notes[d]
965	8:48:40.7	11:54:24	G3 V	14.695	0.761	0.855	80	2	
968*	8:48:42.4	11:55:08	A2 V	11.280	0.130	0.179	99	2	
973	8:48:32.2	11:55:50	F5 V	13.491	0.630	0.707	97	2	
977*	8:48:27.7	11:56:39	B8 V	10.030	-0.07	–	99	1	
985	8:48:27.5	11:57:10	G7 V	15.141	0.878	0.852	62	2	
991	8:48:25.8	11:57:34	G2 V	14.564	0.684	0.796	91	2	
996	8:48:44.3	11:58:07	G5 V	14.972	0.891	0.995	91	2	
1001	8:48:24.3	11:58:29	F0 V	12.440	0.980	–	99	1	F72,RGO171,SI-17
1002	8:48:28.1	11:58:32	G6 V	15.107	0.777	0.883	60	2	
1004	8:48:40.2	11:58:46	G5 V	14.928	0.759	0.810	89	2	
1012	8:48:40.7	11:59:21	G2 V	14.516	0.737	0.874	88	2	
1019	8:48:39.2	11:59:44	G0 V	14.335	0.807	0.997	91	2	
1028*	8:48:30.7	12:00:17	G9 V	15.377	0.848	0.897	66	2	
1029	8:48:37.5	12:00:20	G8 V	15.214	0.793	0.881	72	2	
1032	8:48:42.4	12:00:38	F5 V	13.480	0.573	0.700	98	2	
1041	8:48:41.9	12:01:13	G3 V	14.718	0.729	0.832	83	2	
1050	8:48:34.1	12:01:37	F9 V	14.292	0.658	0.779	84	2	
1057	8:48:35.9	12:02:19	F9 V	14.303	0.675	0.758	81	2	
1061	8:48:29.5	12:02:35	F6 V	13.626	0.568	0.687	97	2	
1065	8:48:43.7	12:03:04	G3 V	14.645	0.800	0.873	77	2	
1078	8:48:43.3	12:04:20	F9 V	14.174	0.656	0.733	97	2	
1079	8:48:37.8	12:04:26	G8 V	15.267	0.818	0.868	63	2	
1088	8:48:32.4	12:05:32	F6 V	13.549	0.621	0.701	97	2	
1089	8:48:28.1	12:05:40	F9 V	14.199	0.666	0.717	91	2	
1095	8:48:24.9	12:08:17	G3 V	14.650	0.700	–	88	1	
1096	8:48:28.8	12:08:18	G2 V	14.540	0.740	–	94	1	
1106	8:48:23.7	12:10:10	G4 V	14.880	0.680	–	91	1	
1111	8:48:23.8	12:12:23	F6 V	13.660	0.540	–	97	1	

Table A.2 continued

ID[a]	α (1950)	δ (1950)	Adopted Sp. Type	m_V^b	B-V	V-I	%[c]	Notes[d]
1112	8:48:39.8	12:12:48	G6 V	15.030	0.810	–	92	1
1181	8:48:58.5	11:43:26	F3 V	13.090	0.730	–	99	1
1204	8:49:05.8	11:51:17	G3 V	14.650	0.900	–	83	1
1208	8:48:48.6	11:53:23	G2 V	14.600	0.840	–	92	1
1212	8:49:03.1	11:53:48	G8 V	15.320	0.782	0.899	83	2
1213	8:48:54.7	11:53:56	F8 V	14.114	0.600	0.716	98	2
1218	8:48:50.5	11:55:07	G2 V	14.590	0.684	0.754	97	2
1220	8:49:01.9	11:55:28	F5 V	13.371	0.572	0.648	99	2
1235	8:48:50.2	11:57:11	G5 V	14.980	0.877	0.951	87	2
1251	8:49:04.6	11:58:54	G4 V	14.790	0.750	0.851	81	2
1255	8:48:52.0	11:59:05	G1 V	14.486	0.666	0.774	94	2
1263*	8:48:48.5	12:00:10	A0 V	11.060	0.190	0.262	99	2
1267	8:49:04.5	12:00:34	A1 V	10.940	0.220	–	99	1
1269	8:48:57.8	12:00:56	G5 V	14.934	0.758	0.791	81	2
1284	8:48:50.2	12:02:28	B9 V	10.940	0.220	0.318	99	2
1289	8:48:46.2	12:02:40	G4 V	14.901	0.762	0.840	94	2
1307*	8:48:48.7	12:05:03	G7 V	15.167	0.807	0.870	80	2
1309	8:48:52.4	12:05:45	G7 V	15.158	0.832	0.866	86	2
1330	8:48:58.5	12:10:49	F9 V	14.140	0.630	–	82	1
1341	8:48:46.4	12:15:34	G4 V	14.740	0.680	–	94	1
1422	8:49:12.1	11:50:33	G2 V	14.580	0.780	–	86	1
1426	8:49:27.4	11:51:52	F9 V	14.250	0.620	–	91	1
1434	8:49:26.7	11:55:26	A1 V	10.700	0.110	–	97	1
1441	8:49:18.7	11:57:23	F4 V	13.151	0.572	0.683	98	2
1452	8:49:19.4	11:59:08	G2 V	14.578	0.672	0.746	86	2
1461	8:49:23.8	12:01:10	F7 V	13.890	0.560	–	95	1
1473	8:49:12.1	12:04:55	G6 V	15.055	0.775	0.827	83	2

Table A.2 continued

ID[a]	α (1950)	δ (1950)	Adopted Sp. Type	m_V^b	B-V	V-I	%[c]	Notes[d]
1477	8:49:09.1	12:05:38	G2 V	14.593	0.718	0.747	91	2
1484	8:49:09.1	12:07:36	G2 V	14.570	0.900	–	88	1
1491	8:49:13.8	12:12:19	F6 V	13.680	0.760	–	94	1
1616	8:49:31.3	12:04:22	G2 V	14.537	0.684	0.768	85	2
2211	8:49:24.4	11:59:30	F7 V	13.762	0.581	0.673	76	2
2213	8:48:27.9	11:59:43	G4 V	14.867	0.726	0.805	57	2
489	8:47:32.1	12:05:02	G2 IV	12.760	0.680	–	97	1
591	8:47:58.0	11:48:08	G2 IV	12.670	0.730	–	98	1; RGO3
598	8:47:50.4	11:51:11	G0 IV	12.650	0.610	–	99	1; RGO38
606	8:47:52.1	11:54:33	G8 IV	12.780	0.860	–	98	1; F4,RGO79,SI-73
751	8:48:03.6	11:56:07	F7 IV	12.770	0.460	–	99	1; F16,RGO113,SI-41
756	8:48:19.2	11:57:04	G0 IV	12.673	0.620	0.726	98	2; F54,RGO119,SI-25
775	8:48:17.4	12:00:50	G0 IV	12.687	0.631	0.711	99	2; F51,RGO254,SIV-60
781	8:48:16.9	12:01:27	G2 IV	12.725	0.739	0.830	97	2; F48,RGO252,SIV-59
792	8:48:11.5	12:03:30	F9 IV	12.040	0.600	0.671	99	2; F30,RGO334;SIV-76
806	8:48:16.0	12:05:48	G5 IV	12.782	0.813	0.893	99	2; F46,RGO411,SIV-81
815	8:48:10.2	12:07:45	F8 IV	12.890	0.510	–	98	1
926	8:48:42.1	11:44:18	G4 IV	12.530	0.810	–	98	1; SI-82
961	8:48:25.5	11:53:02	G2 IV	12.830	0.710	–	99	1; F79,RGO87,SI-62
997*	8:48:35.8	11:58:18	F5 IV	12.126	0.458	0.562	99	2; F124,RGO186
1000*	8:48:39.7	11:58:33	G4 IV	12.835	0.783	0.854	80	2; F144,RGO195,SI-243
1007*	8:48:41.3	11:58:52	F9 IV	12.533	0.589	0.694	99	2; F149,RGO201
1024*	8:48:38.8	12:00:07	F7 IV	12.718	0.553	0.685	99	2; RGO283,SIII-4
1034	8:48:34.4	12:00:39	F9 IV	12.647	0.608	0.723	99	2; F115,RGO278
1045	8:48:34.9	12:01:23	F9 IV	12.540	0.591	0.703	99	2; F119,RGO279
1053	8:48:29.5	12:01:55	G1 IV	12.286	0.676	0.741	99	2; F88,RGO267,SIV-236
1069*	8:48:44.7	12:03:18	G1 IV	12.677	0.684	0.761	99	2; F163,RGO370,SII-17
1076	8:48:31.6	12:04:16	F9 IV	12.831	0.567	0.685	98	2

Table A.2 continued

ID[a]	α (1950)	δ (1950)	Adopted Sp. Type	m_V^b	B-V	V-I	%[c]	Notes[d]
1082	8:48:36.6	12:04:43	F5 IV	11.250	0.410	0.529	99	2; F131,RGO47; F4IV[BB],F0IV[Pe]
1216	8:48:57.9	11:54:56	F8 IV	12.690	0.564	0.675	99	2; F216,RGO142,SII-36
1231	8:48:45.3	11:56:45	K0 IV	12.934	0.917	0.972	98	2; F166,RGO136,SII-22
1245*	8:49:00.7	11:58:05	K0 IV	12.934	0.919	0.940	98	2; F227,RGO222; K0III-IV[BB]
1270	8:49:05.0	12:01:02	F8 IV	12.729	0.577	0.704	99	2; F241,RGO315
1271	8:48:50.2	12:01:02	F8 IV	12.909	0.534	0.665	99	2
1285	8:49:04.2	12:02:31	G1 IV	12.505	0.663	0.764	98	2; F236,RGO388,SIII-53
1310	8:48:57.1	12:05:47	F8 IV	12.760	0.580	0.650	99	2; F216,RGO429,SIII-47
1319	8:49:04.6	12:08:10	K0 IV	12.950	0.950	–	99	1; F237,RGO481,SIII-75
1323	8:48:51.2	12:09:14	G2 IV	12.890	0.720	–	99	1; F192,RGO472,SIII-82
1415	8:49:09.5	11:49:52	F8 IV	12.710	0.570	–	99	1; F256,RGO66,SII-110
1438*	8:49:27.3	11:56:58	G5 IV	12.889	0.817	0.870	98	2; F281,RGO154,SII-129
1456	8:49:09.3	11:59:40	F8 IV	12.705	0.575	0.663	99	2; F255,RGO317
1463	8:49:12.0	12:01:34	K0 IV	12.910	1.000	–	98	1; F262,RGO319,SIII-57
1485	8:49:07.2	12:09:09	F8 IV	12.870	0.550	–	98	1; F248,RGO482,SIII-92
1506	8:49:08.5	12:15:38	F8 IV	12.730	0.570	–	98	1; F252,SIII-114
1508	8:49:15.6	12:16:18	G2 IV	12.730	0.700	–	96	1
1589	8:49:34.7	11:54:45	G0 IV	12.660	0.610	–	98	1; F287,RGO156,SII-139
2208	8:48:48.3	11:59:19	F5 IV	12.777	0.822	0.882	97	2; F181,RGO208,SII-6
2212	8:48:46.5	12:00:31	F9 IV	12.725	0.587	0.704	99	2; F174,RGO299,SIII-1
721	8:48:05.7	11:46:24	K1 III	11.240	1.100	1.070	98	2; RGO6
989	8:48:37.5	11:57:23	K1 III	11.450	1.060	–	99	1; F135,RGO192; K2III[Po]
1016*	8:48:33.0	11:59:33	K2 III	10.300	1.260	1.230	98	2; F105,RGO180;K2III[BB]
1040	8:48:39.7	12:01:07	G4 III	11.520	0.870	0.910	99	2; F143,RGO286; G8IV[BB],K0III+[Po]
1074	8:48:28.5	12:03:59	K1 III	10.590	1.120	1.090	98	2; F84,RGO351

Table A.2 continued

ID[a]	α (1950)	δ (1950)	Adopted Sp. Type	m_V^b	B-V	V-I	%[c]	Notes[d]
1084	8:48:42.0	12:05:09	K1 III	10.480	1.100	–	98	1; F151,RGO419;K0III[BB]
1221	8:48:59.5	11:55:45	K1 III	10.760	1.130	1.100	99	2; F224,RGO143;K1III[BB]
1237*	8:49:06.1	11:57:26	G8 III	10.780	0.940	0.960	98	2; F244,RGO227; G8III-IV[BB]
1254	8:49:01.0	11:59:04	K1 III	11.520	1.050	–	99	1
1277	8:48:58.2	12:01:26	K1 III	11.630	1.050	–	98	1; F218,RGO312,SIII-32
1279	8:48:44.9	12:01:51	K1 III	10.550	1.120	1.090	99	2; F164,RGO295;K1III[Po]
1288	8:48:58.2	12:02:41	K1 III	11.330	1.070	–	99	1; F217,RGO387,SIII-34
1293	8:48:55.2	12:03:04	K0 III	12.094	1.007	1.016	97	2; RGO385,SIII-35
1305	8:48:51.6	12:04:53	K0 III	12.230	0.993	1.002	99	2; F193,RGO426
1316	8:48:59.7	12:08:01	K1 III	10.580	1.100	1.080	99	2; F223,RGO478
1592	8:49:34.6	11:55:47	K0 III	10.470	1.120	1.040	97	2; F286,RGO155,SII-138

* Spectrum plotted in Figure A.3.

a ID numbers after Sanders (1977).

b Probability of membership from Girard et al. (1989).

c Photometry references: 1=BV photometry from Girard et al. (1989), 2=BVI photometry from Montgomery et al. (1993).

d Identification cross-references: F=Fagerholm ID, RGO=Royal Greenwich Observatory ID, S=Sandage ID.

e Previously published spectral types from: [BB]=Burbidge and Burbidge(1959), [Pe]=Pesch (1967), [Po]=Popper (1954).

Table A.3. Field Giants

ID	α (1950)	δ (1950)	Sp. Type
SAO 30509	17:39:05.7	+56:53:46	K7III
HR 4371*	11:14:43.0	+02:17:08	M0III
β And	01:06:55.4	+35:21:21	M0III
HR 4666*	12:13:37.5	+40:56:18	M0.5III
HR 4517*	11:43:17.3	+06:48:34	M1III
HR 5150*	13:38:59.0	−08:27:05	M1.5III
χ Peg	00:12:00.7	+19:55:43	M2III
HR 5181*	13:44:41.9	−17:36:37	M2III
HR 5095*	13:29:21.7	−05:59:53	M2.5III
SAO 63349*	13:04:37.4	+31:22:22	M3III
HR 4362	11:12:32.8	+23:22:06	M3IIb
HR 5226*	13:49:58.2	+64:58:11	M3.5III
HR 8621	22:36:39.5	+56:32:08	M4III
HR 4532*	11:46:13.3	−26:28:17	M4III
HR 4267*	10:53:25.7	+06:27:09	M5.5III
BK Vir*	12:27:48.1	+04:41:34	M7III

* Spectrum plotted in Figure A.3

Table A.4. Useful Spectral Features

λ(Å)	Identification	Notes	Ref.
5847–6058	TiO	Late K through M.	1
5893	Na I	Weak in B. Strength increases with decreasing T_{eff}. Part Interstellar.	1
6080–6390	TiO	Mid K through M.	1
6122	Ca I	Weak in A-F. Strength increases with decreasing T_{eff}.	1
6162	Ca I	Weak in A. Strength increases with . decreasing T_{eff}. Stronger than λ 6122.	1
6346,6382,6389	CaH	Mid K through M	1,2
6497	Ba II, Fe I, Ca I	F through M. Useful relative to Hα.	1,2
6563	Hα	Maximum at A0. Sometimes in emission in M.	1,2
6651–6852	TiO	Mid K through M.	1,2
6750–7050	CaH	Mid K through M. Weaker in giants than in dwarfs.	1,2
6867	Telluric O_2		
7053–7270	TiO	Mid K through M.	1,2
7186	Telluric H_2O		
7749	Fe I	K dwarfs.	1
7750–7861	TiO	M stars.	1,2
7773	O I	Strong in A. Absent by late F.	1
7834	Fe I	K dwarfs.	1
7851–7973	VO	M stars.	1,2
7937	Fe I	K dwarfs.	1
8195	Na I	Strongest in late F, but difficult to distinguish from telluric H_2O at λ 8200.	1,2
8200	Telluric H_2O		
8206–8569	TiO	M stars.	1,2
8498,8542,8662	Ca II	Maximum at mid K. Stronger in giants than in dwarfs.	1,2
8807	Mg I	Seen in all.	1,2
8859–8937	TiO	Late M.	1,2

1 Torres-Dodgen & Weaver 1993
2 Kirkpatrick et al. 1991

Appendix B

Photometric and Spectroscopic Data in L1641

We present relevant data in tabular form for stars in the spectroscopic sample. For each of the four regions surveyed, two tables are shown: one containing source designations (adopted from our spectroscopic survey), positions, and optical and near-infrared photometry, and the other containing derived quantities. Sources whose spectra show Ca II in emission are noted.

Table B.1. L1641 North: Optical and Near–Infrared Photometry

ID	α (1950)	δ (1950)	R	I	J	H	K
58	5:32:51.54	−6:26:31.0	14.29	13.07	11.69	10.88	10.40
70	5:32:51.55	−6:34:16.5	14.62	13.33	12.14	11.46	11.22
191	5:32:52.00	−6:26:23.1	17.62	15.56	13.68	13.05	12.65
137	5:32:52.74	−6:29:18.2	16.50	14.73	13.23	12.53	12.09
95	5:32:53.08	−6:26:07.0	15.33	14.04	12.91	12.19	11.92
709	5:32:54.53	−6:20:14.9	16.64	17.89	16.11	15.30	14.19
65	5:32:56.05	−6:22:36.0	14.12	13.18	12.51	11.48	11.34
108	5:32:57.39	−6:35:33.6	15.73	14.38	12.67	11.85	11.49
54	5:32:57.41	−6:30:16.6	14.62	12.96	11.58	10.87	10.60
210	5:32:58.21	−6:29:39.4	17.57	15.94	14.66	13.95	13.66
225	5:32:58.26	−6:34:55.1	17.51	16.14	14.67	13.78	13.35
148	5:32:58.30	−6:30:32.7	16.73	14.84	13.23	12.59	12.26
222	5:32:58.40	−6:25:34.0	17.63	16.10	14.84	14.20	13.90
97	5:32:59.41	−6:25:11.0	15.57	14.07	12.84	12.10	11.86
69	5:33:00.22	−6:21:01.2	14.71	13.24	11.69	10.80	10.48
61	5:33:00.60	−6:28:39.6	14.11	13.18	12.22	11.52	11.32
57	5:33:00.83	−6:21:34.0	14.18	12.84	11.28	10.49	10.09
121	5:33:02.81	−6:18:21.5	16.12	14.09	11.59	10.66	10.27
25	5:33:08.46	−6:23:42.8	.....	.....	9.64	9.28	9.19
68	5:33:10.42	−6:18:22.2	14.06	13.12	11.99	11.32	11.11
145	5:33:12.30	−6:25:34.2	16.41	14.81	13.48	12.78	12.52
102	5:33:13.55	−6:34:01.9	15.60	14.27	12.66	11.73	11.35
44	5:33:14.73	−6:24:36.1	13.62	12.38	11.02	10.26	9.85
80	5:33:16.68	−6:36:42.4	.....	.....	13.67	12.84	12.41
60	5:33:20.98	−6:31:00.6	14.54	12.73	11.31	10.65	10.32
106	5:33:21.19	−6:35:13.5	15.71	14.26	12.99	12.31	12.03
1	5:33:21.26	−6:33:21.7	.....	.....	11.06	10.45	10.32
98	5:33:21.33	−6:23:26.6	15.39	14.12	12.73	11.92	11.32
100	5:33:21.90	−6:19:49.7	15.60	14.18	12.95	12.24	12.00
126	5:33:21.99	−6:19:26.5	16.23	14.52	13.11	12.39	12.11

Continued, next page.

Table B.1 continued

ID	α (1950)	δ (1950)	R	I	J	H	K
116	5:33:24.13	−6:35:25.6	16.21	14.45	13.99	13.41	13.17
89	5:33:24.44	−6:35:07.6	15.39	13.91	12.65	12.10	11.77
46	5:33:29.19	−6:17:46.0	12.77	12.36	11.93	11.58	11.47
73	5:33:30.40	−6:25:44.5	.....	.....	12.71	12.13	11.98
93	5:33:30.88	−6:17:27.5	15.25	13.98	12.69	11.91	11.44
53	5:33:31.05	−6:18:25.4	14.30	12.85	11.66	11.22	10.80
172	5:33:31.69	−6:16:41.1	16.88	15.13	13.46	13.03	12.60
43	5:33:32.77	−6:18:17.8	.....	.....	8.59	8.56	8.18
7	5:33:33.33	−6:17:56.1	12.86	11.89	10.59	10.10	9.41
125	5:33:33.99	−6:25:36.8	16.29	14.57	13.06	12.48	12.23
161	5:33:34.06	−6:18:08.0	16.28	14.95	13.66	13.06	12.89
77	5:33:34.67	−6:17:21.0	14.62	13.49	12.13	11.50	10.89
118	5:33:34.82	−6:26:56.9	16.07	14.53	13.15	12.55	12.14
20	5:33:37.86	−6:22:33.0	.....	.....	9.88	9.73	9.64
31	5:33:37.86	−6:22:33.4	.....	.....	9.88	9.73	9.64
136	5:33:38.26	−6:36:28.0	16.23	14.70	14.37	13.81	13.55
52	5:33:38.89	−6:31:21.1	13.81	12.90	11.82	10.91	10.26
63	5:33:38.91	−6:27:14.4	14.25	13.09	11.85	11.21	10.94
66	5:33:40.20	−6:16:14.9	13.95	12.88	11.21	10.63	9.75
143	5:33:40.44	−6:33:31.6	16.35	14.76	13.53	12.81	12.55
76	5:33:40.51	−6:34:05.8	14.83	13.52	11.54	10.31	9.49
62	5:33:40.56	−6:20:42.3	14.89	13.11	11.48	11.05	10.52
132	5:33:42.05	−6:26:26.5	16.89	14.73	12.77	12.17	11.79
71	5:33:42.95	−6:18:59.6	14.69	13.35	12.08	11.58	11.09
56	5:33:43.11	−6:20:25.0	14.18	12.99	11.77	11.30	10.85
244	5:33:43.24	−6:26:22.3	18.25	16.44	14.63	14.05	13.68
236	5:33:43.81	−6:20:43.5	17.82	16.33	14.28	13.42	12.94
49	5:33:44.07	−6:21:50.2	13.26	12.56	11.74	11.08	10.90
59	5:33:44.77	−6:35:36.0	14.50	13.11	12.76	12.10	11.82
128	5:33:46.31	−6:25:28.0	16.42	14.51	12.66	11.73	11.27
733	5:33:46.50	−6:25:23.0	15.33	13.52	11.35	10.29	9.79
112	5:33:46.89	−6:27:29.3	15.86	14.42	13.14	12.57	12.25

Table B.1 continued

ID	α (1950)	δ (1950)	R	I	J	H	K
36	5:33:47.24	−6:29:19.3	12.75	12.32	11.76	11.38	11.27
15	5:33:48.67	−6:19:25.2	12.94	12.15	11.13	10.46	10.08
11	5:33:48.93	−6:25:43.7	.....	.....	9.80	9.59	9.49
82	5:33:49.24	−6:19:27.2	14.54	13.68	12.53	11.78	11.52
111	5:33:49.40	−6:16:39.0	15.75	14.33	13.04	12.34	12.14
83	5:33:51.50	−6:30:24.3	15.21	13.90	12.59	11.90	11.68
64	5:33:52.13	−6:22:26.7	14.23	13.26	12.23	11.54	11.14
157	5:33:52.56	−6:23:52.1	16.40	16.44	13.68	12.99	12.20
74	5:33:53.65	−6:33:07.0	14.67	13.54	12.57	11.82	11.62
113	5:33:54.69	−6:19:05.0	16.21	14.37	12.80	12.25	11.97
47	5:33:54.74	−6:32:57.7	13.33	12.49	11.67	10.96	10.79
265	5:33:55.57	−6:25:17.7	19.48	16.56	13.18	11.40	10.16
124	5:33:55.59	−6:27:49.7	15.69	14.33	12.14	11.00	10.10
174	5:33:55.69	−6:29:17.6	16.59	15.14	13.82	13.32	13.04
21	5:33:56.17	−6:28:48.1	.....	.....	8.78	8.28	7.84
129	5:33:56.89	−6:21:25.2	16.29	14.72	13.38	12.77	12.45
285	5:33:57.53	−6:24:58.9	16.68	15.43	13.33	11.95	10.46
154	5:33:57.98	−6:33:37.0	.....	.....	13.66	12.98	12.62
9	5:33:58.58	−6:19:20.0	.....	.....	9.17	8.51	8.21
214	5:33:59.83	−6:26:38.6	17.66	16.09	14.86	13.60	12.74
293	5:33:59.84	−6:28:02.9	19.74	17.03	14.25	13.62	13.14
42	5:34:00.46	−6:28:16.2	13.68	12.48	11.11	10.35	10.05
267	5:34:00.69	−6:22:54.9	.....	.....	15.68	14.90	15.18
140	5:34:02.98	−6:17:32.4	16.46	14.71	13.33	12.73	12.53
72	5:34:03.79	−6:24:57.0	14.51	13.46	12.61	11.44	10.58
142	5:34:03.87	−6:36:38.1	16.10	14.76	14.59	14.01	13.71
273	5:34:04.20	−6:25:43.4	.....	.....	15.10	14.52	14.41
206	5:34:04.31	−6:31:53.8	17.66	15.83	14.59	14.05	13.71
739	5:34:04.70	−6:29:01.0	.....	.....	8.61	8.46	8.34
187	5:34:05.98	−6:29:28.4	17.14	15.44	14.01	13.36	12.98
2	5:34:06.01	−6:21:06.6	.....	.....	11.34	10.57	10.04
6	5:34:06.19	−6:32:01.7	.....	.....	11.71	11.23	11.19

Table B.1 continued

ID	α (1950)	δ (1950)	R	I	J	H	K
55	5:34:06.25	−6:33:21.6	14.72	13.01	10.84	9.68	9.21
103	5:34:06.90	−6:35:46.5	15.52	14.27	13.67	13.07	12.77
119	5:34:10.09	−6:16:11.7	15.75	14.32	13.00	.....	12.07
78	5:34:10.82	−6:35:10.6	14.71	13.59	13.74	12.51	11.31
258	5:34:11.07	−6:17:54.1	18.67	16.51	14.58	14.10	13.61
127	5:34:11.22	−6:35:55.7	15.79	14.62	14.14	13.55	13.24
170	5:34:11.75	−6:26:11.6	16.82	15.15	13.77	13.18	12.94
51	5:34:14.51	−6:31:55.4	13.77	12.82	11.93	11.22	10.93
67	5:34:15.25	−6:35:46.4	.....	.....	11.90	11.01	10.32
220	5:34:15.63	−6:22:31.6	17.65	15.64	13.99	13.44	13.08
147	5:34:17.34	−6:17:14.4	16.21	14.53	13.08	12.47	12.11
205	5:34:18.52	−6:17:50.6	17.48	15.65	14.08	13.45	13.14
155	5:34:18.73	−6:30:57.9	16.61	14.97	13.68	13.10	12.77
81	5:34:18.99	−6:29:55.3	15.28	13.68	12.28	11.59	11.30

Table B.2. L1641 North: Effective Temperatures and Luminosities

ID	Sp. Type	$\log(T_{eff})$	A_v	$L/L_\odot$	W(Hα)	Notes
58	M2	3.544	0.40	-0.04	24	
70	M2.5	3.534	0.21	-0.26	...	...
191	M3.5	3.512	3.49	-0.56	...	...
137	M4	3.498	0.85	-0.67	80	...
95	M2.5	3.534	0.19	-0.57	...	...
709	E	...	...	...	...	...
65	K7	3.602	1.09	-0.24	...	...
108	F8	3.792	6.71	0.53	...	...
54	M3.5	3.512	0.98	0.02	...	...
210	M3.5	3.512	0.83	-1.23	59	...
225	K7	3.602	3.73	-0.83	...	...
148	M5	3.477	0.0:	-0.78	13	...
222	M3	3.525	1.00	-1.26	...	...
97	M3	3.544	0.79	-0.48	...	...
69	M2	3.544	1.89	0.12	...	...
61	M0	3.580	0.13	0.15	...	...
57	M2.5	3.534	0.49	0.11	10	...
121	M5	3.477	0.76	-0.04	14	...
25	F7	3.799	0.73	1.12	...	...
68	M0	3.580	0.19	-0.15	...	...
145	M3	3.525	1.41	-0.68	13	...
102	K3	3.675	5.24	0.19	...	...
44	M1	3.562	1.37	0.35	14	...
80	M0.5	3.571	1.27	-0.31	...	...
60	M4	3.498	1.13	0.12	...	...
106	M2.5	3.534	1.18	...	...	...
1	K3	3.675	0.64	0.34	...	...
98	M4	3.498	0.0:	-0.56	30	Ca II
100	M2	3.544	1.59	-0.42	10	...
126	M4	3.498	0.53	-0.66	11	...

Continued, next page.

Table B.2 continued

ID	Sp. Type	log(T_{eff})	A_v	$L/L_\odot$	W(Hα)	Notes
116	M4	3.498	0.81	-0.58	...	...
89	M3.5	3.512	0.0:	-0.58	...	...
46	G7	3.735	0.33	0.06	...	...
73	K5	3.643	0.0:	-0.44	...	...
93	M3	3.525	0.0:	-0.52	60	...
53	M3	3.525	0.49	-0.05	...	...
172	M6	3.447	0.0:	-0.88	13	...
43	B6	4.114	0.91	2.40	...	...
7	M0	3.580	0.36	0.43	20	...
125	M4	3.498	0.60	-0.63	...	...
161	M3	3.525	0.0:	-0.90	...	...
77	M1	3.562	0.68	-0.17	120	...
118	M3.5	3.512	0.25	-0.69	45	...
20	F5	3.809	0.0:	0.98	...	...
31	A5	3.984	0.64	1.45	...	...
136	M3	3.525	1.00	-0.68	...	...
52	M0	3.580	0.0:	-0.10	14	...
63	M1.5	3.553	0.49	-0.08	...	...
66	M0	3.580	1.04	0.25	22/40	Ca II
143	M3.5	3.512	0.59	-0.81	...	...
76	K5	3.643	4.80	0.54	18	...
62	M4.5	3.488	0.09	-0.06	10	...
132	M6	3.447	0.0:	-0.61	17	...
71	M2.5	3.534	0.50	-0.20	...	...
56	M2	3.544	0.16	-0.10	...	...
244	M4.5	3.488	0.25	-1.31	188	...
236	K5	3.643	5.98	-0.43	13	...
49	K3	3.675	1.26	0.13	...	...
59	M3	3.525	0.12	-0.13	...	...
128	M5	3.477	0.0:	-0.56	36	...
733	M2:	3.544	4.06	0.48	...	...
112	M3	3.525	0.41	-0.65	...	...

Table B.2 continued

ID	Sp. Type	log(T_{eff})	A_v	$L/L_\odot$	W(Hα)	Notes
36	G6	3.750	0.54	0.16	...	...
15	K5	3.643	1.53	0.36	11	...
11	F7	3.799	0.0:	0.98	...	...
82	K7	3.602	0.56	-0.31	...	...
111	M2.5	3.534	0.94	-0.54	63/105	...
83	M2.5	3.534	0.32	-0.43	...	...
64	M0	3.580	0.40	-0.22	75	...
157	M3	3.525	0.0:	-0.91	...	...
74	M0.5	3.571	1.03	-0.30	...	...
113	M5	3.477	0.0:	-0.61	14	...
47	K3	3.675	2.21	0.26	...	...
265	M1	3.562	11.89	0.60	10	...
124	K7	3.602	3.65	0.17	71	Ca II
174	M3	3.525	0.53	-0.91	...	...
21	K0	3.720	0.45	1.30	...	...
129	M3.5	3.512	0.45	-0.76	...	...
285	E	...	...	...	225	Ca II
154	M4.5	3.488	0.63	-0.88	...	...
9	K1	3.706	2.27	1.32	...	...
214	M1	3.562	3.47	-0.97	...	...
293	M3.5III	3.544	7.55	-0.30	10	...
42	M0.5	3.571	1.47	0.33	...	...
267	M3	3.525	1.45	-1.56	15	...
140	M4	3.498	0.79	-0.72	...	...
72	M0.5	3.571	0.57	-0.37	13	...
142	M2.5	3.534	0.50	-0.81	...	...
273	M4.5	3.488	0.0:	-1.52	...	...
206	M4	3.498	1.24	-1.17	...	...
739	B8	4.041	1.82	2.25	...	...
187	M4	3.498	0.43	-1.03	...	...
2	G8	3.729	3.73	0.64	...	...
6	G6	3.750	1.27	0.25	...	...

Table B.2 continued

ID	Sp. Type	log(T_{eff})	A_v	$L/L_\odot$	W(Hα)	Notes
55	K5III	3.643	7.31	1.09	...	...
103	G4	3.763	5.81	0.37	...	...
119	M3	3.525	0.35	-0.60	...	...
78	K8	3.602	2.19	-0.22	110	Ca II
258	M0	3.580	7.82	-0.38	...	...
127	K3	3.675	4.25	-0.11	...	...
170	M3.5	3.512	1.05	-0.85	...	...
51	M0	3.580	0.23	-0.12	...	...
67	M0	3.580	1.82	0.46	148	...
220	M6	3.447	0.0:	-1.09	17	...
147	M4	3.498	0.28	-0.67	10	...
205	M4.5	3.488	0.36	-1.07	...	...
155	M3.5	3.512	0.87	-0.83	...	...
81	M3.5	3.512	0.61	-0.30	12	...

Table B.3. L1641 South: Optical and Near–Infrared Photometry

ID	α (1950)	δ (1950)	R	I	J	H	K
9	5:39:12.15	-8:08:31.6	...	...	11.90	11.23	11.07
61	5:39:14.59	-8:03:57.6	...	...	13.04	12.43	12.21
127	5:39:19.25	-8:08:01.4	...	...	14.74	14.14	13.66
92	5:39:20.39	-8:06:02.6	...	...	13.21	12.33	11.99
147	5:39:23.96	-8:05:28.5	...	...	14.62	14.02	13.55
18	5:39:25.37	-8:01:55.5	...	...	9.43	8.68	7.98
52	5:39:29.43	-8:08:55.9	...	...	11.77	10.79	10.34
119	5:39:30.31	-8:00:35.7	...	...	12.40	11.16	10.34
41	5:39:37.16	-8:07:51.3	...	...	13.40	12.82	12.69
130	5:39:37.26	-8:08:15.4	...	...	13.01	12.27	11.86
90	5:39:41.24	-8:02:27.9	...	...	13.27	12.46	12.07
355	5:39:43.00	-8:06:46.9	19.43	17.25	14.34	13.54	12.92
6	5:39:43.22	-8:04:19.4	12.12	11.70	10.91	10.47	10.34
173	5:39:46.30	-8:08:57.3	18.04	16.08	13.90	13.29	12.87
171	5:39:46.71	-8:02:27.6	17.89	16.16	14.28	13.61	13.21
5	5:39:47.39	-8:09:27.4	13.17	12.39	11.15	10.56	10.32
37	5:39:47.44	-8:03:58.4	14.85	12.75	9.62	8.39	7.69
107	5:39:48.18	-8:07:11.7	17.10	15.58	13.10	12.01	11.50
235	5:39:49.34	-8:11:23.7	18.66	16.64	13.99	13.02	12.16
30	5:39:51.27	-8:07:46.4	14.53	13.29	11.21	10.33	9.90
34	5:39:51.32	-8:08:38.7	14.72	14.03	13.04	12.39	12.25
154	5:39:53.36	-8:08:51.9	17.69	15.94	14.09	13.32	12.94
14	5:39:53.39	-8:05:04.4	14.15	13.30	12.06	11.46	11.19
53	5:39:53.45	-8:09:16.5	15.68	14.75	13.60	12.98	12.80
19	5:39:53.92	-8:09:32.7	14.33	13.42	11.97	11.27	11.02
84	5:39:54.46	-8:05:33.2	16.63	15.16	13.25	12.56	12.27
162	5:39:54.50	-8:08:50.9	17.82	16.12	14.02	13.31	12.87
7	5:39:55.28	-8:07:28.9	12.37	11.39	9.76	9.27	8.91
179	5:39:55.32	-8:06:29.1	17.93	16.18	13.76	12.83	12.43
220	5:39:57.13	-8:08:09.2	18.45	16.48	13.81	12.76	12.26

Continued, next page.

Table B.3 continued

ID	α (1950)	δ (1950)	R	I	J	H	K
33	5:39:57.38	-8:09:51.3	14.52	13.56	12.09	11.37	11.04
110	5:39:59.45	-8:10:31.7	16.94	15.26	13.21	12.25	11.49
43	5:39:59.78	-8:11:07.3	15.07	13.91	12.11	11.34	10.97
422	5:40:00.03	-8:08:14.1	19.91	17.87	14.89	13.94	13.23
21	5:40:00.33	-8:06:28.2	14.28	13.18	11.98	11.33	11.07
44	5:40:01.18	-8:11:39.3	15.08	13.95	12.20	11.41	11.15
13	5:40:01.28	-8:09:58.6	13.74	12.73	11.11	10.52	10.21
108	5:40:01.29	-8:11:16.7	18.20	16.45	13.71	12.55	11.73
305	5:40:02.55	-8:08:28.4	19.52	17.30	14.93	13.97	13.46
69	5:40:02.80	-8:10:38.2	16.03	14.71	13.27	12.83	12.54
272	5:40:03.37	-8:12:25.0	19.13	16.99	14.64	13.87	13.60
68	5:40:03.44	-8:11:13.7	16.26	14.84	12.80	11.94	11.23
142	5:40:03.64	-8:09:47.6	17.59	15.90	13.60	12.55	12.10
172	5:40:04.12	-8:13:07.7	18.36	16.70	15.02	14.45	14.16
35	5:40:04.52	-8:10:33.4	14.75	13.65	11.87	11.12	10.81
114	5:40:05.58	-8:08:47.2	17.18	15.54	13.27	12.27	11.84
46	5:40:05.99	-8:11:39.3	15.39	14.30	12.70	11.97	11.71
12	5:40:06.24	-8:10:35.8	11.66	10.76	9.38	8.81	8.52
201	5:40:06.31	-8:07:10.6	18.33	16.48	14.44	13.73	13.37
47	5:40:06.40	-8:08:31.5	15.51	13.97	11.76	10.83	10.41
82	5:40:06.78	-8:07:59.0	16.94	15.27	13.05	12.22	11.57
137	5:40:07.03	-8:03:56.1	17.46	15.66	13.63	13.02	12.68
174	5:40:07.35	-8:09:43.6	18.07	15.94	13.23	12.18	11.62
60	5:40:08.24	-8:08:44.8	16.10	14.63	12.46	11.54	11.15
169	5:40:08.45	-8:03:15.6	17.81	16.44	15.03	14.75	14.10
195	5:40:08.51	-8:11:28.6	18.23	16.28	13.97	13.10	12.74
155	5:40:08.55	-8:08:25.4	17.40	15.59	13.25	12.48	12.05
3	5:40:09.48	-8:08:35.8	10.47	9.94	9.28	9.10	8.95
59	5:40:09.86	-8:11:20.5	15.83	14.40	12.05	11.05	10.65
202	5:40:10.01	-8:03:32.7	18.26	16.35	14.16	13.50	13.10
182	5:40:11.11	-8:08:39.2	18.18	16.36	14.12	13.37	13.02
250	5:40:11.22	-8:10:10.7	18.92	16.94	13.76	12.56	12.04

Table B.3 continued

ID	α (1950)	δ (1950)	R	I	J	H	K
4	5:40:11.46	-8:09:02.5	12.75	11.92	10.64	10.20	9.95
372	5:40:12.25	-8:11:38.4	19.71	17.58	14.70	14.03	13.50
8	5:40:13.90	-8:18:23.3	...	...	13.35	12.47	12.16
76	5:40:15.76	-8:06:33.4	16.25	15.27	13.53	12.97	12.65
144	5:40:15.81	-8:06:28.0	16.90	15.53	13.44	12.84	12.50
273	5:40:16.41	-8:02:41.4	18.85	17.89	16.39	15.62	16.43
86	5:40:17.62	-8:02:35.2	16.51	15.52	14.04	13.49	13.25
39	5:40:17.90	-8:04:52.1	14.87	14.02	12.69	12.20	12.01
164	5:40:18.06	-8:16:35.5	14.87	14.03	13.42	12.46	11.71
2	5:40:18.10	-8:07:41.6	10.71	10.39	9.95	9.79	9.70
50	5:40:19.15	-8:07:59.8	15.53	14.47	13.29	12.73	12.52
49	5:40:19.89	-8:07:46.3	15.86	14.61	12.80	11.95	11.29
153	5:40:20.14	-8:02:39.0	17.62	16.78	15.39	14.85	15.08
16	5:40:21.34	-8:09:17.9	14.14	13.60	12.75	12.19	12.04
1	5:40:21.53	-8:06:34.7	10.69	10.40	9.96	9.81	9.69
64	5:40:21.64	-8:05:00.3	16.02	15.17	14.07	13.51	13.18
112	5:40:21.80	-8:03:00.3	17.04	16.09	14.76	14.11	14.03
88	5:40:22.95	-8:07:16.9	17.08	15.50	13.56	12.81	12.47
65	5:40:23.02	-8:03:21.2	15.88	14.95	13.56	13.12	12.80
126	5:40:23.17	-8:05:25.2	17.28	15.73	13.71	12.95	12.63
79	5:40:23.37	-8:03:35.7	16.34	15.39	13.80	13.25	12.94
122	5:40:23.90	-8:10:02.7	17.36	15.66	13.66	12.84	12.49
73	5:40:24.00	-8:03:26.4	16.25	15.35	13.89	13.45	13.25
143	5:40:24.01	-8:07:16.8	17.73	15.95	14.02	13.32	12.97
38	5:40:24.89	-8:08:22.7	15.19	13.85	12.02	11.32	10.98
32	5:40:25.74	-8:09:38.7	14.69	13.83	12.41	11.77	11.52
48	5:40:26.10	-8:02:18.3	15.33	14.27	13.03	12.49	12.26
63	5:40:27.10	-8:05:20.6	15.97	15.17	13.90	13.23	13.13
58	5:40:27.34	-8:08:37.0	15.86	14.49	12.80	12.12	11.79
134	5:40:27.46	-8:09:00.7	17.53	16.26	14.70	13.66	12.98
109	5:40:27.65	-8:07:58.9	16.98	15.50	13.83	13.23	12.87
193	5:40:28.13	-8:10:14.4	18.40	16.46	14.31	13.80	13.30

Table B.3 continued

ID	α (1950)	δ (1950)	R	I	J	H	K
24	5:40:30.49	-8:06:20.9	14.37	13.43	12.14	11.40	11.22
22	5:40:31.03	-8:03:53.4	10.76	10.45	10.04	9.85	9.77
93	5:40:31.77	-8:05:41.4	16.79	15.79	14.29	13.52	13.48
138	5:40:33.03	-8:06:24.9	17.58	16.09	14.65	14.01	13.81
106	5:40:34.02	-8:02:20.6	15.53	14.57	12.98	12.08	11.28
56	5:40:34.65	-8:04:43.3	15.91	14.99	13.55	12.86	12.59
54	5:40:34.98	-8:10:42.5	15.98	14.82	12.95	12.10	11.50
51	5:40:36.12	-8:03:52.7	15.45	14.33	12.52	11.61	11.31
29	5:40:36.45	-8:09:59.6	...	...	12.29	11.66	11.41
25	5:40:37.53	-8:06:09.2	...	...	12.05	11.12	10.51
81	5:40:40.43	-8:02:24.5	...	...	14.00	13.55	13.18
42	5:40:41.60	-8:09:15.2	...	...	12.05	11.48	11.19
125	5:40:44.38	-8:12:50.8	...	...	14.48	13.48	12.83

Table B.4. L1641 South: Effective Temperatures and Luminosities

ID	Sp. Type	$\log(T_{eff})$	A_v	$L/L_\odot$	W(Hα)	Notes
9	K7	3.602	0.16	-0.10	...	...
61	M1.5	3.553	0.0:	-0.62	...	...
127	M2	3.544	0.0:	-1.30	...	...
92	M0	3.580	1.89	-0.46	...	...
147	M2.5	3.535	0.0:	-1.27	...	...
18	K5	3.643	1.30	1.01	18	Ca II
52	M0	3.580	2.87	0.22	...	...
119	K8	3.591	5.34	0.24	...	...
41	K7	3.602	0.0:	-0.72	...	...
130	M5	3.477	1.08	-0.56	...	...
90	M2	3.544	1.44	-0.57	...	...
355	M6	3.447	0.0:	-1.26	...	...
6	K3	3.675	0.0:	0.28	...	...
173	M4	3.498	2.06	-0.81	...	...
171	M3	3.525	2.25	-0.91	...	...
5	K4	3.662	1.74	0.39	...	...
37	MIII	3.544	5.91	1.37	...	...
107	K5	3.643	6.14	0.06	...	...
235	M3	3.525	4.06	-0.60	50:	...
30	K3	3.675	4.76	0.72	...	...
34	K5	3.643	0.95	-0.47	...	...
154	K8III	3.591	5.68	-0.40	...	...
14	K8	3.591	0.11	-0.18	...	...
53	M0	3.580	0.10	-0.81	...	...
19	K5	3.643	2.28	0.10	...	...
84	M2	3.544	1.92	-0.50	...	...
162	M1.5	3.553	3.88	-0.60	...	...
7	A0	4.000	6.19	2.09	...	...
179	M2.5	3.534	3.06	-0.60	...	...
220	M1	3.562	5.94	-0.29	...	...

Continued, next page.

Table B.4 continued

ID	Sp. Type	log(T_{eff})	A_v	$L/L_\odot$	W(Hα)	Notes
33	K8	3.591	0.74	-0.12	100	...
110	M2	3.544	3.25	-0.35	65	...
43	K5	3.643	3.91	0.22	...	...
422	M1.5	3.553	6.00	-0.72	...	...
21	M1	3.562	0.46	-0.14	...	...
44	M0	3.580	1.39	-0.11	...	...
13	G6	3.750	4.04	0.79	...	...
108	K8	3.602	6.13	-0.19	27	...
305	M3.5	3.512	4.50	-0.95	...	...
69	M2.5	3.535	0.40	-0.69	...	...
272	M3	3.525	4.81	-0.78	...	...
68	M1	3.562	2.50	-0.25	134	Ca II
142	M0	3.580	4.88	-0.30	...	...
172	M2.5	3.534	2.50	-1.17	...	...
35	K5	3.643	3.53	0.28	...	...
114	K6	3.622	6.19	-0.00	...	...
46	M0	3.580	1.09	-0.34	...	...
12	B5	4.176	6.32	2.74	...	...
201	M3.5	3.512	2.19	-1.00	...	...
47	M1	3.562	3.23	0.25	...	...
82	M3.5	3.511	1.06	-0.56	30	...
137	M3.5	3.511	1.89	-0.71	...	...
174	M2	3.544	6.06	-0.06	15:	...
60	K6	3.622	5.13	0.21	...	...
169	M2.5	3.535	0.66	-1.36	...	...
195	M1.5	3.553	5.44	-0.41	...	...
155	M4	3.498	1.13	-0.65	...	...
3	B5	4.176	4.05	2.54	...	...
59	K7	3.602	4.14	0.27	...	...
202	M4	3.498	1.75	-0.95	48	...
182	M3	3.525	2.81	-0.79	...	...
250	M0	3.580	6.69	-0.17	...	...

Table B.4 continued

ID	Sp. Type	log(T_{eff})	A_v	$L/L_\odot$	W(Hα)	Notes
4	A0	4.000	5.28	1.64	...	...
372	M3	3.525	4.75	-0.82	36:	...
8	B5	4.176	8.84	1.42	...	...
76	G4	3.754	4.00	-0.16	...	...
144	M2	3.544	1.31	-0.64	12:	...
273	M0	3.580	0.31	-1.90	28:	...
86	G4	3.754	4.07	-0.36	...	...
39	F5	3.809	3.75	0.25	...	...
164	M1	3.562	0.0:	-0.88	...	...
2	A6	3.903	1.19	1.45	...	...
50	M1	3.562	0.25	-0.68	...	...
49	M3	3.525	0.0:	-0.64	220	Ca II
153	M1	3.562	0.0:	-1.67	...	...
16	K1	3.706	0.67	-0.28	...	...
1	A0	4.000	1.85	1.55	...	...
64	K8	3.591	0.03	-0.99	...	...
112	F9	3.785	4.13	-0.60	...	...
88	M2	3.544	2.63	-0.55	...	...
65	G2	3.768	3.80	-0.18	...	...
126	M2.5	3.534	1.81	-0.72	76	...
79	K6	3.622	1.88	-0.67	...	...
122	M1.5	3.553	3.88	-0.45	...	...
73	K1	3.706	3.06	-0.48	...	...
143	M1	3.562	4.75	-0.50	24:	...
38	M1	3.562	1.98	0.01	...	...
32	K5	3.643	2.08	-0.10	...	...
48	M1	3.562	0.24	-0.58	...	...
63	K5	3.643	1.64	-0.74	...	...
58	M2.5	3.535	0.69	-0.47	...	...
134	M1	3.562	1.52	-1.11	340	Ca II
109	M1	3.562	2.85	-0.62	...	...
193	M5	3.477	0.19	-1.20	...	...

Table B.4 continued

ID	Sp. Type	log(T_{eff})	A_v	$L/L_\odot$	W(Hα)	Notes
24	G4	3.754	3.79	0.37	...	...
22	F4	3.819	0.42	0.99	...	...
93	G6	3.750	3.99	-0.49	...	...
138	M2.5	3.534	1.44	-1.13	...	...
106	M0.5	3.571	0.01	-0.57	100	Ca II
56	G5	3.760	3.60	-0.23	...	...
54	M1	3.562	0.88	-0.48	67	...
51	K2	3.690	4.15	0.16	...	...
29	K5	3.643	0.24	-0.25	...	...
25	K5	3.643	2.94	0.14	32	...
81	G5	3.760	0.86	-0.70	...	...
42	M4	3.498	0.0:	-0.30	...	...
125	M2	3.544	3.11	-0.87	...	...

Table B.5. C-K Region: Optical and Near−Infrared Photometry

ID	α (1950)	δ (1950)	R	I	J	H	K
51	5:37:53.82	-8:15:00.5	16.82	15.23	13.29	12.44	11.92
49	5:37:55.32	-8:15:47.0	16.40	15.06	...	...	...
18	5:37:55.83	-8:18:08.5	14.58	13.55	...	...	...
50	5:37:57.43	-8:10:34.7	16.93	14.91	12.76	11.65	11.16
56	5:37:57.65	-8:10:26.7	17.13	15.28	13.05	11.94	11.38
91	5:38:00.52	-7:57:06.6	16.12	14.68	...	...	...
6	5:38:00.74	-8:09:03.4	12.71	11.79	10.64	9.73	8.91
73	5:38:01.60	-8:12:47.1	17.22	15.44	13.47	12.32	11.62
47	5:38:02.93	-8:09:06.8	16.78	15.03	13.26	12.33	11.66
62	5:38:04.20	-8:08:35.0	17.31	15.83	14.90	14.43	14.06
39	5:38:08.19	-8:08:08.8	16.57	15.02	13.35	12.57	12.12
65	5:38:09.62	-8:05:50.8	17.54	15.49	13.79	13.07	12.72
52	5:38:09.77	-8:14:47.5	17.30	15.33	13.33	12.32	11.87
7	5:38:13.06	-8:05:32.4	12.90	11.48	9.78	8.96	8.21
131	5:38:16.67	-8:03:47.9	18.64	16.72	13.26	11.74	10.79
38	5:38:17.06	-8:14:02.1	16.68	14.54	11.53	10.19	...
10	5:38:18.94	-7:59:22.4	12.20	11.75	...	...	...
2	5:38:21.94	-8:06:53.1	12.86	11.80	10.17	9.32	8.69
4	5:38:22.11	-8:06:04.7	12.89	11.74	10.34	9.51	9.16
41	5:38:22.38	-8:08:41.6	16.64	14.97	11.60	10.14	9.34
24	5:38:22.57	-8:06:23.3	14.89	13.42	12.09	11.17	10.56
5	5:38:23.80	-8:07:27.1	12.10	11.23	10.03	9.35	8.96
32	5:38:24.57	-8:10:25.0	16.00	14.52	12.66	11.76	11.30
11	5:38:26.92	-8:00:01.9	12.98	12.34	11.75	11.20	11.07
28	5:38:26.93	-7:57:55.8	15.32	14.52	...	...	...
8	5:38:27.67	-8:16:46.2	13.14	12.45	...	...	...
1	5:38:31.20	-8:14:44.6	12.18	11.69	11.34	10.94	10.82
35	5:38:32.45	-8:07:49.7	16.48	15.04	14.10	13.61	13.38
30	5:38:33.51	-7:57:08.6	15.45	13.99	...	...	...
64	5:38:35.51	-8:07:31.0	17.65	15.41	13.30	12.52	12.04

Continued, next page.

Table B.5 continued

ID	α (1950)	δ (1950)	R	I	J	H	K
36	5:38:35.99	-8:15:22.3	16.83	14.63	...	...	...
34	5:38:36.06	-7:59:59.5	16.05	14.86	14.04	13.48	13.31
155	5:38:36.95	-7:58:31.1	18.99	16.53	...	...	...
60	5:38:37.89	-8:05:42.0	17.52	16.01	15.17	14.35	14.24
165	5:38:42.17	-8:11:27.7	20.91	17.10	13.57	11.94	11.13
124	5:38:45.91	-8:06:54.7	19.80	16.70	12.90	11.21	10.32
14	5:38:47.92	-7:58:35.4	13.54	12.86	...	...	...
16	5:38:49.83	-8:09:23.9	14.68	13.10	11.70	10.78	10.36
29	5:38:51.48	-8:16:13.9	16.24	15.12	...	...	...
40	5:38:53.85	-8:09:00.9	16.96	15.22	13.95	13.52	13.15
17	5:38:54.79	-8:02:08.9	14.57	13.79	13.16	12.54	12.38
25	5:38:56.29	-8:16:48.9	15.47	14.12	...	...	...
3	5:39:01.11	-8:07:20.2	11.88	11.07	10.45	9.80	9.21
139	5:39:01.98	-7:59:43.8	19.43	16.73	...	...	...
57	5:39:03.14	-8:06:40.5	17.41	15.81	14.70	14.17	13.70
31	5:39:04.19	-8:03:37.5	16.16	14.55	13.38	12.78	12.55
68	5:39:06.33	-8:06:13.4	17.85	15.73	13.01	11.54	10.36
26	5:39:06.79	-8:09:39.6	16.08	14.68	13.71	13.03	12.80
63	5:39:07.98	-8:00:58.6	17.34	15.98	15.34	14.84	14.75
9	5:39:12.14	-8:08:31.7	...	...	11.91	11.23	11.07
42	5:39:19.27	-8:08:01.5	...	...	14.74	14.15	13.66
117	5:39:19.86	-8:05:01.9	...	...	14.21	13.16	12.61
33	5:39:20.38	-8:06:02.7	...	...	13.21	12.34	11.99
58	5:39:23.98	-8:05:28.7	...	...	14.63	14.02	13.55
84	5:39:26.12	-8:12:23.4	...	...	15.37	15.07	14.78
23	5:39:29.43	-8:08:56.0	...	...	11.78	10.79	10.34
19	5:39:37.16	-8:07:51.2	...	...	13.40	12.82	12.70
54	5:39:37.28	-8:08:15.2	...	...	13.01	12.27	11.86
66	5:39:39.81	-8:01:22.6	...	...	13.54	12.76	12.25

Table B.6. C-K Region: Effective Temperatures and Luminosities

ID	Sp. Type	log(T_{eff})	A_v	$L/L_\odot$	W(Hα)	Notes
51	K7	3.643	3.15	0.03	...	...
49	K7e	3.602	4.52	-0.16	...	...
18	M0	3.580	4.70	-0.22	...	...
50	M3	3.525	3.28	-0.11	...	...
56	M3	3.525	3.85	-0.34	25	...
91	M3e	3.525	6.02	-0.68	...	...
6	K0e:	3.720	1.39	0.85	47	Ca II
73	M3	3.525	4.39	-0.56	38	...
47	M3e	3.525	4.23	-0.49	230	Ca II
62	M3	3.525	6.32	-1.33	...	...
39	K5:	3.643	3.27	-0.02	...	...
65	M5	3.477	5.16	-0.92	...	...
52	M3.5	3.512	4.15	-0.48	...	...
7	F0-G0e	3.809	0.0:	1.79	...	...
131	M0:	3.580	3.18	-0.00	...	...
38	K5:	3.643	0.47	1.10	...	...
10	K0	3.720	3.20	0.35	...	...
2	K1e:	3.706	0.72	1.10	16	Ca II
4	K7	3.602	1.31	0.76	...	...
41	K7	3.602	1.71	0.60	...	...
24	M2.5	3.534	3.34	-0.12	13	...
5	K7:	3.602	1.46	0.70	...	...
32	¡K7	3.643	2.70	0.21	...	...
11	K7	3.602	3.57	-0.06	...	...
28	K7	3.602	6.01	-0.75	...	...
8	K7	3.602	4.35	0.03	...	...
1	K0:	3.720	2.81	0.28	...	...
35	M1	3.562	5.00	-0.75	...	...
30	M3	3.525	5.25	-0.38	...	...
64	M6vr	3.447	4.87	-0.81	42	...

Continued, next page.

Table B.6 continued

ID	Sp. Type	$\log(T_{eff})$	A_v	$L/L_\odot$	W(Hα)	Notes
36	M5	3.477	5.14	-0.18	...	...
34	M2	3.544	5.59	-1.00	...	...
155	K7	3.643	0.93	1.28	...	...
60	M3	3.525	6.54	-1.42	...	...
165	K7	3.602	0.12	1.23	...	...
124	M1:	3.562	1.05	0.83	...	...
14	K5	3.643	3.93	0.08	...	...
16	M2	3.544	2.60	0.19	10	...
29	M0	3.580	5.93	-0.71	...	...
40	M4.5	3.488	5.60	-1.06	...	...
17	K7	3.602	4.74	-0.61	...	...
25	M3	3.525	5.80	-0.56	...	...
3	K1e:	3.706	1.42	0.82	110	Ca II
139	M6	3.447	6.53	-0.59	...	...
57	M3.5	3.512	6.13	-1.27	...	...
31	M3.5	3.512	4.80	-0.73	...	...
68	K7e	3.602	2.37	0.34	40	Ca II
26	M3	3.525	5.26	-0.90	...	...
63	M1	3.562	6.38	-1.30	...	...
9	M0	3.580	3.54	-0.14	...	...
42	M2.5	3.534	6.45	-1.32	...	...
117	K7	3.602	4.88	-0.67	...	...
33	M0	3.580	4.36	-0.48	...	...
58	M3.5	3.512	6.23	-1.31	...	...
84	M4.5	3.488	7.72	-1.63	...	...
23	M1:	3.562	2.64	0.19	...	...
19	K7	3.602	5.20	-0.72	...	...
54	M5	3.477	4.33	-0.58	...	...
66	K5:	3.643	4.72	-0.60	...	...

Table B.7. V380 Region: Optical and Near–Infrared Photometry

ID	α (1950)	δ (1950)	R	I	J	H	K
114	5:32:49.78	-6:39:03.00	16.31	14.81	12.57	11.61	11.27
46	5:32:50.29	-6:49:17.05	14.17	13.42	12.49	11.92	11.71
180	5:32:50.42	-6:43:05.51	...	...	14.22	13.79	13.69
35	5:32:52.13	-6:50:46.06	13.50	12.74	11.84	11.23	11.04
124	5:32:53.54	-6:46:08.53	16.85	15.28	13.84	13.24	12.92
36	5:32:54.31	-6:47:52.85	13.21	12.76	12.18	11.83	11.78
84	5:32:54.66	-6:47:32.80	15.73	13.87	12.27	11.59	11.24
54	5:32:54.67	-6:49:17.68	14.82	13.67	12.48	11.82	11.57
66	5:32:54.87	-6:44:14.83	15.56	13.98	12.48	11.90	11.62
29	5:32:55.67	-6:42:39.44	12.59	12.18	11.67	11.31	11.29
37	5:32:59.31	-6:49:48.00	13.90	12.97	11.56	10.75	10.10
165	5:33:02.03	-6:46:43.76	17.62	16.07	14.89	14.22	14.09
162	5:33:04.90	-6:52:24.55	17.58	15.85	13.79	13.29	12.93
39	5:33:05.19	-6:47:09.19	14.35	12.99	11.63	10.85	10.47
175	5:33:05.85	-6:38:16.76	17.97	15.93	13.83	13.05	12.40
32	5:33:06.74	-6:39:23.00	12.77	12.34	11.79	11.42	11.33
76	5:33:08.23	-6:41:34.28	15.62	14.16	12.76	12.01	11.69
9	5:33:10.81	-6:47:03.18	...	...	10.68	10.41	10.34
5	5:33:15.01	-6:45:42.24	...	...	10.93	10.45	10.37
89	5:33:19.67	-6:47:09.72	16.32	14.73	13.39	12.81	12.58
55	5:33:23.19	-6:42:53.00	15.20	13.73	12.46	11.79	11.56
12	5:33:31.23	-6:48:53.74	12.66	12.03	11.24	10.71	10.59
73	5:33:31.35	-6:42:17.42	15.71	14.26	12.85	12.15	11.84
20	5:33:31.53	-6:44:30.91	13.06	12.16	11.12	10.28	9.53
30	5:33:31.67	-6:40:02.58	13.22	12.32	11.28	10.77	10.44
51	5:33:32.22	-6:38:32.52	14.64	13.53	12.65	11.38	10.62
34	5:33:34.27	-6:44:22.96	13.69	12.75	10.86	10.06	9.41
56	5:33:34.99	-6:42:48.96	14.42	13.74	12.94	12.43	12.25
83	5:33:35.53	-6:46:03.57	16.42	14.61	13.06	12.47	12.16
16	5:33:35.54	-6:52:03.07	...	...	9.29	9.03	8.92
123	5:33:35.74	-6:44:25.14	17.72	15.53	13.41	12.81	12.34
78	5:33:36.00	-6:48:49.66	15.57	14.45	13.41	12.78	12.58

Continued, next page.

Table B.7 continued

ID	α (1950)	δ (1950)	R	I	J	H	K
72	5:33:39.08	-6:44:32.75	16.25	14.18	12.35	11.79	11.38
15	5:33:39.14	-6:48:30.06	13.23	12.16	11.02	10.38	10.12
109	5:33:41.42	-6:44:56.05	17.06	15.24	12.78	11.86	11.41
45	5:33:42.48	-6:50:24.68	14.78	13.42	12.30	11.37	10.60
220	5:33:42.60	-6:42:22.11	18.84	16.61	14.43	13.94	13.57
132	5:33:45.34	-6:47:32.56	17.26	15.75	14.43	13.44	12.89
7	5:33:46.14	-6:51:26.69	...	...	10.52	10.23	10.14
188	5:33:49.23	-6:38:04.75	18.41	16.25	14.19	13.63	13.34
231	5:33:49.85	-6:47:40.36	18.63	17.08	15.91	15.37	14.99
99	5:33:53.65	-6:46:02.52	17.20	15.02	13.12	12.58	12.25
118	5:33:54.04	-6:52:27.36	16.67	15.43	14.26	13.78	13.46
82	5:33:56.03	-6:43:29.29	16.50	14.57	12.86	12.29	11.99
69	5:33:59.26	-6:46:28.94	16.07	14.21	11.23	9.51	8.12
28	5:33:59.51	-6:44:45.28	...	...	8.36	7.68	6.50
130	5:34:00.57	-6:50:30.28	17.84	15.59	13.57	13.02	12.84
59	5:34:02.23	-6:46:19.47	15.20	13.89	12.76	12.03	11.66
40	5:34:02.56	-6:50:31.55	13.81	13.27	12.62	12.09	12.06
163	5:34:03.08	-6:40:27.58	18.14	16.14	14.40	13.72	13.18
125	5:34:03.60	-6:40:37.07	17.21	15.33	13.71	13.17	12.93
200	5:34:04.31	-6:44:32.68	19.55	16.77	14.85	13.06	11.79
229	5:34:04.61	-6:43:49.78	19.36	17.02	15.32	14.78	14.07
48	5:34:06.85	-6:41:41.33	14.43	13.50	12.48	11.82	11.63
153	5:34:06.99	-6:46:07.26	18.06	15.98	12.95	11.57	10.70
88	5:34:07.53	-6:38:31.84	15.33	14.44	13.42	12.85	12.70
67	5:34:08.37	-6:45:09.20	15.11	14.18	13.24	12.61	12.41
170	5:34:09.46	-6:51:58.30	18.42	16.25	14.16	13.78	13.19
31	5:34:18.04	-6:51:27.26	...	...	11.70	11.14	10.99
129	5:34:18.39	-6:48:58.41	17.38	15.74	14.34	13.95	13.79
159	5:34:20.65	-6:41:35.40	18.28	16.09	15.16	14.76	14.44
8	5:34:21.86	-6:51:18.92	...	...	10.30	10.02	9.94
70	5:34:24.20	-6:43:14.43	15.41	13.96	11.97	11.06	10.57
161	5:34:24.35	-6:43:39.58	18.17	16.11	13.92	13.02	12.45
68	5:34:24.44	-6:50:43.37	15.86	14.14	12.60	12.04	11.73

Table B.8. V380 Region: Effective Temperatures and Luminosities

ID	Sp. Type	$\log(T_{eff})$	A_v	$\log(L/L_\odot)$	Notes
114	K0	3.720	6.88	0.47	...
46	K5	3.643	1.31	-0.21	...
180	M5	3.477	0.0:	-1.18	...
35	K4	3.662	1.56	0.10	...
124	M3	3.525	1.31	-0.84	...
36	G3	3.760	0.75	0.04	...
84	M4.5	3.488	0.56	-0.33	...
54	M0.5	3.571	1.19	-0.25	...
66	M2	3.544	2.69	-0.11	...
29	G1	3.772	0.62	0.25	...
37	M0	3.580	0.19	0.02	...
165	M3.5	3.512	0.31	-1.38	...
162	M4	3.498	0.62	-0.92	...
39	M3	3.525	0.0:	-0.09	...
175	M6	3.447	0.0:	-1.03	...
32	G5	3.760	0.50	0.15	...
76	M3.5	3.512	0.0:	-0.56	...
9	F5	3.809	0.17	0.68	...
5	K0	3.720	0.15	0.41	...
89	M3.5	3.512	0.56	-0.75	...
55	M3	3.525	0.62	-0.36	...
12	K2	3.690	1.06	0.34	...
73	M3	3.525	0.56	-0.52	...
20	M0	3.580	0.0:	0.18	...
30	M0	3.580	0.0:	0.11	...
51	M0	3.580	1.25	-0.30	...
34	K5	3.643	2.50	0.57	...
56	K1	3.706	1.56	-0.26	...
83	M4.5	3.488	0.25	-0.68	...
16	F2	3.838	0.41	1.34	...
123	M5	3.477	1.75	-0.67	...
78	M1	3.562	0.62	-0.69	...

Continued, next page.

Table B.8 continued

ID	Sp. Type	$\log(T_{eff})$	A_v	$L/L_\odot$	Notes
72	M5	3.477	1.00	-0.33	...
15	M0.5	3.571	0.69	0.28	...
109	M0	3.580	5.75	0.12	...
45	M2	3.544	1.25	-0.20	...
220	M5.5	3.462	1.06	-1.16	...
132	M3	3.525	0.87	-1.12	...
7	F7	3.799	0.03	0.69	...
188	M5	3.477	1.56	-1.00	...
231	M1	3.562	3.31	-1.40	...
99	M4	3.498	3.44	-0.35	...
118	M2	3.544	0.50	-1.06	...
82	M5	3.477	0.12	-0.62	...
69	K3	3.675	8.56	1.11	...
28	A1	4.000	2.93	2.34	...
130	M6	3.447	0.19	-0.91	...
59	M2.5	3.534	0.31	-0.49	...
40	G9	3.730	0.87	-0.18	...
163	M3	3.525	4.00	-0.78	...
125	M5	3.477	0.0:	-0.98	...
200	M2	3.544	10.12	-0.27	...
229	M6	3.447	0.75	-1.55	...
48	M0	3.580	0.12	-0.35	...
153	M2	3.544	5.75	0.02	...
88	M0.5	3.571	0.0:	-0.75	...
67	M0	3.580	0.19	-0.65	...
170	M6	3.447	0.0:	-1.16	...
31	K5	3.643	0.0:	-0.03	...
129	M4	3.498	0.06	-1.20	...
159	M2	3.544	6.44	-0.79	...
8	F6	3.806	0.14	0.81	...
70	M0	3.580	3.38	0.19	...
161	M3	3.525	4.25	-0.56	...
68	M5	3.477	0.0:	-0.53	...

Didelon, P. 1982, AAS, 50, 199

Elias, J.H., Frogel, J.A., Matthews, K., & neugebauer, G. 1982, AJ, 87, 1029

Elmegreen, B.C. 1992, III Canary Islands Winter School (Cambridge University Press)

Fukui, Y., Takaba, H., Iwata, T., & Mizuno, A. 1988, ApJ, 325, L13

Girard, T.M, Grundy, W.M., Lopez, C.E., & van Altena, W.F. 1989, AJ, 98, 227

Hartigan, P., Kenyon, S.J., Hartmann, L., Strom, S.E., Edwards, S., Welty, A.D., & Stauffer, J. 1991, ApJ, 382, 617

Hartigan, P., Strom, K.M., & Strom, S.E. 1994, ApJ, 427, 961; HSS

Hartigan, P., Edwards, S., & Ghandour, L. 1995, ApJ, 452, 736

Hartmann, L., & Kenyon, S.J., 1990 ApJ, 349, 190

Herbig, G.H., & Jones, B.F. 1981, AJ, 86, 1232

Hillenbrand, L.A., Strom, S.E., Vrba, F.J., & Keene, J. 1992, ApJ, 397, 613

Hillenbrand, L.A. 1995, Ph.D. Thesis, University of Massachusetts

Hodapp, K-W & Deane, J. 1993, ApJS, 88, 119; HD

Hughes, J., Hartigan, P., Krautter, J., Kelemen, J. 1994 AJ, 108, 1071

Jacoby, G.H., Hunter, D.A., and Christian, C.A. 1984, ApJS, 56, 257 (JHC)

Johnson, H.L. 1952, ApJ, 116, 640

Jones, B.F. & Stauffer, J.R. 1991, AJ, 102, 1080 (JS)

Kenyon, S. & Hartmann, L. 1995 ApJ in press

Kirkpatrick, J.D., Henry, T.J., & McCarthy, D.W. 1991, ApJS, 77, 417

Königl, A. 1991, ApJ, 370, L39

Lada, E.A., DePoy, D.L, Evans, N.J. II, & Gatley, I. 1991 ApJ 371, 171

Landolt, A. 1983, AJ, 88, 439

Mateo, M. 1988, ApJ, 331, 261

Meyer, M.R. 1996, Ph.D. Thesis, University of Massachusetts

Mihalas, D. & Binney, J. 1981 Galactic Astronomy (W.H. Freeman & Co.: San Francisco)

Miller, G.E. & Scalo, J.M. 1979 ApJS, 41, 513

Montgomery, K.A., Marschall, L.A., & Janes, K.A. 1993, AJ, 106, 181 (MMJ)

Mould, J.R. & Wallis, R.E. 1977, MNRAS 181, 625

NASA HST Guide Star Catalog, 1992.

Öhman, Y. 1936, Stockholms Observatoriums Annaler, 12, 3

Palla, F. & Stahler, S.W. 1993, ApJ, 418, 414

Parsamian, E. S. & Chavira, E. 1982, *Bol. Inst. Tonantzintla*, 3, 69

Pesch, P. 1967, ApJ, 148, 781

Popper, D.M. 1954, AJ, 59, 445

Popper, D.M. 1948, ApJ, 108, 490

Pravdo, S.H., Rodriguez, L.F., Curiel, S., Canto, J., Torrelles, J.M., Becker, R.H., & Sellgren, K. 1985, ApJ, 293, L35

Randich, S., & Schmitt, J.H.M.M. 1994, AA, in press

Rebeirot, E. 1966, Pub. Obs. Haute-P. 8, no.4

Rieke, G.H., & Lebofsky, M.J. 1985, ApJ 288, 618

Sanders, W.L. 1977, AAS, 27, 89

Schmidt-Kaler, T.H. 1982, Physical Parameters of Stars, Landolt-Bornstein New Series, Vol2b, Astronomy and Astrophysics, Stars and Star Clusters, ed. K. Shaifers & H.H. Voigt (New York:Springer)

Smithsonian Astrophysical Observatory Star Catalog 1966 (Smithsonian Pub. 4652, Washington, D.C.:GPO)

Soderblom, D.R. & Stauffer, J.R. 1984, AJ, 89, 1543

Stahler, S.W. 1983, ApJ 274, 822

Stauffer, J.R. 1982, PASP, 94, 678

Sterzik, M.F., Alcalá, J.M., Neuhäuser, R., Schmitt, J.H.M.M. 1995, A&A, 297, 418

Strom, K.M., Newton, G., Strom, S.E., Seaman, R.L., Carrasco, L., Cruz-Gonzalez, I., Serrano, A., & Grasdalen, G.L. 1989, ApJS, 71, 183

Strom, K.M., Strom, S.E., Wilkin, F.P., Carrasco, L., Cruz-Gonzalez, I., Recillas, E., Serrano, A., Seaman, R.L., Stauffer, J.R., Dai, D., & Sotille, J. 1990, ApJ, 362, 168

Strom, K.M., Strom, S.E., and Merrill, K.M. 1993, ApJ, 412, 233; SSM

Strom, S.E., Edwards, S., & Skrutskie, M.F., 1993, Protostars and Planets III, E.H. Levy & J.I. Levine, Eds., The University of Arizona Press

Swenson, F.J., Faulkner, J., Rogers, F.J., & Iglesias, C.A. 1994, ApJ, 425, 286; FJS

Torres-Dodgen, A.V. & Weaver, W.B. 1993, PASP, 105, 693

Upgren, A.R., Weis, E.W., & DeLuca, E.E. 1979, AJ, 84, 1586

Wall, D. 1994, private communication

Warren, W.H., & Hesser, J.E. 1978, ApJS, 36, 497

Weis, E.W. 1981 PASP, 93, 437

Wilson, O.C. 1963, ApJ, 138, 832

References

Abt, H. A. 1986, PASP, 98, 307

Allen, L.E., & Strom, K.M. 1995, AJ, 109, 1379

Bally, J., Langer, W..D., Stark, A.A., & Wilson, R.W. 1987, ApJ 312, L45

Barbier 1963, Pub. Obs. Haute-P. 6, no.36

Bessell, M. & Brett, J.M. 1988, PASP, 100, 1134

Bessell, M. 1991, AJ, 101, 662

Bidelman, W. P. 1956, PASP, 68, 318

Blaauw, A. 1991, The Physics of Star Formation and Early Stellar Evolution, ed. J. Lada & N.D. Kylafis, Kluwer: Dordrecht), p. 125

Boesgaard, A.M. & Budge, K.G. 1988, ApJ, 332, 410

Bolte, M. 1991, ApJ, 376, 514

Brand, J. & Wouterloot, J.G.A. 1991, in *Low Mass Star Formation in Southern Molecular Clouds*, ESO Sci. Report No. 11.

Brown, A.G.A., de Geus, E.J., & de Zeeuw, P.T. 1994 A&A, 289, 101

Burbidge, E.M. & Burbidge, G.R. 1959, ApJ, 129, 513

Cabrit, S., Edwards, S., Strom, S.E., & Strom, K.M., 1990 ApJ, 354, 687

Cohen, J.G., Persson, S.E., Elias, J.H., Frogel, J.A. 1981 ApJ 249, 481

Cohen, M. & Kuhi, L.V. 1979, ApJS, 41, 743

Corbally, C.J. & Garrison, R.F. 1983, J. Astr. Soc. Canada, 77, 28

Corbally, C.J. & Garrison, R.F. 1986, AJ, 92, 90

Crawford, D.L., & Barnes, J.V. 1969, AJ, 74, 818

D'Antona, F. & Mazzitelli, I. 1994, ApJS, 90, 467; DM93

Danks, A.C., & Dennefeld, M. 1994, PASP, 106, 382

Dickman, R.L., & Herbst, W. 1990, ApJ, 357, 531